B. A. R. C.-1024

B. A. R. C.-1024

भारत सरकार
GOVERNMENT OF INDIA
परमाणु ऊर्जा आयोग
ATOMIC ENERGY COMMISSION

RESEARCH & DEVELOPMENT

Activities of the
NEUTRON PHYSICS DIVISION
for the period
January 1977 - December 1978

Edited by
M. Ramanadham and O. P. Joneja

भाभा परमाणु अनुसंधान केन्द्र
BHABHA ATOMIC RESEARCH CENTRE
बंबई, भारत
BOMBAY, INDIA
1979

B.A.R.C.-1024

GOVERNMENT OF INDIA
ATOMIC ENERGY COMMISION

B.A.R.C.-1024

RESEARCH & DEVELOPMENT
Activities of the
NEUTRON PHYSICS DIVISION
for the period
January 1977 - December 1978

Edited by
M. Ramanadham and O. P. Joneja

BHABHA ATOMIC RESEARCH CENTRE
BOMBAY, INDIA
1979.

INIS Subject Category : ~~E21, A31, A13, E14~~

Descriptors

RESEARCH PROGRAMS

BARC

NEUTRON DIFFRACTION

NEUTRON REACTIONS

REACTOR PHYSICS

REACTOR KINETICS

PLASMA

THERMONUCLEAR REACTIONS

X-RAY DIFFRACTOMETERS

FABRICATION

CRYSTALLOGRAPHY

SOLIDS

PHASE STUDIES

NUCLEAR EXPLOSIONS

UNDERGROUND EXPLOSIONS

SEISMIC DETECTION

SEISMOLOGY

CONTENTS

FOREWORD

The research and development programmes of the Neutron Physics Division cover the fields of reactor neutron physics, fusion and plasma neutronics, biological and high precision crystallography, solid state phenomena and seismology. The workshop facilities for the Division are provided by the Physics Group Workshop whose staff is affiliated to the Nuclear Physics Division. We have also had the benefit of collaboration and support from several other Divisions in BARC.

During the period of the report, the detailed physics calculation and the engineering design of Purnima-II, the BeO-reflected U^{233} (Uranyl nitrate solution) fuelled experimental thermal reactor were completed. The fabrication of most of the component assemblies is also over. Work on a U^{233}-fuelled 30 KW mini-pool neutron source reactor for neutron radiography to be located in RRC also made significant progress.

Computational physics is an important aspect of reactor physics research and extensive capability has been developed in the Division in this field. Many new computer programs, including some based on the Monte Carlo method, have been written and several international computer codes have also been adapted for local computers. Theoretical analysis of the characteristics of fast systems and a number of computer calculations have led to the development of a versatile and useful relation for the variation of k_{eff} with core and reflector dimensions and with density. Although the relation was originally derived for spherical hard fast assemblies only, it has been found applicable also for describing neutron leakage from non-spherical and small thermal systems.

A new programme has recently been initiated on fusion and plasma neutronics. Experiments have been carried out using a Mather-type dense plasma focus device to study the mechanism of neutron production from high temperature deuterium plasmas. Neutrons, believed to be of thermonuclear origin, have been detected in these experiments. Neutrons have also been detected in exploding wire experiments using deuterated cotton fibres. The above experiments are being extended using high-energy capacitor banks. Experiments have been done to measure the amount of tritium produced in natural lithium assemblies using Li^6-samples, on irradiation with 14 Mev neutrons. These experiments are part of our studies on fusion reactor blankets. An applied research programme of great interest relates to the use of neutrons in oil exploration.

The first indigenously-designed and fully automatic x-ray diffractometer was commissioned in the Division during the period of this report. The complete hardware and electronics for the system have been fabricated in Trombay and the diffractometer is controlled by the ECIL Computer TDC-312. Recent diffraction work in both neutron and x-ray crystallogra-

phy has tended to be on molecules of biological interest. In view of the high precision of the data now available from the Trombay diffractometers, a programme relating to the determination of charge density distributions in crystals and molecules using combined x-ray and neutron data is being initiated. A new programme has also been started on the x-ray structure determination of large biological molecules like proteins.

Many interesting phase transformations in solids have been studied during this period. Extensive work has been carried out on the high pressure isothermal martensitic alpha-to-omega transformation in Group-IV elements. An experimental set up for studying electron states in solids using positron annihilation has been set up recently and this will use high-intensity Cu^{64} sources. A theoretical programme for calculating shock Hugoniot equation of states of metals from first principles was also initiated and interesting results have been obtained for Al, Pb and Th. The rock mechanics effects of underground peaceful nuclear explosion have been studied using both computer simulation methods and analytical techniques. Studies in the very interesting field of ferroelasticity have resulted in the discovery of several new ferroelastic materials and the proposal of a new possible class of materials called ferrogyrotropics.

The Seismic Array Station at Gauribidanur continues to operate very satisfactorily and to detect all the major underground nuclear explosions. The data processing computer capability at the Station was enhanced during the period with the addition of a PDP 11/40-based system. The Seismology Section has built up extensive capability for indigenous fabrication of seismometers and other electronic units needed in the work. UNDP has recently placed an order for 20 units of timing systems developed in the Seismology Section; these units will be deployed in the seismic stations in South-East Asia. The Section has also a collaborative seismic project with Bharat Gold Mines Ltd., Kolar to record and monitor rock-burst signals. It has completed the establishment of a network of seven surface sensors at Kolar together with the telemetry and recording system.

The above are only some of the highlights of the research activities of the Division which are described in much greater detail in the report that follows. The report covers the two-year period 1977-78.

R. Chidambaram

1. REACTOR NEUTRON PHYSICS

1.1 Purnima Reactor Programme

1.1.1 Purnima II: BeO Reflected ^{233}U Uranyl Nitrate Solution Critical Experiment - Status Report*

(K. Chandramoleshwar, P.K. Job, V.R. Nargundkar, C.S. Pasupathy, M. Srinivasan and K. Subba Rao

A general layout of Purnima II is depicted in Fig. 1.1. A major portion of the fabrication jobs are complete. The twin glove boxes fabricated at the Radiometallurgy Division are under installation at Purnima vault. The zircaloy core vessel and the stainless steel storage tank have already been fabricated and subjected to both radiography and helium leak tests. A new set of nuclear instrumentation for Purnima II executed by the Electronics Division is ready. The design is similar to the systems being installed at other research reactors at Trombay. The control mechanisms for this reactor have been designed and fabricated by the Reactor Control Division. Shop tests of the weir cup and level probe mechanism are complete. An incore capacitance level probe specially designed and developed for this reactor has been field tested. The reproducibility and reliability of operation of the peristaltic pump employed for transfer of fissile solution from storage tank to the core vessel has been thoroughly investigated. Plumbing work on the various pipelines carrying fuel solution is in progress. All the BeO reflector modules have been assembled and stacked in place. The Fuel Reprocessing Division has completed the chemical purification and separation of the ^{233}U uranyl nitrate stock solution.

Suitable steps in the radiological safety aspects have been taken. Equipment needed to convert the reactor vault into a shoe cover area has been installed. Hand and clothing contamination monitor station has been set up. The Pu-in-air monitor has been suitably modified for use as ^{233}U in-air alpha monitor. Other radiation monitoring instruments have also been procured and tested. The efficiency of HEPA filters in the exhaust system has been rechecked and established to be better than 99.5%. The method of deducing the maximum permissible fissile inventory limit (IMAX) in the system based upon the experimentally determined extrapolated critical mass has been established. The maximum permissible critical level has been stipulated on the basis of 10% free volume in the core vessel above the fuel solution.

A Safety Analysis Report for Purnima II was prepared and is currently being evaluated by the Reactor Safety Committee. The procedure for the first approach to critical has been outlined in this report.

---

* In collaboration with Reactor Control Division and Fuel Reprocessing Division.

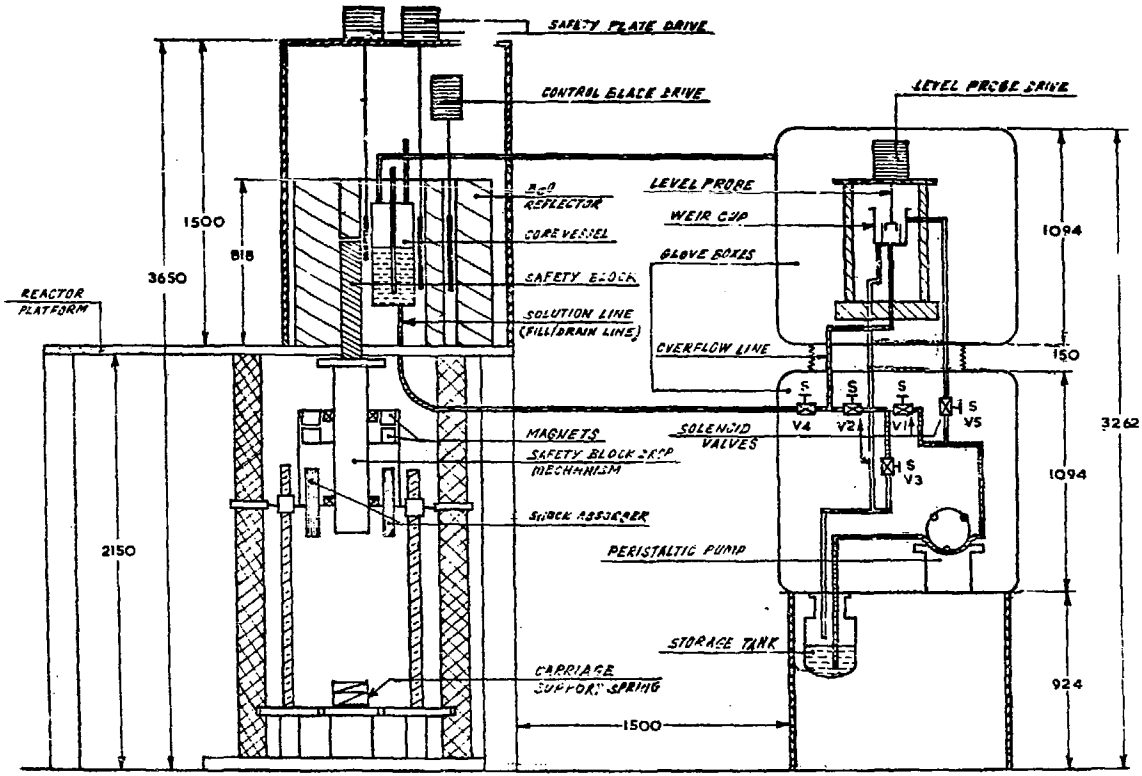

Fig. 1.1 Layout of reactor assembly and glove boxes: schematic elevation (dimensions in mm)

1.1.2 Physics Calculations for Purnima II

(K. Subba Rao, P.K. Job, C.S. Pasupathy and M. Srinivasan)

A number of reported[1] experimental ^{233}U solution critical systems were analysed using 18 group Bells cross section set and 16 group Hansen and Roach (H.R.) set. The 16 group H.R. set with anisotropic treatment for hydrogen gave excellent agreement with the experimental k_{eff} values. All the physics design calculations for Purnima II were therefore repeated using this set. Few group cross section sets were generated from the 16 group H.R. set using appropriate weighting functions to be used in two dimensional transport theory calculations. The Monte Carlo calculations are described in Sec. 1.1.3. The k_{eff} as a function of core solution height

Table 2.1 Variation of K_{eff} as a Function of Solution Height and Concentration (TWOTRAN 2 Group Results)

Uranium conc. in solution (g/L)	H/U^{233}	Core height, h (cm)	Uranium mass (g)	K_∞	K_{eff}+
		25.0	297		0.939
		30.0	357		0.985*
70	364	35.0	416	1.866	1.023
		36.0	428		1.030
		44.07	524		1.069
		50.0	594		1.088
		20.0	306		0.929
		29.1	445		1.030*
90	281	30.0	458	1.933	1.040*
		34.28	524		1.075
		50.0	764		1.146
		20.0	374		-
		25.0	467		1.030*
110	228	28.04	524	1.977	1.057
		30.0	560		-
		50.0	934		-
		20.0	441		-
		23.70	523		1.030*
130	191	23.73	524	2.064	1.031
		30.0	662		-
		35.0	773		1.136
		50.0	1104		1.204

+ Corrected for group collapsing effects
* Graphically interpolated

obtained for 70, 90, 110 and 130 g/L concentrations, are summarised in Table 2.1.

The safety block and safety plate worth calculations were carried out both in the cylindricised ring geometry using TWOTRAN and 2DB codes as well as in the exact geometry using Monte Carlo code KENO and diffusion code WHIRLAWAY. The worths were also obtained as a function of their position. The block worth was estimated to be equal to 60 mk. The total reactivity worth of the two safety plates corresponding to 350 mm stroke between their up and down position was calculated to be ~100 mk for operating core heights in the range of 200 to 400 mm. The variation of reactivity of safety block and plates as a function of position is given in the Safety Analysis Report [2] .

REFERENCES

[1] McNeany, S.R. and Jenkins, J.D., Nucl. Sci. Eng., 65, 441 (1978).

[2] Srinivasan, M. et al., BARC/I-488, (1978)

1.1.3 Monte Carlo Calculations for Purnima II

(V.R. Nargundkar)

(a) K_{eff} of Purnima II Reactor

The Monte Carlo code KENO-II was used to obtain k_{eff} for Purnima-II system and to estimate the reactivity worths of boral safety plates, BeO safety block etc, using the exact three dimensional geometry. 200 neutrons were used in a batch and typically 8000 neutron histories were traced. Some of the results are shown in Table 3.1.

Table 3.1 Calculated Reactivity Worths for Purnima-II System Using H.R. Set (^{233}U Solution Core: 70 g/L Concentration)

Core Solution Height (h)	30 cm	35 cm
Reference system K_{eff}	0.965 ± 0.011	1.031 ± 0.012
Boral Safety Plates Worth	91 ± 14 mk	124 ± 18 mk
BeO Safety Block Worth	35 ± 14 mk	53 ± 14 mk

(b) Storage Tank K_{eff}

Calculations were also done to estimate the k_{eff} of the cylindrical fuel solution storage tank of Purnima II. This tank is made of 6 mm

thick SS having 15.6 cm ID and 50 cm height and is shielded by 15 cm thick lead all around in rectangular geometry. The K_{eff} values for different solution concentrations and ^{233}U inventories are summarised in Table 3.2.

Table 3.2: Storage Tank K_{eff} for Various Concentrations and Inventories of ^{233}U (I = ^{233}U inventory; h = solution height)

Concentration (g/L)	I = 500 g		550 g		600 g		650 g	
	h	k_{eff}	h	k_{eff}	h	k_{eff}	h	k_{eff}
70	-	-	-	-	44 cm	0.830	-	-
90	29 cm	0.806	32 cm	0.814	35 cm	0.840	37.8 cm	0.838
110	-	-	-	-	28.5cm	0.830	-	-
130	-	-	-	-	24.1cm	0.803	-	-

For an inventory of 600 g of ^{233}U at 70 g/L concentration, the bare and 20 cm (infinite) water reflected k_{eff} values are 0.602 and 0.754 respectively. These values are much less than 0.830 obtained with 15 cm lead reflector. The standard deviation of k_{eff} in these calculations was ~10 mk.

1.1.4 Protection Capability of Safety System of Purnima II Reactor

(S. Das and M. Srinivasan)

In order to evaluate the protection capability of the safety system of Purnima II in the event of an inadvertent insertion of reactivity, detailed kinetic analysis of energy release for a number of ramp reactivity inputs was carried out [1]. Power excursion was initiated by adding reactivity at a ramp rate to an initially just critical reactor (power level = 10mW) and was terminated by a trip caused by control instrumentation (either linear safety channel or period channel). In the study, all system delays (electronic, fixed and inertial) were taken into account. For both safety block drop and safety plate fall, there was initially a free fall in the millisecond region after which reactivity was removed slowly during damped fall.

Fig. 4.1 gives plots of reactivity, reactor power and integrated energy in a hypothetical (severe) prompt critical start up 'accident' for a reactivity insertion rate of 10 \$/s wherein safety block acts to terminate the excursion. Following trip initiation at an indicated reactor power of 1.3W, there is 100 ms of fixed and inertial delay after which reactivity removal commences (free fall reactivity removal rate = 50\$/s and acts for 60 ms; damped fall reactivity removal rate is 1 \$/s acting for 4s). The reactor is brought to a constant subcritical level of 7\$ in 4.34s. Total integrated energy released during the entire course of the 'excursion'

is $\sim 4.3 \times 10^{15}$ fissions (0.14 mega-joules) corresponding to a rise in solution temperature of only 5°C. Table 4.1 summarises the energy release (E) and temperature (T) when safety plate removes reactivity, corresponding to the three stages during the excursion (The definition of the stages I, II and III are evident from Fig. 4.1).

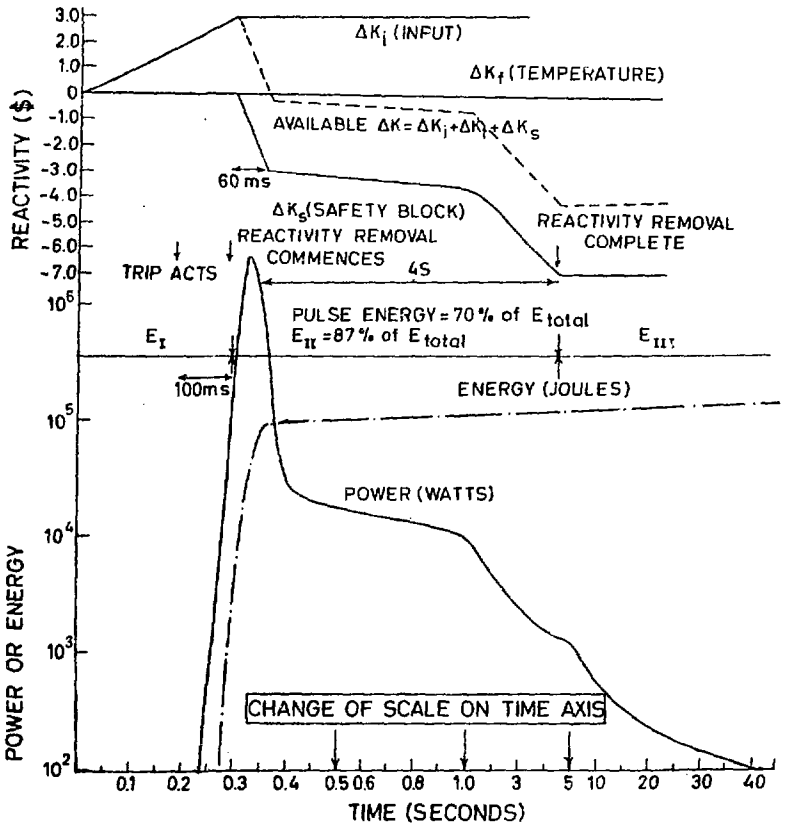

Fig. 4.1 Analysis of a hypothetical prompt critical accident in Purnima II. Linear channel acts and safety block falls for reactivity input = 10 $/sec.

Taking prevention of core boiling as the safety criterion, protection capability of safety plate when linear channel initiates trip has been deduced to be ~ 4.5 $/s. Corresponding figure for safety block is $\gtrsim 10$$/s. Analysis also shows that if the period channel initiates trip, even with a reactivity insertion rate of 10$/s, total integrated energy, E_T, released in the entire excursion is less than one joule and solution temperature rise is less than one degree centigrade.

Table 4.1: Energy Release and Solution Temperature When Linear Safety Channel Initiates Trip and Only One Safety Plate Acts

Ramp rate ($/s)	E_I (J)	E_{II} (J)	E_{III} (J)	$E_T=E_I+E_{II}+E_{III}$ (J)	T_I (°C)	T_{II} (°C)	T_{III} (°C)
0.1	1.24	0.07*	<0.2	1.51	30	30	30
0.4	1.16	0.27*	<0.2	1.63	30	30	30
1.0	6.26	4.25	<1	11.5	30	30	30
3.0	2.26 $\times 10^3$	7.8 $\times 10^3$	$< 10^3$	11.1 $\times 10^3$	30.1	30.4	30.5
5.0	4.6 $\times 10^5$	Boils	-	Boils	47	100	-
8.0	Boils	-	-	Boils	100	-	-

* Before reactivity removal was complete, power level had decayed to less than 10 milliwatt.

To be on the conservative side the gas void reactivity feedback resulting from bubbles generated by radiolytic decomposition of water was neglected. However the role of radiolytic gas voids in shutting down the reactor during a fast power excursion was considered in detail earlier [2] and the magnitude of the resulting dynamic pressure wave calculated. At present a model that takes into account the dynamics of bubble formation and their migration to the core solution surface is being developed to explain the series of characteristic reactivity and power oscillations observed in CRAC [3] experiments during slow ramp reactivity additions.

REFERENCES

[1] Das, S. and Srinivasan, M., Proc. Symp. on Power Plant Safety and Reliability, BARC, Bombay (Jan. 1979).

[2] Das S. Neutron Physics Section Annual Report, BARC-937, pp. 53-56 (1977).

[3] Le'corche', P. and Seale, R. L., Oak Ridge Criticality Data Centre, Report Y-CDC-12 (1973).

1.2 Analytical and Monte Carlo Methods of Calculations of Neutronics of Fission Systems

1.2.1 Trombay Criticality Formula for Small Fast Assemblies

(Anil Kumar, K. Subba Rao and M. Srinivasan)

Although sophisticated code packages based on multigroup transport,

diffusion and monte carlo methods are available to calculate accurately neutron leakage and k_{eff} for any system of interest, it is often useful to have simple formulae and correlations which can be used to make quick calculations and spot-checks of the 'reasonableness' of computer outputs and give a deeper insight into the basic physical phenomena involved. The Trombay Criticality Formula is one such relation which has been found to be remarkably useful in the context of high leakage fast assemblies for estimating k_{eff} changes due to various types of perturbations in system geometrical parameters such as size, shape and density.

The basis of the Trombay Criticality Formula, which has been elaborated in detail elsewhere [1-5], is the observation that changes in system geometrical parameters do not lead to significant shift in the neutron energy spectrum or k_∞ of the system and consequently variations in neutron leakage probability and k_{eff} can be essentially attributed to changes in core geometrical parameters such as its mean chord length, ($\hat{\ell}$). The elegance of the concept of mean chord length is that it is directly obtained from the volume (V) to surface area (S) ratio of the core through $\hat{\ell} = 4V/S$ and thus serves as the link between neutron leakage probability and core geometrical size and shape.

Trombay Criticality Formula (TCF) states:

$$k_{eff} = k^*_\infty \left[1 - \exp\left(-\theta \frac{\hat{\ell}}{\hat{\ell}_c}\right)\right]$$

$$= k^*_\infty \left[1 - \exp\left(-\theta \frac{\hat{\ell}}{q\,\hat{\ell}^{b}_{sph}\,\eta}\right)\right] \qquad \text{--------- (1)}$$

where k^*_∞ is a constant close to k_∞ or η of the core composition; $\theta = \ln[k^*_\infty/(k^*_\infty - 1)]$; $\hat{\ell}$ ($\hat{\ell}_c$) is mean chord length of core (critical core) for fixed reflector parameters; $\hat{\ell}^{b}_{sph}$ is mean chord length of bare spherical critical core having identical core composition; $\eta (\leq 1)$ is a parameter indicative of the degree of reflection; $q (\simeq 1)$ is a correction factor accounting for the slight difference in $\hat{\ell}$ of non-spherical and spherical cores having same neutron leakage.

There are a number of areas of application of the Trombay Criticality Formula (TCF) starting from the simple problem of calculation of k_{eff} of a lump of fissile material having arbitrary shape and density and estimation of the increase in reactivity following compaction of highly enriched fissile fuel during transportation accidents to more involved situations as in array criticality problems in the context of fuel storage. Another likely application is the use of mean chord length based interpolation schemes for following k_{eff} changes in sophisticated LMFBR

core melt down codes, with a view to effect some savings in computer time. Temperature coefficients of reactivity of small fast systems due to density changes can also be readily computed [6] through TCF.

REFERENCES

[1] Anil Kumar, Srinivasan, M., Basu, T.K. and Subba Rao, K., Atomkernenergie 30, 39 (1977).

[2] Anil Kumar and Srinivasan, M., Atomkernenergie 31 249 (1978).

[3] Anil Kumar, Subba Rao, K. and Srinivasan, M., paper under publication in Atomkernenergie (1979).

[4] Anil Kumar, and Srinivasan, M., paper presented at third national symposium on radiation physics held at Waltair, India (February, (1979).

[5] Anil Kumar and Srinivasan, M., paper under publication in Nuclear Technology (1979).

[6] Srinivasan, M., Job, P.K. and Anil Kumar, p. 64-69, BARC-937 (1977).

1.2.2 Finite Element Techniques in Reactor Physics Calculations

(G. V. Acharya)

An attempt is being made to apply the finite element technique to multi group, multiregion systems The problem has been formulated as a self-adjoint variational principle, which ensures covergence. The space angle flux is approximated in terms of univariate polynomials for the spatial and angular variables separately. A special method is adopted for solving the matrix equation that yields the neutron fluxes at the nodes. Using this method a computer programme is being written to find the k_{eff} of a bare spherical reactor under one group approximation.

It is intended to study the problem for the non self-adjoint form of the transport equation, in future. Also it is intended to develop a code for a cylindrical geometry for a two-dimensional case, wherein the finite element method is applied to spatial variables and Sn technique is applied to angular variables.

1.2.3 Monte Carlo Calculation for Intermediate Energy Standard Neutron Field (ISNF)

(K. Subbukutty, O. P. Joneja, S.B.D. Iyengar and M. P. Navalkar)

As a substitute to the NBS intermediate energy neutron facility which

employs enriched U^{235} [1] , a natural uranium loaded assembly is suggested. The fast neutrons generated due to fission in the natural uranium source gets degraded as a result of scattering in carbon and finally preferential absorption in B^{10} results in the intermediate energy spectra. Detailed Monte Carlo calculations have been done [2] considering different source thicknesses, densities and location of the source. The average energy, median energy etc compare reasonably well with the NBS facility using thin enriched uranium sources.

REFERENCES

[1] Gillam, D. M., Grundl, J. A. and Eisenhauer, C. M., BNL-NCS-22500, p 188 (1977).

[2] Joneja, O. P., Subbukutty, K., Iyengar, S. B. D. and Navalkar, M. P. International Conference on neutron physics and Nuclear data for reactors and other applied purposes, Harwell, Sept. 1978.

1.2.4 Exponential Biasing for the Calculation of Transmission Through LiH Cylinder

(K. Subbukutty, N. N. Ajitanand* and M. P. Navalkar)

While the usual variance reduction techniques with an addition of non-leakage through other sides is sufficient to estimate the transmission ratio in LiH assembly, it is found inadequate to estimate the transmitted spectrum. In this case the statistics becomes poor ar no meaningful conclusion can be drawn from the output. To impro the statistics a method known as exponential biasing is introduced. In this method the mean free path is stretched if the neutron travels in the direction of interest while its weight is adjusted to counter the bias introduced. Thus in the case of transmission the number of particles leaking through the interested face will increase while the transmitted weight and transmission ratio remain unchanged. Although it improves the statistics considerably, it is felt that the transmitted spectrum statistics is still too low to draw any valid conclusion based on it.

1.2.5 Time-Dependent Calculation by Neutralised Collision Method

(K. Subbukutty, S. B. D. Iyengar and M. P. Navalkar)

The neutralised collision method can be considered as one of the many variance reduction techniques available to increase the statistical accuracy of the calculation.

In this method, the random change in weight due to collision is replaced by a continuous change of weight which is a function of time and

---

* Nuclear Physics Division

occurs at a rate depending on the energy of the particle and the medium in which it moves. The collision parameters are changed such that the expected number of neutrons emerging from a collision is made unity. This has to be done in such a way that the number of secondary neutrons per primary neutron remains the same, as before. If the parameters Σ_t (macroscopic total cross-section) and C (number of secondary neutrons per collision) are changed to Σ_t' and C' respectively and 'a' is the exponential ratio of continuous change of weight, we have, in one group formalism.

$$v \Sigma_t C = v \Sigma_t' C' \qquad \text{---(1)}$$

$$v \Sigma_t C + (1 - v\Sigma_t) = v \Sigma_t' C' + (1 - v \Sigma_t') + a \qquad \text{---(2)}$$

where v represents the velocity of the neutron From (1) & (2) we get

$$a = v \Sigma_t' (C/C' - 1) \qquad \text{---(3)}$$

Since the weight is not to change in collsion

$$C' = 1$$

and therefore ,

$$\Sigma' = C \Sigma_t \qquad \text{---(4)}$$

$$a = v \Sigma_t (C - 1) \qquad \text{---(5)}$$

Thus the neutrons are tracked (a) with $1/C\Sigma_t$ as the mean free path, (b) there is no change of weight on collision and (c) there is continuous change of weight given by

$$\omega (t - t_0) = \omega (t_0)\, e^{a(t - t_0)} \qquad \text{---(6)}$$

Since

$$C = (v \Sigma_f + \Sigma_s) / \Sigma_t \qquad \text{---(7)}$$

and

$$a = v (v \Sigma_f + \Sigma_s - \Sigma_t) \qquad \text{---(8)}$$

Thus the main features of neutralised collision method which differs from conventional Monte Carlo method are

1. Use of $(v \Sigma_f + \Sigma_s)^{-1}$ as the mean free path to find collision probability and point of collision.

2. Continuous change of weight given by equation (6)

The neutron density is obtained from the weight at each time.

1.3 Design of a 30KW U^{233} Fuelled Mini Pool Neutron Source Reactor to be set up at RRC

1.3.1 Status Report

(C.S. Pasupathy and M. Srinivasan)*

A small ^{233}U fuelled light water moderated and cooled tank type neutron source reactor (30KW power, 10^{12} n/cm^2/sec flux) is being set up at the Radiometallurgy Laboratories of RRC. This reactor would mainly be used for neutron radiography of irradiated FBTR fuel subassemblies. Table 1.1 summarises the main characteristics of this reactor.

Table 1.1: Main Characteristics of the Reactor

Fuel Composition	20 wt% U-Al alloy
Meat Dimensions	1 x 54 x 250 mm^3
Plate Dimensions	2 x 62 x 260 mm^3
Clad Material	Aluminium
Water Gap Between Fuel Plates	6 mm
Number of Fuel Plates/Subassembly	24
Number of Subassemblies	3
Overall Core Dimensions	194 x 204 x 260 mm^3
Thermal Neutron Flux in Core	$\sim 10^{12}$n/cm^2/sec.
Side Reflector Material	BeO followed by H_2O
Side Reflector Thickness	200 mm + infinite water reflector ($\sim$700 mm)
Axial Reflector Material	40 vol% BeO-H_2O followed by infinite H_2O
Power Density at 30KW	3KW/litre
Heat Flux on Fuel Plate Surface	$\sim$1.4 Watts/cm^2
Total Heat Transfer Area	2.1 x 10^4 cm^2
Fuel Plate Temperature at 30KW	$\sim$85°C
Typical Bulk Pool Temperature	$\sim$45°C
Average Coolant Velocity in Core	44mm/s

The reactor consists of a BeO assembly approximately 60 x 60 x 60 (ht) cm^3 in size immersed in a 2.0 m dia SS tank containing demineralised water. A 194 x 204 x 260 (height)mm^3 core is placed in a central vertical channel of the BeO reflector assembly. The core is made of ^{233}U-Al alloy (20 wt% of uranium flat fuel plates of the MTR type). Fig. 1.1 is a schematic view of the reactor.

The reactor is cooled by natural convection circulation of the pool water. Heat transfer calculations have been made to obtain the flow velocities and temperature rise (ΔT) across the core using the code

---

* In collaboration with Shri Anand Kumar and Shri Kannan of RRC.

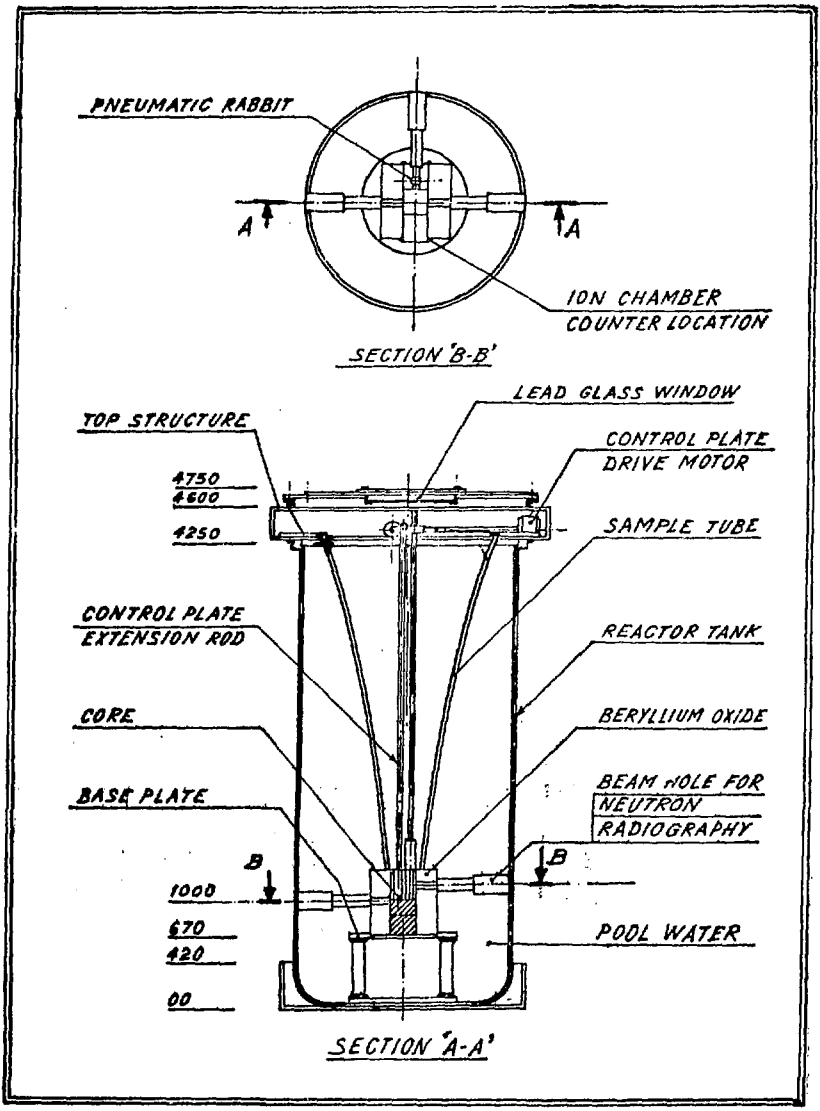

Fig. 1.1 Schematic view of the mini pool neutron source reactor

Table 1.2: Coolant Velocity and Temperature Rise Across Core Obtained from Program HOTPLATE

Power in KW	Heat flux* in watts/ cm^2 (q)	(Gr Pr) No	Heat Transfer coeff in $Btu/ft^2hr^\circ F$ ($\bar{h}$)	Coolant velocity+ in cm/sec ($\bar{v}$)	Temperature rise across the ΔT (°C)	Film drop (Tc - Tw) (°C)	Max fuel temp for coolant inlet temp of 40°C (Tc) (°C)
10	0.48	9.3×10^8	60.3	1.8	5.6	18.3	63.9
20	0.95	2.5×10^9	77.1	3.0	6.5	26.3	72.8
30	1.43	6.6×10^9	92.6	4.4	7.3	33.3	84.6
50	2.38	$\sim 10^{11}$	160	5.9	10.0	25.5	75.5
100	4.76	$\sim 10^{11}$	185	7.7	13.7	37.2	90.9

* Total fuel plate area = 2.1×10^4 cm^2

\+ This is the velocity averaged over hydrodynamic boundary layer thickness of 2.7 mm on both sides of each plate.

HOTPLATE for various reactor powers. Table 1.2 summarises the results. It is seen that the maximum fuel surface temperature even for a power level of 100 KW is $<100^{\circ}C$ which is well below the fuel alloy melting point of $650^{\circ}C$.

Detailed physics calculations for the initial design of the reactor assembly are under way using two and three dimensional diffusion theory codes, (2DB and WHIRLAWAY), two dimensional transport theory code TWOTRAN and Monte Carlo code KENO.

The reactor is being installed in the basement area under the hot cells of RML building. The civil works inclusive of special alterations to the building to accommodate this reactor are complete. A separate once through ventilation system (with air conditioning) connected to the RML stack has been installed and tested. A Preliminary Design and Safety Analysis Report is under preparation.

Detailed specification for the control system, shielding, auxiliary water system such as demineraliser and heat exchanger, pneumatic rabbit facility, radiography facility etc are in progress.

1.4 Development of Techniques and Instrumentation for and Actual Measurements of Flux and Spectrum in Reactors and Fusion Blanket Assemblies

1.4.1 Neutron Spectrum Measurements and Unfolding Methods

(D.V.S. Ramakrishna, O.P. Joneja and M.P. Navalkar)

Fast neutron spectrum unfolding from the measured specific activity data is an effective method for finding neutron spectrum in reactor assemblies. Several functional forms and methods are developed for determining the fast neutron spectrum [1, 2, 3]. The concept of minimization of the variation of the amplitude factor is found to work satisfactorily. It is now extended to include a double parameter function coupled to a Monte Carlo scheme for selection of activity and cross-section set using a Gaussian error function. The analysis done with the IAEA specific activity data is found to satisfy the minimization criteria.

In connection with the pressure vessel surveillance programme of IAEA, fast neutron spectrum in the tray-rod position of CIRUS reactor has been determined [4] using several threshold detectors. However, it is observed that for a better spectrum shape specially in the lower energy side, it is desirable to conduct experiments with the following set of detectors i.e., Al, Ni, Fe, Ti, Rh and In.

Double parameter functional representation appears to be satisfactory spectrum approximation, but needs to be tested for several different reactor spectra.

REFERENCES

[1] Ramakrishna, D. V. S., Joneja, O. P. and Navalkar, M. P., Proc. of Nuclear Physics and Solid State Physics Symposium, Vol. II 356-360 (1968).

[2] Joneja, O. P., Ramakrishna, D. V. S., and Navalkar, M. P., Report KFA-Jul-1196 (1975).

[3] Joneja, O. P., Ramakrishna, D. V. S. and Navalkar, M. P., Atomkernenergie 30, 45(1977).

[4] Joneja, O. P., Ramakrishna, D. V. S. and Navalkar, M. P., Third National Symposium on Radiation Physics, Waltair, Feb. 1979.

1.4.2 Unfolding of Neutron Spectrum from Activation Data

(K. Subbukutty, S. B. D. Iyengar and M. P. Navalkar)

For spectrum unfolding the assumed functional form may have one or more parameters to be determined or the number of energy groups can be suitably selected for a given set of activation data such that the equations are over determined and hence least squares method can readily be applied. The program STAYSL' which is adapted for 'BESM-6' employs covariance matrices for both flux and cross section as additional informations to over determine the set of equations.

STAYSL [1] has been written in FORTRAN-IV for PDP-10 machine and is therefore not directly compatible with BESM-6. Hence appropriate changes have been made to make the programmes operative on BESM-6 and it has been verified using a listed example. The present version of STAYSL has been used to unfold the spectrum of PURNIMA for a set of measured activities and the results are compared with those obtained using a code based on minimisation method developed by Joneja et al [3].

REFERENCES

[1] Perey, F. G., ORNL ITM-6062, ENDF-254 (1977).

[2] Subbukutty, K., Iyengar, S. B. D. and Navalkar, M. P., Third National Symposium on Radiation Physics, Waltair, Feb. 1979.

[3] Joneja, O. P., Ramakrishna, D. V. S. and Navalkar, M. P., Atomkernenergie 30, 45(1977).

1.4.3 Direct Measurement of Thermal Neutron Flux

(D. V. S. Ramakrishna, M. R. Phiske and M. P. Navalkar)

Activation of 1/v detector gives information of the thermal neutron

density and the flux can be obtained by multiplying with the neutron velocity which is temperature dependent. It is difficult to measure the temperature accurately in power reactors and as such the flux measurements by foil activation are subjected to errors. A method to measure directly the flux without the knowledge of neutron temperature is developed making use of glass beads containing B^{10} and 1/v detector material such as Co, In or Dy. B^{10} makes the detector black to thermal neutrons and thereby the activity of the 1/v detector responds directly to the flux. The absolute source strength of the Co bead is determined by γ-γ coincidence.

Small glass beads of about 2 mm diameter are made from the matrix* having the composition of H_3BO_3 (37%), SiO_2(28.5%), Co_3O_4 (13.5%) and Al_2O_3(8.5%) and LiO(12.5%). The method has been tested to determine the flux and the axial buckling in the irradiation position A-7 in Apsara reactor.

1.4.4 Multiple Activation Detectors

(O. P. Joneja and M. P. Navalkar)

Availability of SAMPO computer code enables proper integration of photo peak events for a given photopeak energy in the presence of other Gamma ray energies, reasonably well separated from each other. It was therefore proposed to fabricate an alloy consisting of several threshold detectors, such that only one or two foils may be required to be irradiated and counted for finding the fast neutron spectrum at the site of interest in a reactor. From the consideration of half life, reaction cross-section, and gamma energies, the following two alloys are proposed.

1) Al-Ni-In (37.4 - 62.2 - 0.4) wt %
2) Mg-Fe-In (48.6 - 50.7 - 0.7) wt%

The first alloy was prepared in the chemistry division and was found to exhibit uniformity in composition along the axis of the cylindrical ingot. The results are quite encouraging and the aspect of foil fabrication and using them for reactor spectrum studies is being looked into.

1.4.5 He^3 Sandwich Spectrometry**

(O. P. Joneja, J. S. Coachman and M. P. Navalkar)

Several design features have been incorporated to obtain a suitable matched pair for He^3 sandwich spectrometry. The spectrometer has been

---

* Fabricated in Metallurgy Division, BARC
** In Collaboration with Technical Physics Division

employed to find the fast neutron spectrum of a 5 Curie Pu-α-Be neutron source. It is capable of exhibiting neutron peak structure in the source spectrum; however the energy calibration requirements are much more stringent and pose some difficulties at present. The problem is being looked into from the point of view of the fabrication procedure.

1.4.6 Response Calculation of a Self-Powered Detector

(K. Subbukutty, B. Lal* and M. P. Navalkar)

To calculate the current produced by the instantaneous S-P detector for in core measurements, a Monte Carlo program is written for cylindrical geometry, the inner and outer cylinders being cobalt and Al_2O_3. All the processes such as photoelectric, Compton, pair production and annihilation of positron are considered. Point cross-section is used for various types of interaction and linear interpolation is employed to calculate intermediate values. The electron energy, its range and thereby escape from the considered media are computed to find the aggregate current. A current of 1.2×10^{-23} amp/length/flux was obtained which compares well with the reported experimental value[1].

REFERENCES

[1] Goldstein, N. P., IEEE Trans. Nucl. Sci. Feb. 73, Vol. MS-20 Number 1.

1.4.7 International Intercomparison for Unfolding of γ-Ray Spectrum

(K. Subbukutty, N. N. Ajitanand+ and M. P. Navalkar)

For international intercomparison of unfolding methods, code SAMPO has been employed for finding the Gamma spectrum from Ge(Li) data supplied by IAEA. The code evaluates shape factors for standard input spectra and utilizes these values for calculating true peaks, false peaks, areas etc.

1.4.8 Fabrication of 1024 Channel Pulse Height Analyser

(J.S. Coachman)

A 1024 channel pulse height analyser has been designed and fabricated by Shri S. Ragupathy of Division of Radiological Protection. Based on his design, a similar one is being assembled. Some of the salient features include, besides the use of IC's, electronic switching of modes, three different read outs modes, read out of clock time, storage capacity of 10^6 counts per channel, integral non-linearity of 0.1%, differential non-linearity of 2% etc.

---

* Multi-Disciplinary Research Section.

\+ Nuclear Physics Division

1.5 Pulsed Neutron Experiments and Their Interpretation in Reactors and Other Assemblies

1.5.1 Prototype Pulsed Neutron-Logging Equipment*

As a part of BARC-ONGC,R & D collaboration work, prototype pulsed neutron logging equipment was developed and fabricated. A pulsed logger is used to differentiate saline water zones and oil zones by using neutron life time method, the average life of neutrons in oil and saline water being 200μsecs and 60μsec respectively. The logger consists of a high voltage supply consisting of 30 KV transformer, two 500 pf 30 KV capacitors and a neutron tube**. The tube acts as a rectifier in positive half cycle of the input voltage and provides -84 KV at the target end of the neutron tube which acts as an accelerating voltage for deuteron ions. The sealed neutron tube, 30 mm in diameter and 170 mm in length, has hot cathode PIG ion source, replenisher and the tritium target assembly. The imported neutron tube was successfully tested using control and bore hole electronics developed by the Electronics Division. The following parameters were obtained.

i) Pulse Width-100 μsec
ii) Repetition rate-400 cycles
iii) Neutron output-5 x 10^6n/sec has been obtained with the following conditions:

Magnetization Current (for transformer)	125 ma
Replenisher Current	1.9 Amps at 5.5 volts
Filament Current	1.8 Amps at 2.7 volts

iv) The neutron yield and off pulse to on pulse ratio was determined using time interval distribution analyser. The maximum variation in the neutron yield was found to be 0.2% from the average.

v) Using a proton recoil spectrometer the emergent spectrum of neutrons from the tube was found out. It confirms the d-t reaction.

The accelerator part and the bore hole electronics is housed in a carbon steel pipe of 73.5 mm I.D. and 89 mm O.D. and approximately 11 feet in length. The mains 230 volts supply is fed through double armoured three core cable which is also used to carry detector pulses to the surface electronics.

---

* Electronics Division, Reactor Control Division, Primary Isotopes Section, Nuclear Physics Division, Ore Extraction Section, Neutron Physics Division and Central Workshop.

** Being developed by the Primary Isotopes Section.

1.5.2 Carbon-Oxygen Method for Oil Logging using the Pulsed Neutron Generator

(D. V. S. Ramakrishna, S. K. Sadavarte, M. R. Phiske, Jagir Singh and M. P. Navalkar)

Laboratory experiments are carried out to develop the carbon-oxygen logging method to identify the presence of hydro-carbons in oil well, irrespective of water salinity in the formations. Results of initial measurements in pure oil and water barrels are promising. A bore hole model which can give the porosity of 30% and variable oil and water saturations is fabricated to simulate the bore hole conditions. A 2' dia and 3' long cylindrical tank is filled with glass sand of about 100 mesh size in which glass tubes of 3.0 cm dia. are imbedded at four different pitch circle diameters such that they act as channels for introducing the oil and water regions. Regid pvc tubes whose outer diameters match with the inner diameters of the glass tubes are chosen as containers for oil and water. There is a central opening of 6" dia. in the tank to accommodate the target tube and the detecting system. C/O measurements using the bore hole model are under way in order to establish the method.

1.5.3 Development of He-3 Counters for Oil-Well Logging Applications

(Y. D. Dande*, G. V. Shenoy*, R. S. Udyawar* and M. P. Navalkar)

To avoid bore hole effects in oil-well logging with Pulsed Neutron equipment, one needs to measure the neutron intensity at times greater than 1500μs after the neutron burst. With the present ONGC imported equipment using BF_3 detectors (7 in parallel), the signal to noise ratio is rather poor at these times. In the programme of replacement of imported equipment of ONGC for oil exploration, a joint R & D programme between ONGC and BARC for development of more efficient detectors was undertaken.

A single He-3 detector has been developed to replace the cluster of 7 BF_3 tubes. With a neutron detection efficiency of more than twice that of the BF_3 cluster, this detector has shown much superior demarcation of oil and water zones in the field trials at Ankleshwar oil fields. With this improvement in detection efficiency, it is felt that the spatial resolution of the log, as well as the useful life of the Neutron tube will be substantially enhanced.

The detectors are at present undergoing extensive field tests and a detailed performance report from ONGC is awaited.

---

* Nuclear Physics Division.

I. 5. 4 NaI(Tl) Detectors for Elevated Temperature*

The use of thallium activated sodium iodide crystal scintillators for oil logging operations demands the detector to be operated through zones of elevated temperatures. The temperature dependence of response is therefore an important consideration. A study of high temperature performance characteristics was undertaken to decide the right activator concentration and to optimize the crystal growth parameters for the best detector performance.

The pulse height was found to decrease with temperature for all the detectors having activator concentration in the range 0.0005 to 0.005 mole fraction. The coefficient obtained for temperature variation is 2.245 $\pm$ 0.07 kev/deg irrespective of activator concentration. The counting efficiency is found to depend on both the activator concentration and temperature. The coefficient of temperature variation ranges from 0.66%/deg to 0.3%/deg depending upon the activator concentration.

The results of our measurements suggest that the energy transfer mechanism from host lattice to the sparsely dispersed Tl luminescent centers is a temperature dependent. phenomenon.

---

* Technical Physics Division and Neutron Physics Division

2. FUSION AND PLASMA NEUTRONICS

2.1 Utilization of 14 Mev Neutrons and Fusion Blanket Neutronics

The present day CTR concepts are based on D-T burner and aim at self breeding of tritium within the blanket assemblies. As a result, the blanket engineering has attained significant importance. At present tritium produced due to neutron induced reactions in natural lithium is measured by several indirect methods. There exist a considerable gap between theoretical calculations and experimental observations. In continuation of our efforts to improve upon the existing techniques and developing new methods for measuring tritium production, the following concepts are being pursued.

2.1.1 Solid State Track Recording Technique

(D. V.S. Ramakrishna, O. P. Joneja, S. K. Sadavarte, M. R. Phiske and M. P. Navalkar)

The method involves the irradiation of cellulose nitrate film in contact with a lithium source and recording the α-tracks produced due to $Li^6(n,\alpha)t$ and $Li^7(n,\gamma\alpha)t$ reactions. Preliminary results obtained in water moderated assembly[1]containing lithium cylinders of about 2 kg quantity showed discrepancy of about 30% to the estimated value of the tritium produced and as such only relative measurements are possible. In order to use this method on absolute basis, investigations are in progress to identify and discreminate the α-tracks with respect to triton tracks and other light particle event tracks in the film on the basis of the diameter of the track holes formed. Separate measurements are planned using monoenergetic beam from Vande graaf accelerator to study the track diameters as a function of particle energy and their masses.

REFERENCES

[1] Annual report of Neutron Physics Section (1976).

2.1.2 Thermoluminiscent Dosimetery

(O. P. Joneja, S. P. Kathuria*, and M. P. Navalkar)

Thermoluminiscent charge (10-20 mgm) consisting of Li^6, Li^7 and natural lithium was sealed in specially fabricated glass tubes and subjected to irradiation in the existing lithium assembly. Samples after about six hours of irradiation were annealed and left for self irradiation in a low background environment. The decay of tritium generated within the glass capsule deposits energy in the TLD sample, which can be released by suitably heating the sample. The TLD response thus obtained is a measure of total tritium present in the sample, which can be easily co-related to the tritium breeding in the lithium assembly.

---

* Health Physics Division.

The response obtained at different times was found to be linear and it was observed that a period of about 45 days of self irradiation is desirable to get the current well above the background level ($\sim 10^{-9}$ amp.). It is therefore proposed to conduct experiments with enhanced neutron flux, more TLD charge and preferably larger irradiation time.

2.1.3 Liquid Scintillation Technique

(O. P. Joneja, T. S. Iyengar* and M. P. Navalkar)

The method has been employed for finding the tritium generated due to neutron induced reactions in lithium. Initially several samples of lithium (100-200 mgm), tightly sealed in plastic vials were irradiated in the thermal column of Apsara reactor. The tritium generated is suitably transformed into liquid phase and β decay of tritium is then studied by liquid scintillation technique. The measurements were carried out in the actual cylinderical lithium assembly ($\sim$2 kgms) at two different positions, and it is observed that countable activity is registered after about 4.5 hours of irradiation with a deuteron current of $\sim$80 μAmp.

The concept of charge holding mechanism is being reviewed because of the perturbation effects and from the point of view of the space availability for irradiation. Some experiments are underway with different plastic tubes for solving the problems.

2.1.4 Double Ionization Chamber Method

(O. P. Joneja, M. R. Phiske and M. P. Navalkar)

A new method is developed for finding directly the tritium breeding of a given lithium assembly. It incorporates suitable changes so as to overcome difficulties associated with the silicon surface barrier technique. The system consists of two ionization chambers separated by a common earthing ring which holds the radiating material. The neutron interaction produces charged particles which travel into different ionization chambers and get detected.

Analytical calculations and Monte Carlo simulation for the system response have been worked out. The latter has been extended to take into account the energy losses in the various media under consideration. A typical response obtained is shown in Fig. 4.1. An experimental response along with the calculated one is shown in Fig. 4.2.

The detector head was subjected to neutron irradiation in a paraffin block and an integral counting was accomplished employing a gating pulse obtained due to double coincidence events. Thermal flux was also determined with the help of gold foil irradiation. It is observed that the experimental

---

* Health Physics Division.

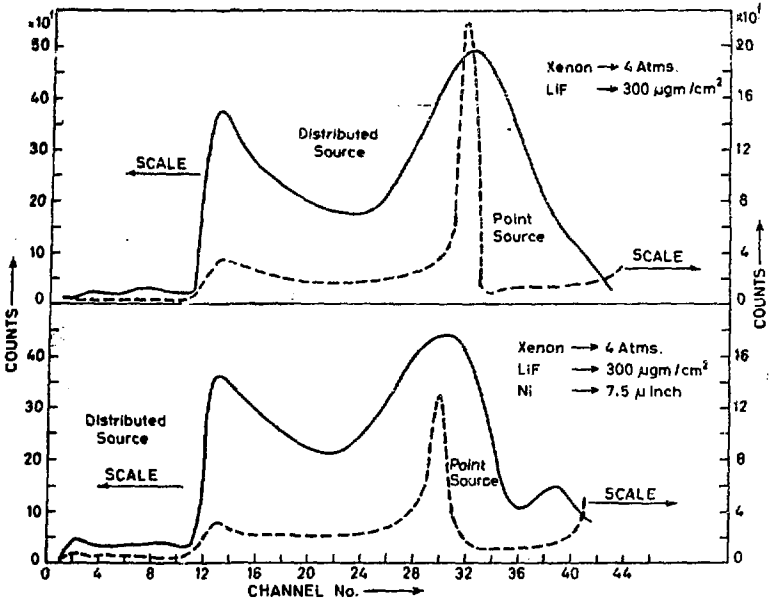

Fig. 4.1 Double ionization chamber response calculated by point source and distributed source assumption

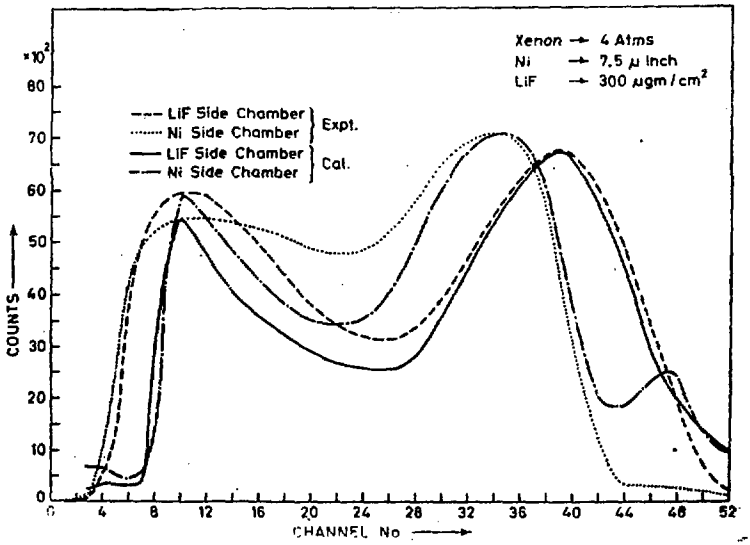

Fig. 4.2 Experimental and calculated response of a double ionization chamber

results agree within 11% with calculations. The response calculations are being done for a wider energy range and thereby its application extended to cover fast blankets.

2.1.5 Tritium Breeding Calculations in Different Assemblies

(K. Subbukutty, O. P. Joneja and M. P. Navalkar)

1. Tritium Breeding in Spherical Cylindrical Geometries

A 27 group cross-section set was used to calculate tritium production due to Li^6 and Li^7 reactions separately as a function of radius. A maximum total breeding ratio of 1.72 ± 10% per 14 Mev neutron is found for a spherical lithium assembly surrounded by graphite reflector. The contribution of tritium from Li^6 and Li^7 becomes equal at radius of 1.5 meters.

The same 27 group cross section set for Li^6 and Li^7 was also used for calculating tritium breeding, in cylindrical geometry. Breeding is calculated as a function of radius for several heights such that H = 2 R. It is seen that maximum breeding remains constant after a radius of about 2 meters [1]

REFERENCES

[1] Joneja, O. P., Subbukutty, K. and Navalkar, M. P. Atomkernenergie, 33, 11 (1979).

2.1.6 Absolute Measurement of $^{56}Fe(n, p)\ ^{56}Mn$ Cross-Section at 14.7 Mev Using a Neutron Telescope

(D. Sharma*, M. G. Shahani*, U. V. Phadnis* and S. K. Sadavarte)

A neutron telescope developed in DRP has been employed to measure the cross-section of $Fe^{56}(n, p)\ Mn^{56}$ reaction. The method consists of irradiating 99.9% pure iron foils attached to the surface of the telescope. The telescope measures the incident neutron flux whereas the induced activity is measured with proportional counters. The value of $Fe^{56}(n, p)\ Mn^{56}$ cross-section corrected for scattered neutron contribution is found to be 98.5 ± 4 mb.

---

* Division of Radiological Protection

2.1.7 Investigation of (n, 2n) and (n, f) Rates in Iron Shielded Uranium Sample Irradiated with 14 Mev Neutrons

(K. Subbukutty, D. V. S. Ramakrishna and M. P. Navalkar)

Monte Carlo calculation of transmitted spectrum from 14 Mev source through iron shield of various thicknesses is done. A parallelopiped geometry is used for this purpose. The emerging spectrum is used to compute the average ratio of fission to (n, 2n) for U^{238}. 27 group cross-section is used for iron. Results are shown in Fig. 7.1.

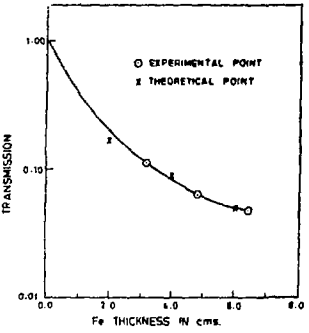

Fig. 7.1 14 Mev neutron transmission through iron shield of various thicknesses compared with theoretical results

2.2 Experimental and Theoretical Investigation of Plasma Fusion Neutron Production Methods

2.2.1 Fusion Neutron Production Experiments

(Anurag Shyam, S. K. H. Auluck and M. Srinivasan)

Efforts are underway to study the mechanism of neutron production by D-D and D-T fusion reactions in various pinch experiments such as plasma focus and exploding wires.

a) Plasma Focus

A Mather type deuterium plasma focus has been fabricated and tested at the Purnima Laboratories, Fig. 1.1. When a fast (low inductance, high current) capacitor bank is discharged through the focus, a flash-over takes place across the insulator producing a plasma. The radial current ($\vec{J}$) which flows through this plasma interacts with the magnetic field ($\vec{B}$) induced by the current flowing in the inner electrode and the resultant $\vec{J} \times \vec{B}$ force pushes the plasma along the axis to the end of the inner electrode where it is focussed to form a high temperature ($\sim 10^7$K) and high density ($\sim 10^{19}$ particles/cm^3)

plasma pinch. Consequently neutrons are produced partly due to thermonuclear fusion and partly due to accelerated deuterons. The run down time of the plasma along the coaxial electrode is adjusted by optimising the gas pressure in such a way that at the time of focusing maximum current flows through the plasma.

The plasma focus at Purnima Laboratories is a low energy device running on 100 joules and producing~5 x 10^5 neutrons/discharge at 4 torr deuterium gas pressure. The neutrons are detected by a high efficiency silver

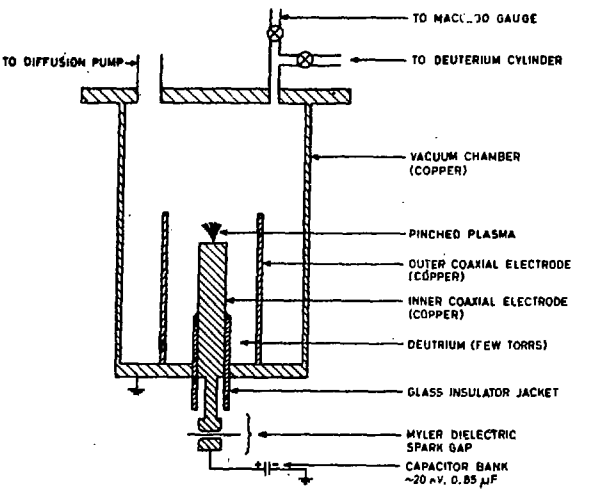

Fig. 1.1 Mather type plasma focus device

activation counter[1]. This focus has produced neutrons with the lowest reported[2] energy input. The neutron yield is found to scale up as $E^{1.73}$ and $I^{4.29}$, E and I being the capacitor bank energy and current respectively.

b) Exploding Wire

When a low inductance capacitor bank is discharged through a thin (~10^{-5} m diameter) fibre containing deuterium or deuterium and tritium the fibre explodes due to heating. Consequently the fibre vapours expand till the density is low enough for Townsend discharge to take place. This discharge ionises the vapour and renders the resultant plasma highly conducting. The heavy current flowing through the plasma interacts with its own magnetic field and this $\vec{J} \times \vec{B}$ force implodes the plasma (linear z pinch effect). The implosion heats and compresses the plasma to high densities (~10^{19} particles/cm^3) and high temperatures (~10^6 to 10^{7}°K) as in the plasma focus. Neutrons are produced by D-D or D-T reactions by thermonuclear fusion and accelerated deuterons.

In the experiments performed at Purnima Laboratories, 12.5 micron diameter, .1 cm long cotton fibres dipped in heavy water were used. The fibres absorbed ~3 times their weight of heavy water. Ammonium nitrate was dissolved in the D_2O to make the fibres conducting. The fibre was exploded on a 500 joule capacitor bank. An average neutron yield of 8×10^4 neutrons per discharge was detected.

A 21 KJ, 50 KV, 35 nH fast capacitor bank is under fabrication. In order to understand the exact mechanism of neutron emission in these experiments detailed diagnostic studies are being planned.

REFERENCES

[1] Anurag Shyam et al., p. 85-86, BARC-937 (1977).

[2] Anurag Shyam and Srinivasan M., App. Phys. 17, p. 425-426 (1978).

3. BIOLOGICAL CRYSTALLOGRAPHY AND AUTOMATION

3.1 Neutron Diffraction Studies of Biological Molecules

3.1.1 A Neutron Diffraction Study of the Structure of DL-Aspartic Acid

(M. Ramanadham, A. Sequeira, H. Rajagopal and S.N. Momin)

Analysis of the crystal and molecular structure of DL-aspartic acid (DL-ASP), $NH_3^+.CH(CH_2COOH).COO^-$, by neutron diffraction technique has been completed. The crystals belong to the monoclinic space group C2/c with 8 molecules per unit cell. The unit-cell parameters are: a = 18.96 (2), b = 7.429(7), c = 9.203(9)Å and β = 124.12(5)°. More than 1500 independent observations with $(\sin\theta/\lambda) \leq 0.5 Å^{-1}$ were recorded on the computer controlled neutron diffractometer, D4, at a neutron wavelength of 1.036Å. The model structure consisting of positional and anisotropic thermal parameters for all the atoms in the molecule was refined along with the scale and extinction parameters by the method of least-squares to an R-value of about 0.04.

A stereoscopic picture of the molecule is shown in Fig. 1.1.

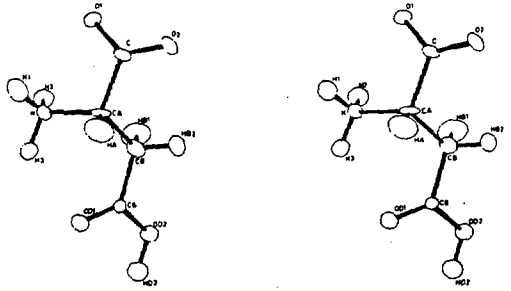

Fig. 1.1 Stereoscopic picture of DL-aspartic acid molecule

Structural parameters like bond lengths, angles, etc., involving the non-hydrogen atoms compare favourably with those obtained in the x-ray study [1] of DL-ASP. However, the present study provides high precision data on the stereochemistry of hydrogen atoms in the structure. The general features of the structure and conformation of DL-ASP are in good agreement with the results obtained from the neutron diffraction studies of other amino acids [2].

There are four distinct inter-molecular H-bonds per DL-ASP molecule. The carbonyl oxygen of the side-chain carboxyl group is an acceptor

for a weak H-bond from the protonated α-amino group. The bending angle of this H-bond is 21°. The other two H-bonds from $-NH_3^+$ group have one of the two oxygen atoms of the ionized α-carboxyl group as acceptor. The second oxygen atom of this group is involved in a strong, almost linear O-H---O bond from the -OH group of the side chain carboxyl group. The two C-O bonds of $-COO^-$ group have lengths, which are in conformity with the strengths of the H-bonds accepted by the oxygen atoms.

REFERENCES

[1] Rao, S. T. (1973) Acta Cryst. B29, 1718.

[2] Ramanadham, M. and Chidambaram, R. (1978) in "Advances in Crystallography", Ed. R. Srinivasan; Oxford and IBH, New Delhi pp. 81-103.

3.1.2 On the Planarity of the Peptide Group in Glycyl-L-Threonine. $2H_2O$

(M. Ramanadham and A. Sequeira)

The crystal structure analysis of glycyl-L-threonine. $2H_2O$ (GLT. $2H_2O$), NH_3^+. CH_2. CONH. CH($CHOHCH_3$). $COO^- + 2H_2O$, which was undertaken in our laboratory [1], is the first neutron diffraction study of a dipeptide with one amino-acid residue different from glycine. In an earlier Report we have discussed the planarity of the peptide group in GLT molecule on the basis of the model which was picked up from an earlier stage of refinement. Results obtained at this stage were in good agreement with the conclusions arrived at by Ramachandran and co-workers regarding the non-planar distortions on the basis of theoretical calculations [2] and x-ray diffraction studies of simple peptide structures [3]. Since then more data were added and the model was further refined. The present values of $\Delta\omega, \theta_C$ and θ_N are respectively 2.9(5)°, -2.9(15)° and 0.5(15)°. These values suggest that the peptide group is non-planar, even though the non-planar distortions are quite small. However, unlike in the other two neutron diffraction studies of dipeptides, θ_N is smaller than θ_C. The data set contained a large number of weak reflections, with a significant number of them being 'negative'. Therefore, we tried to refine the structure by replacing the negatives with zero values, retaining negatives as they were and using only those reflections for which $F_o^2 > \sigma(F_o^2)$. The trend (that $\theta_N < \theta_C$) persisted in all the three situations but the actual values were different by as much as half a degree. For example, when we ignored reflections with $F_o^2 \leq \sigma(F_o^2)$ the resulting values of $\Delta\omega, \theta_C$ and θ_N were, 3.0°, -2.2° and 1.0° respectively. We made use of the weighted least-squares planes to assess the significance of these values. We performed χ^2-tests using the sum of the squares of deviations from the planes. For the least squares plane containing C_1^α, C_1, N_2, C_2^α atoms (contains ω-angle) this number is 28.47. This is much larger than 6.63, which is the expected

value at 99% confidence level. Therefore, one can say that the non-planarity due to pure ω-rotation is quite significant at that level. Similar numbers computed for LS-planes consisting of C_1^{α}, C_1, O_1, N_2 atoms (contains θ_C) and C_1, N_2, C_2^{α}, H_2 atoms (contains θ_N) are 5.51 and 0.19 respectively. Both these numbers are smaller than the exptected value of 6.63 at 99% confidence level, which means that the non-planar distortions in the planar trigonal configurations of bonds around C and N are not significant at this level.

We are looking at methods of treating the weak intensities in a better way, in order to confirm whether $(\theta_N < \theta_C)$ is a real structural feature of GLT in this crystal. On the basis of the results available at present, one can only say that the peptide group has rather small non-planar distortions.

REFERENCES

[1] Sequeira, A., Rajagopal, H. and Padmanabhan, V. M. Annual Report of the Neutron Physics Section, BARC, 1977, pp 11-14.

[2] Ramachandran, G. N., Lakshminarayanan, A. V. and Kolaskar, A. S. (1973), Biochim. Biophys. Acta, 303, 8.

[3] Ramachandran, G. N. and Kolaskar, A. S. (1973), Biochim. Biophys. Acta, 303, 385.

3.2 High-Precision Diffraction Studies of Crystal Structures, Extinction Effects, Etc.

3.2.1 A Neutron Diffraction Study of the Structural Disorder in Ammonium Copper Chloride Dihydrate

(S. N. Bhakay-Tamhane, A. Sequeira and R. Chidambaram)

A high precision neutron diffraction study of the structural disorder in ammonium copper chloride dihydrate $(NH_4)_2\ CuCl_4.2H_2O$ [space group $P4_2/mnm$, $a = b = 7.596$, $c = 7.979$ Å, $Z = 2$] has been carried out in its room temperature phase. The data set, consisting of 494 reflections (202 independent), at a wavelength of 1.036Å upto $\sin\theta/\lambda = 0.56$Å^{-1} was collected on the TDC-312 computer-controlled neutron diffractometer at CIRUS. The final R index on F is 0.022 with anisotropic type II extinction being corrected for. The weights in the least squares refinement found to be most appropriate are those based only on counting statistics.

Earlier 2-D neutron diffraction study indicated order of NH_4^+ whereas our results clearly indicate orientational disorder of NH_4^+ between two available tetrahedral sites, with occupancies 0.65 and 0.35 as shown in

Fig. 1, 1. Our findings are in conformation with those of specific heat measurements. In the favourable orientation the N is bonded to 4 Cl(II)

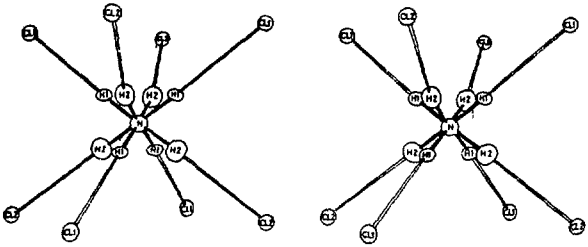

Fig. 1.1 Stereoscopic view of ammonium ion surroundings (The thermal ellipsoids of hydrogens are population weighted)

at 3.357 Å while in the other orientation, it is bonded to 4 Cl(I) at 3.370 Å. The H_2O hydrogens are bonded to two Cl(II) at 2.186 Å and do not show any disorder unlike as reported from earlier infra-red studies but confirming the findings of a recent laser-Raman study [1]. The general unit cell structure of the compound is as shown in Fig. 1.2.

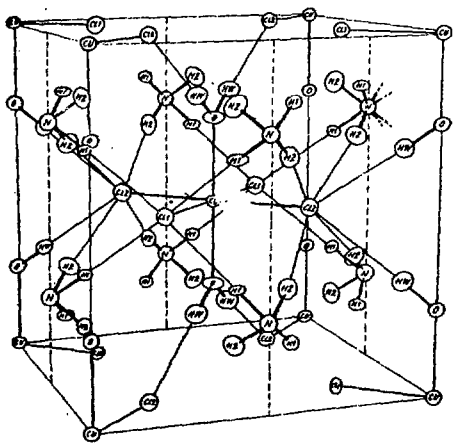

Fig. 1.2 The unit-cell structure of ammonium copper chloride dihydrate

REFERENCES

[1] Bansal, M. L., Sahni, V. C. and Roy, A. P., BARC report 966 (1978).

3.2.2. Highly Anisotropic Extincition in KCl Crystals: A Case Study

(A. Sequeira, H. Rajagopal and R. Chidambaram)

The data-set consisting of 54 reflections in an octant of the reciprocal space was measured from a single crystal of size 2.2 x 2.6 x 4.2 mm, at a neutron wavelength of 1.026Å., using the computer-controlled neutron diffractometer.

The data refined to a low-value of 0.0154 when an isotropic extinction correction was applied. Nevertheless, there were significant systematic residual discrepancies between the F_o and F_c values of the strong reflections indicating the existence of Type II anisotropic extinction. When the refinement was continued applying Zachariasen's Type II anisotropic extinction correction, it converged to a suprisingly low R-value of 0.0066

In view of the unusually high accuracy of the data set, attempts were made to distinguish further between the possible primary and secondary extinctions as well as to test the validity of the Becker and Coppens theory which suggests the replacement of the particle radius (r) by (r sin 2θ) in the case of Type II crystals. The results summarised in Table 2.1, do not favour the (r sin 2θ) correction suggested by Becker and Coppens, and also do not permit a clear choice between the primary and the secondary extinction effects.

Table 2.1 Refinements Based on Various Extinction Corrections

Parameter	Secondary				Primary		
	Isotropic		Anisotropic		Isotropic		Anisotropic
	A	B	Type 1	Type 2	A	B	A
R(F) %	1.54	1.66	0.98	0.67	1.52	1.68	0.68
$R(F^2)$ %	3.39	3.61	2.05	1.22	3.33	3.69	1.26
$Rw(F^2)$ %	3.75	4.20	2.65	1.96	3.73	4.21	1.98
B(K)	1.830 (64)	1.579	1.833	1.804 (30)	1.820	1.573	1.821
B(Cl)	1.874 (63)	1.762	1.877	1.862 (30)	1.879	1.761	1.888
$\rho \times 10^{-4}$	0.1130	0.2874	-	-	4.13	6.52	-

(A) = Zachariasen model
(B) = Zachariasen model with r(sin 2Θ) replacing (r)

3.2.3 Crystallographic Computing

(H. Rajagopal and A. Sequeira)

The Trombay crystallographic least squares program TRXFL has

been extensively modified to incorporate the application of the primary and the secondary extinction corrections both in the isotropic and in the anisotropic forms.

3.3 X-ray Crystal Structure Determination of Small Molecules of Biological Importance

3.3.1 X-ray Studies of Peptides

(V.S. Yadava and V. M. Padmanabhan)

As a part of programme to study the crystal structure and conformation of simple peptides, we have carried out the following structure investigations:

(a) The Crystal and Molecular Structure of L-Prolyl-L-Alanine Monohydrate

The peptide L-prolyl-L-alanine, $C_8N_2O_3H_{14}$, crystallizes in the monoclinic space group $P2_1$ with one molecule of water of crystallization. The cell dimensions are a = 6.58 (1), b = 5.52 (1), c = 14.18 (2) Å, β = 100.0(2)°, Z = 2. The structure has been determined from three-dimensional X-ray diffraction data using the symbolic addition method and refined by least-squares with anisotropic thermal parameters to an R-index of 0.094.

The crystal structure is a disordered one. The pyrrolidine ring exists in two conformations in the ratio 3:2. The C^γ atom of the ring is statistically situated on both sides of $NC^\alpha C^\beta C^\delta$ plane. The van der Waals energy calculations for the two C^γ positions also give a lower energy value for $C^{\gamma 1}$ position. The coefficients of van der Waals potentials for various atom pairs used being those given by Pavel et al.[1]. The bond lengths and angles for the peptide have values close to those expected except those for the pyrrolidine ring. The peptide and carboxyl groups are planar. The dimensions of the carboxyl group suggest that the molecule is a zwitterion. The molecule is in extended conformation (ψ = 167.8°, ϕ = 61°) and in trans configuration (ω = 170°).

The crystal structure projected down b-axis is shown in Fig. 1.1. The hydrogen bonds through water molecules stabilize the structure. The hydrogen bonds involving the amide N atoms as donors are longer than those involving the terminal $-NH_2$ group.

(b) The Crystal and Molecular Structure of L-Valyl-L-Tyrosine Monohydrate.

The peptide L-valyl-L-tyrosine, $C_{14}N_2O_4H_2O$, crystallizes in the

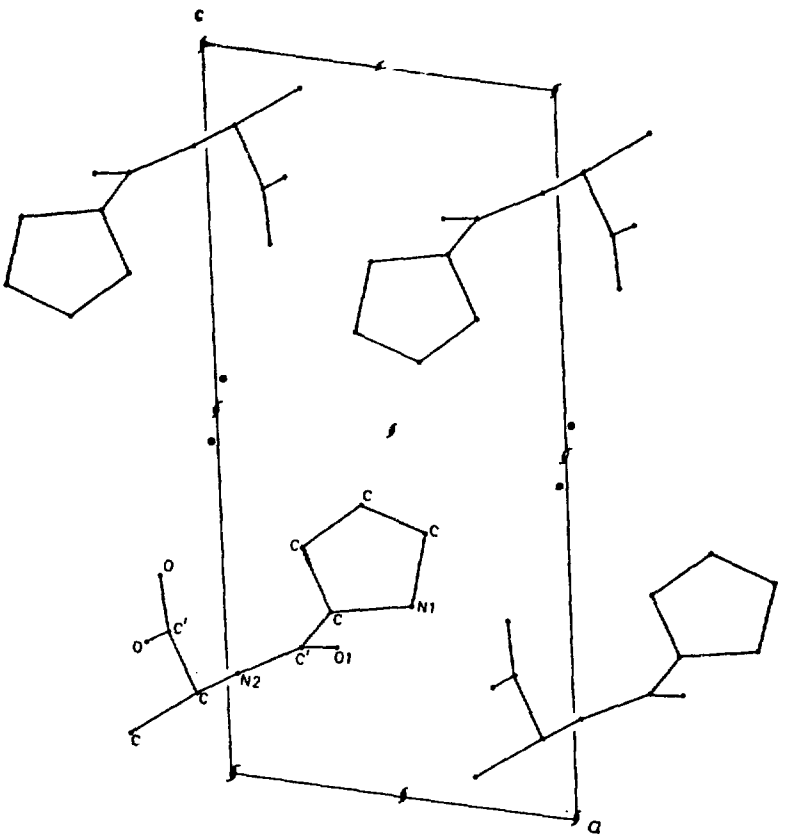

Fig. 1.1 Projection of the unit cell of L-prolyl-L-alanine monohydrate down b-axis

orthorhombic space group $P2_12_12$ with one molecule of water of crystallization. The cell dimensions are a = 14.05(2) b = 19.05 (2), c = 5.50(1) Å, Z = 4. The structure has been determined from three-dimensional X-ray diffraction data by direct methods using MULTAN and refined by least squares with individual isotropic thermal parameters to an R-value of 0.11. At the present stage of refinement, it is noted that the peptide is in extended conformation and the molecules are hydrogen-bonded through

the water molecule. The crystal structure projected down c-axis is shown in Fig. 1.2.

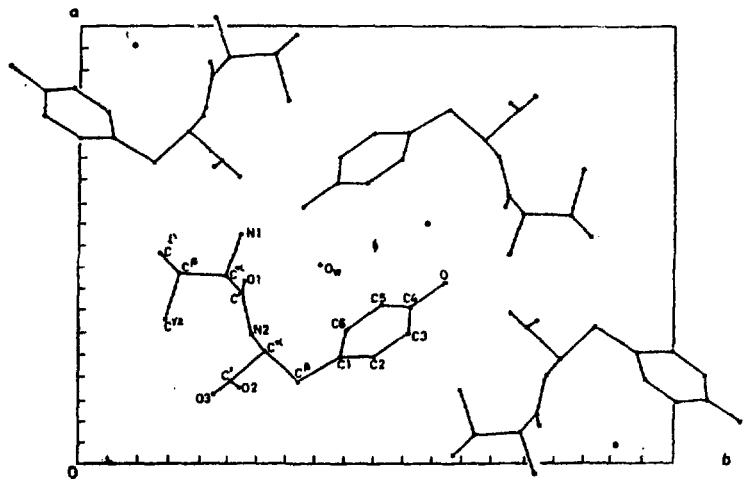

Fig. 1.2 Projection of the unit cell of L-valyl-L-tyrosine monohydrate down c-axis

REFERENCE

[1] Pavel, N.V., Quagliata, C. and Scarcelli, N. (1976) Z. Krist. 144, 64.

3.3.2 Crystal Structure of a Heterocyclic Steroid

(Surendra Sinh and V.M. Padmanabhan)

The biological activity of any steroid is closely related to the shape of the parent steroidal skeleton as well as the functional groups attached to it. The heterocyclic steroids are important because of their greater pharmacological activity and also reduced side effects in some cases. The compound 17-Thia-3-Methoxy - Estra - 1, 3, 5 (10) Triene-17 Dioxide (Mol. formula $C_{18}H_{24}O_3S$ and called Estra Sulfone) has been synthesized in Bio-Organic Division, BARC [1]. Its structure has been determined to ascertain its stereochemistry.

The compound crystallises in space group $P2_1/a$ with a = 13.480 (2)Å

b = 10.563(2)Å, c = 11.205(1)Å, β = 93.97(.01)° and with 4 molecules in the unit cell. X-ray diffraction data for the compound has been collected both by photographic (Weissenberg) method and counter method (CAD-4 Diffractometer at IISc, Bangalore). The structure has been solved by direct methods using MULTAN and has so far been refined to R = 7.11% for counter data and R = 11.24% for photographic data. Counter data is also being collected on our TDC-312 controlled x-ray diffractometer for comparison.

The structure projected down the b-axis is shown in Fig. 2.1. The four molecules are held together by the van der Waals forces only.

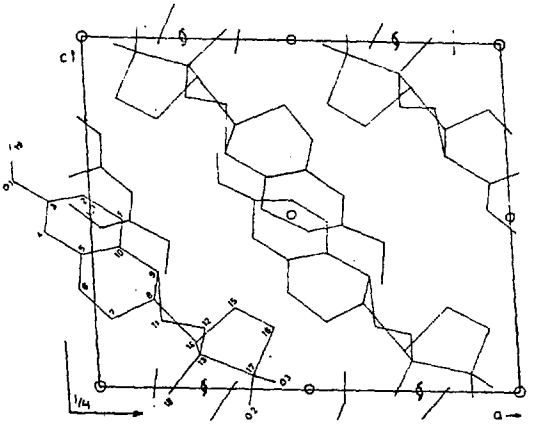

Fig. 2.1 Projection of the unit cell of Estra Sulfone molecule down b-axis

The ring A is planar and shows typical aromaticity and delocalisation of π electrons to produce a mean bond length of 1.398 Å and the bond angles are quite close to 120°. Ring B shows a distorted half-chair conformation with atoms 5, 6, 9 and 10 lying in one plane and atoms 8 and 7 being below and above this plane by 0.33 and 0.36Å respectively. Ring C has a chair conformation with atoms 8, 9, 11, 12, 13 and 14 being alternately below and above the least-squares plane passing through them. The chair conformation being slightly distorted due to the presence of sulphur at position 17 in ring D. The ring D is in a conformation in between that of a half-chair and β envelope as shown by the value of its pseudo rotation parameters as defined by Altona et al.[2]

Δ = 10.8° ϕ_m = 42.4°, the atoms 15, 16 and 17 forming a plane and 14 and 13 being below and above the plane by 0.13 and 0.52 Å respectively.

The overall shape of the molecule suggests that it is in 8α - 9α - 13β - 14β conformation.

REFERENCES

[1] Bhide, G.V. and Jogdeo, P.S. (1979) Steroid (in Press)

[2] Altona et al. (1968) Tetrahedron, 24, 13.

3.4 X-Ray Diffraction Analysis of Biological Macromolecules

3.4.1 Proposed Programme of Research

(K.K. Kannan, M. Ramanadham and S. Sinh)

The important processes of biological systems are catalysed by certain macromolecules called enzymes. A number of physico chemical techniques have been used by many investigators with a view to understand their functions at the molecular level. Of these methods the application of x-ray diffraction techniques to crystalline proteins (enzymes) has given a wealth of information on the tertiary structure of these important biomolecules as well as on the interaction of specific inhibitors and substrates with the enzymes.

For a successful application of the x-ray diffraction method [1] the protein of interest should be available in good quality and quantity. The protein solution should also be highly homogeneous. The most important requirement however is the crystallizability of the protein. The crystals should diffract well to atleast 2.8Å resolution. The other necessary requirement is the preparation of heavy atom derivatives [2] by reacting heavy metal compounds with the enzymes in the crystalline state or by cocrystallization after reacting them in solution.

The diffraction data (x-ray reflections) are most advantageously collected by the multiple film oscillation technique and processed on high speed microdensitometers and digital computers. A computer-controlled x-ray diffractometer can also be used for the data collection. The processed data are then used to locate the heavy atom substitution sites in the heavy atom derivatives by difference Patterson methods. The heavy atom sites are refined by the least squares method and used to calculate the phase angles by the multiple isomorphous replacement method. The electron density map is then computed, contoured and interpreted [3] in a model building machine [4]. The electron density maps may also be

interpreted very accurately and quickly using a computer-controlled graphic display.

The most important purpose of the protein crystallographic studies is the elucidation of the structure of enzyme-inhibitor complexes and substrate analogues. The interaction of the inhibitors and substrate analogues with the enzyme is elucidated by interpreting the difference Fourier maps in the optical comparator [5], and the mechanism of the enzyme action interpreted. The results of these interpretation could also form the basis for designing specific drugs with minimal side effects.

We are engaged in the elucidation of the structures of mammalian carbonic anhydrase isoenzymes (Fig. 1.1) and their complexes with different inhibitors and metal-ion prosthetic groups. We are refining the structure

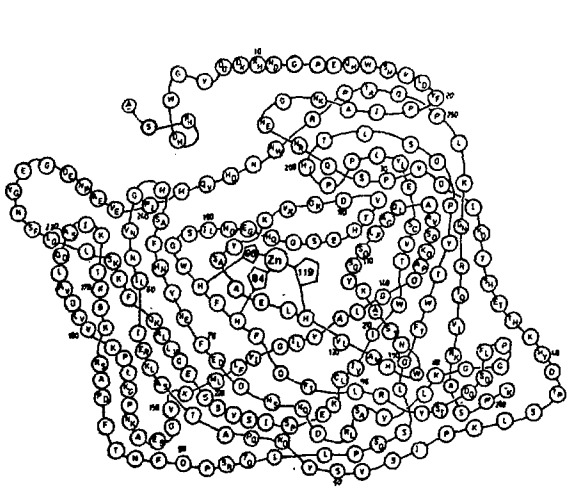

Fig. 1.1 Schematic drawing of the three-dimensional structure of human erythrocyte carbonic anhydrase B and C with the amino acid sequence written in the single letter code. Whenever the two sequences are monohomologous the B enzyme sequence is given at the top and that of the C enzyme at the bottom. Deletions are represented by the '-' sign.

of the human carbonic anhydrase form B and form C to 2Å resolution and the structure of triclinic hen egg white lysozyme to 1.5 Å resolution.

We are also determining the tertiary structure of a presynaptic toxin notexin, from Australian tiger snake venom by the application of multiple isomorphous method and molecular replacement method. We also plan to crystallize other presynaptic toxins belonging to the notexin family and to study their structural and functional relationship by x-ray diffraction methods.

REFERENCES

[1] Blundell, T. L. and Johnson, L. N. (1976) "Protein Crystallography" Academic Press.

[2] Green, D. W., Ingram, V. M., and Perutz. M. F. (1954), Proc. Roy. Soc. Lond. A 225, 287.

[3] Kannan, K. K. (1977) in Advanced Methods in Protein Sequence Determination (Ed. S. B. Needleman). Mol. Biol., Biochem. and Bio Phys. 25, 75.

[4] Richards, F. M. (1968), J. Mol. Biol. 37, 225.

[5] Kannan, K. K., Petef, M., Fridborg, K., Cid-Dresdner, H., and Lovgren, S. (1977), FEBS Letters, 73, 115.

3.4.2 The Structure Determination of Notexin, a Presynaptic Toxin

(K. K. Kannan, Hilda Cid,* K. Fridborg* and S. Ramakumar+)

Notexin is a strongly basic protein consisting of a single polypeptide of 119 aminoacid residues cross-linked by seven disulfide bridges [1]. The molecular weight of the protein is about 13,500. Notexin has three interesting biological activities: (i) a lethal (intravenous mouse LD_{100} = 25 μg/Kg), paralytic, "neurotoxic" action which is due to pre-synaptic interference with the release of acetylcholine from the motor nerve terminals [2], (ii) a myotoxic action whereby direct local application in vivo causes degenerative necrosis of skeletal muscle within three days [3] and (iii) notexin exhibits moderate phospholipase A activity against ovolecithin and the rate of hydrolysis is greatly enhanced in the presence of deoxycholate [4].

Notexin is highly homologous to some other elapid venom phospholipases having little or no neurotoxic or myotoxic activity and shows 43% identity in sequence to bovine and porcine phospholipases A2. Many other snake venom toxins that exhibit presynaptic action similar to notexin are however multi-subunit toxins. Thus notexin is a unique monomeric

*Wallenberg Laboratory, Uppsala, Sweden. +Dept. of Physics, IISc, Bangalore.

presynaptic toxin.

Notexin has been crystallized by Kannan et al [5] from 1.5 M ammonium sulfate solution at pH 8.5 in .05 M tris-SO_4. The unit cell dimensions are:
a = b = 75.03 Å, c = 49.04 Å and γ = 120° and belong to the trigonal space group $P3_121$ or $P3_221$. Low resolution data (5Å) was collected using CAD4 Nonius diffractometer at Indian Institute of Science, Bangalore, India. High resolution data to 2Å resolution has since been collected using an oscillation camera and a rotating anode x-ray generator at the Wallenberg Laboratory, Uppsala. The films were measured on a high speed drum scanner and the data processed on an IBM 370/155 computer.

Two heavy atom derivatives have also been prepared. One of the heavy atom derivatives was prepared by iodinating a histidine residue in the active site of notexin in the crystalline state. This destroys the phospholipase activity. Another heavy atom derivative has been obtained by reacting strontium ion with Notexin crystals. Diffraction data has been collected for these derivatives with the oscillation camera and rotating anode generator and processed in the same way as with the native enzyme. Further work is in progress to locate the heavy atom sites and refine them in order to calculate the best Fourier map to arrive at the high resolution structure.

In the meantime the fast rotation function program due to Dr. A. Crowther has been set up for the DEC 10 computer at TIFR in order to use the molecular replacement method to determine the structure of notexin by direct methods. The known structure of the homologous bovine phospholipase [6] was placed in a large orthogonal triclinic unit cell and the structure factors calculated. The calculated amplitudes of this model structure were used together with the observed structure amplitudes of notexin and the rotation function was calculated. The rotation function is being interpreted to determine the orientation of the notexin molecule in its unit cell determined. Work is also in progress to calculate the translation parameter of the notexin molecule and a molecular replacement Fourier for notexin with the high resolution native notexin data.

REFERENCES

[1] Karlsson, E., Eaker, D. and Ryden, L. (1972). Toxin, 10, 405.

[2] Harris, J.B., Karlsson, E. and Thesleff, S. (1973). Br. J. Pharmac. 47, 141.

[3] Harris, J.B., Johnson, M.A. and Karlsson, E., (1975). Clin. Exp. Pharmac. Physiol. 2, 383.

[4] Halpert, J., Eaker, D., and Karlsson, E. (1976). FEBS Lett. 61, 72.

[5] Kamman, K.K., Lovgren, S., Cid-Dreselnu, H., Petef, M., and Eaker, D., (1977) Toxicon, 15, 434.

[6] Dijkstra, B.W., Drenth, J., Kalk, K.H. and Vandermaelen, P.J. (1978) J. Mol. Biol. 123, 1.

3.5 Instrumentation Development for Structural Research

3.5.1 Design and Development of Indigenous On-Line Computer-Controlled X-Ray Diffractometer

(V.M. Padmanabhan, A. Sequeira, S.N. Momin, J.N. Soni Surendra Sinh, H. Rajagopal, V.S. Yadava, R.N. Khunte and R. Chidambaram)

To meet the present accelerated pace of single crystal structure investigations, it is necessary to have sophisticated methods of automatic data acquisition utilising on-line computers.

A TDC-312 computer-controlled four-circle neutron diffractometer has already been operating for some years at Cirus reactor [1]. A fully indigenous TDC-312 controlled x-ray diffractometer has now been commissioned. This diffractometer designed for collecting three-dimensional intensity data, has a 23 cm diameter full circle orienter (Fig. 1.1) fabricated in the Physics Group Workshop. All the axes, viz. ω, χ, ϕ for crystal orientation and 2θ for detector movement have been aligned to intersect within an accuracy of 0.015 mm and the tilt between the χ and ϕ axes is within a tolerance of 0.07°. The four angle shafts can be driven through precision worm gears by SCR-controlled DC motors (maximum speed 35°/min). The shaft movements are tracked to an accuracy of 0.01° with the help of digitisers.

The x-rays are detected by a NaI scintillator. A 6 digit display for the detector counts, and a 5-digit selective display for the angle positions is available on the computer console.

The 4K software package is similar to the one used for the neutron diffractometer and is based on the algorithm developed by Busing et al [2]. The salient features of the software which has four subprograms are: (i) crystal orientation, matrix calculation from unit cell parameters and setting angles for two reflections (ii) elimination of back-lash and overshoot errors during motor movement by always arriving at the destination in a forward slow mode and (iii) over 40 teletype commands which enable the user to have a dialogue with the diffractometer and to execute various operations such as initializing and driving the motors, choice of scan mode, and automatic data collection with teletype printout.

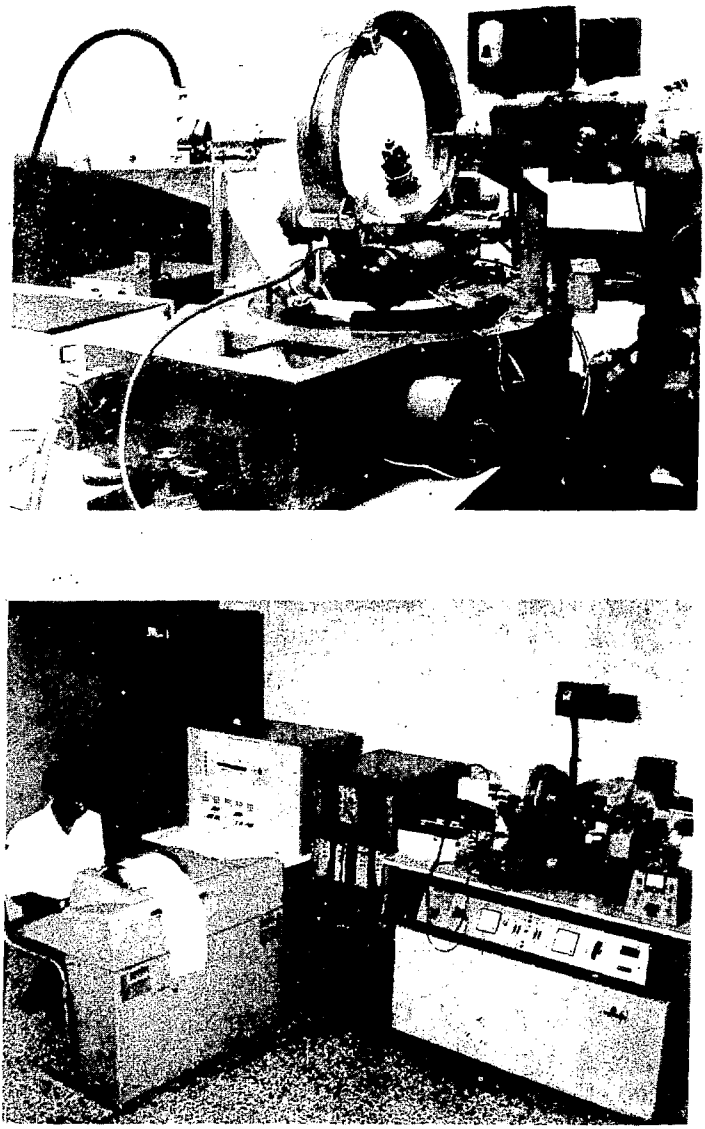

Fig. 1.1. On-line computer-controlled x-ray diffractometer and the TDC-312 control system

REFERENCES

[1] Sequeira, A. et al. (1978), Pramana 10, 289

[2] Busing, W.R. et al. (1968), ORNL-4143.

3.5.2 Design and Fabrication of a Highly Stabilised X-Ray Generator*

As it is essential to have a stabilised x-ray generator for carrying out reliable diffraction work, particularly for work involving accurate measurement of diffracted intensities, the design and fabrication of a full-wave rectified, smoothed and stabilised power supply has been undertaken. The prototype power supply, housed in a tank filled with transformer oil has been fabricated at VEC site by Shri S.S. Ramamurthy and his group with the following components (i) H.V. transformer (220V/65KV 100 ma, 50 c/s) (ii) rectifier elements with full wave bridge configuration (iii) oil filled condenser for filtering (0.1 μf, 60KV). (iv) series current limiting resistance stack (50kΩ, 800 W), (v) voltage divider chain and (vi) x-ray filament transformer (220V/7V, 11V; 4A, 80 KV isolation). The current and voltage (H.T.) stabilization is done by separate control circuits and each has a set of selectable reference points, on which the stabilization is achieved. Protective relays are included in the circuits, to safeguard the generator from the x-ray tube faults, earth faults etc. The power supply was tested with a resistive load upto 52 KV and 50 mA (at Variable Energy Cyclotron Project site, Calcutta). The prototype is now being reassembled at Trombay for testing as an integral unit, with an expected stability of 0.03 % in current and high voltage at mains voltage variation of $\pm$ 10% and with a ripple less than 40 V/ma.

---

* In collaboration between Neutron Physics Division, VEC Project, Chemistry and Metallurgy Divisions.

3.5.3 On-Line Computer Controlled Neutron Diffractometer System: Memory Expansion

(H. Rajagopal, S.N. Momin, A. Sequeira)

The TDC-312 controlled neutron diffractomer system has been updated by expanding the memory from 4K to 8K words to enhance its program, data and device handling capacity.

The 4K software package has been updated by incorporating command swapping of the SET-UP and the DATA-COLLECTION programs and thus eliminating the alternate loading procedures of the 4K-version. The development of the software for the refinement of cell and orientation parameters as well as automatic determination of the crystal orientation are in progress. As projected memory map of the 8K software is shown in Table 3.1.

Table 3.1: Memory Map of 8k Software

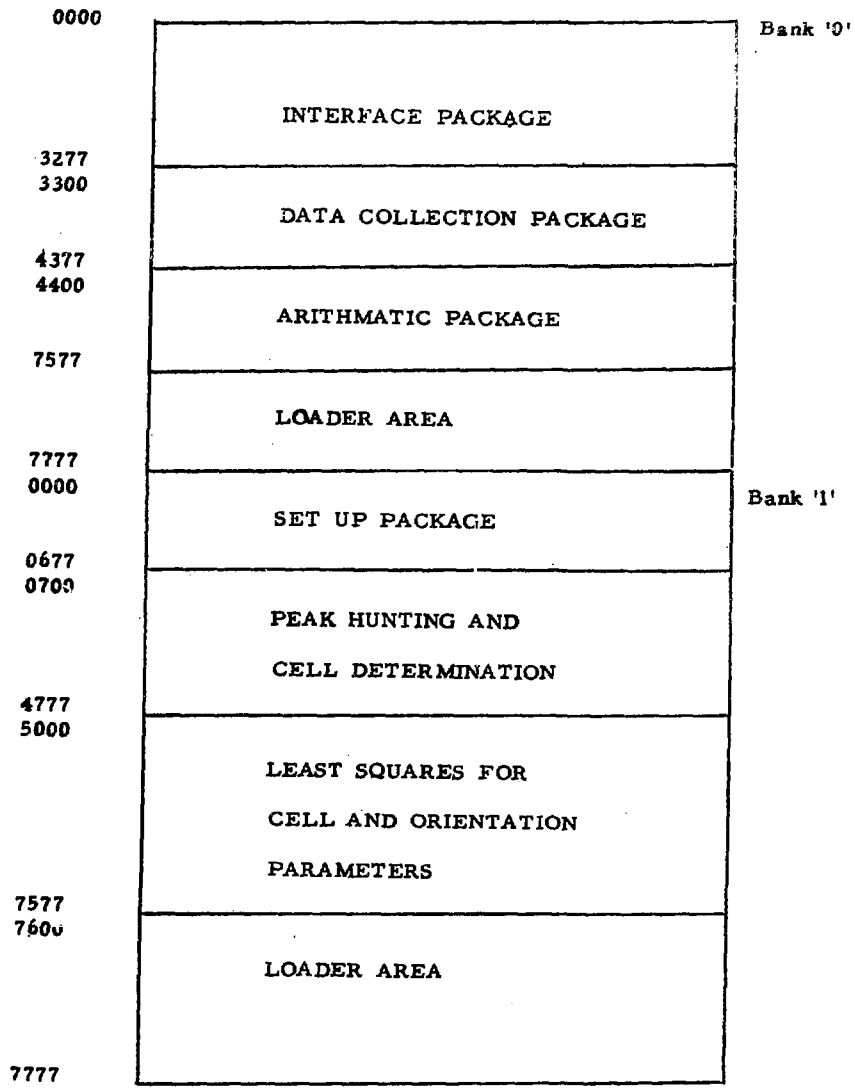

3.5.4 Magnetic Tape Controller for the TDC-312 Computer Controlled Diffractometer System

(S. N. Momin and R. N. Khunte)

In order to enhance the data and program storage capacity of the computer-controlled diffractometer system, a suitable magnetic tape controller has been designed to interface a 'Pertec' make synchronous digital magnetic tape transport (6840-75-25 tape) with TDC-312 computer. The controller uses 3 cycle data interrupt facility of the TDC-312 computer for data transfer and interrupt I/O bus for control and status transfer as shown schematically in the block diagram of Fig. 4.1.

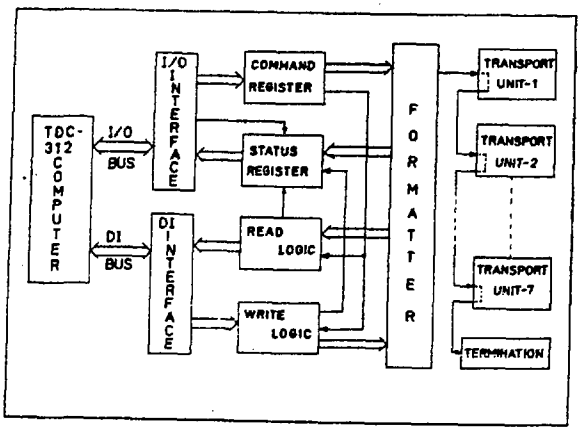

Fig. 4.1 Magnetic tape controller schematic block diagram (The present design is based on an earlier design developed in the R. Cn. D.)

The controller accepts commands and presents status to the computer via I/O bus of the computer. Device addresses $(30)_8$ and $(31)_8$ are used for interfacing the controller with the computer. Command to be performed on the transport unit is first loaded from accumulator into command register (CR) using instruction load command register (LCR). Once the command is successfully initiated the important bits of the command are transferred from CR to command buffer register (CBR) where these are stored undisturbed till its execution is over. CR is then free to accept the next command which can be executed only when the previous command is over. This feature of the controller enables the 'on fly' operation for read and write commands and prevents the tape from stopping into inter record gaps, which saves time in reading or writing

consecutive records.

Status information of the controller and the transport is stored in a status register (SR) and can be read into accumulator using read tape status register (TSR) instruction. SR contains device flag or magnetic tape flag (MTF) which is used to indicate the completion of the command being executed and it is set whenever the execution of a command is completed. The locations $(0030)_8$ and $(0032)_8$ in memory bank '0' are used to retain word count (WC_1 & WC_2) and $(0031)_8$ and $(0033)_8$ locations are used to indicate current address (CA_1 & CA_2) governing data transfer.

The controller can be interfaced with upto seven transport units and can read or write 7 or 9 - track IBM compatible tapes recorded in NZRI format. The present 'Pertec' tape transport is a 7-track, read-after-write type recording head with read-write speed of 25 inches/sec. at 556/800 Characters/inch density which gives data transfer rates of 13,500/20,000 Characters/Sec.

The layout and fabrication of various cards of (1) Read-Write Logic (2) Control Register Logic (3) Status Register Logic (4) Data Interrupt Logic (5) Input/Output Interface Logic have been completed along with module card holder. The back panel wiring layout and testing of these logic cards are in progress. The system is expected to be commissioned shortly.

3.5.5 High Resolution Powder Diffractometer-D_1

(A. Sequeira)

The resolution of the double crystal diffractometer D_1, has been improved by tightening the in-pile collimation (α_0) from 0.6 (FWHM) to 0.15, and by replacing the Ge(111) monochromator with pyrolytic graphite (002). Powder diffraction patterns of U-fuel pellets, before and after effecting the above changes, are shown in Fig. 5.1. The average resolution has improved by a factor of two and the ratio of the peak height to peak width has improved nearly four times. The improved resolution is expected to facilitate testure studies of polycrystalline samples with low crystallographic symmetry such as uranium.

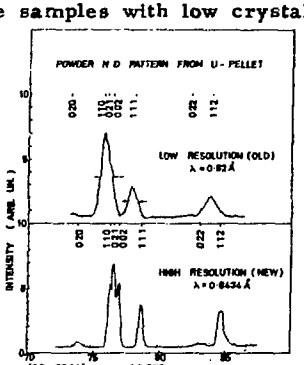

Fig. 5.1 Powder diffraction patterns of U-fuel pellets

4. SOLID STATE PHENOMENA

4.1 High-Pressure, High-Temperature Equation of State and Shock Propagation in Solids and High-Z Plasmas

4.1.1 Electronic Grüneisen Parameter in Shock Hugoniot Equation of State of Aluminium

(B. K. Godwal, S. K. Sikka and R. Chidambaram)

The shock Hugoniot equation of state for aluminium has been computed from first principles. The pseudopotential method, with parameters taken from Fermi surface measurements, has been employed to evaluate the 0K isotherm, ionic vibration contributions and thermal electronic excitation contributions. The nuclear Grüneisen parameters used in the analysis have been derived from phonon frequencies. These are found to be in better agreement with the experimental values measured by Neal[1], compared to those derived empirically by Slater's method from the 0K isotherm. The computed electronic Grüneisen parameter values depart considerably from the value 0.5, used often in analysing shock compression experiments. This leads to different Hugoniot temperatures compared to those derived by Al'tshuler et al [2], although the P-V curve is in good agreement with their experimental results [Fig. 1.1.]

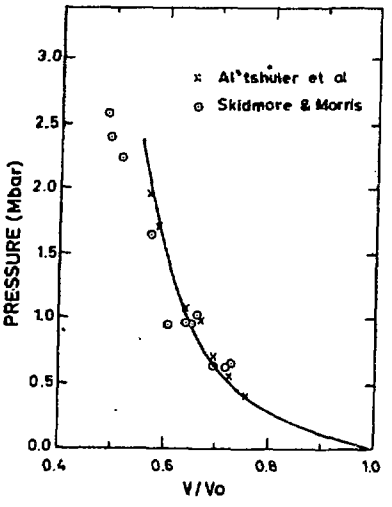

Fig. 1.1 Comparison of calculated Hugoniot (-) for Al with experimental data of Al'tshuler et al. and Skidmore and Morries

REFERENCES

[1] Neal, T. (1976) Phys. Rev. B14, 5172.

[2] Al'tshuler, L.V., Kromer, S.B., Braznik, M.I., Vladimirov, L.A., Speranskya, M.P. and Funtikov, A.I. (1960), Sov. Phys. JETP 11, 766.

4.1.2 Electronic Thermal Grüneisen Parameter for Thorium

(B.K. Godwal)

The variation of electronic thermal energy, pressure and electronic Grüneisen parameter (γ_e) with temperature have been computed for some compressed states (V/Vo = 0.55, 0.60) of thorium, using the augmented plane wave method. This was to check whether the values of γ_e derived from the Thomas-Fermi statistical atom model used in shock equations of state (i.e. $\gamma_e \simeq 0.5$) are appropriate for high Z elements. This study was undertaken because earlier theoretical studies on Al [1] and metallic iodine [2] suggested γ_e values different than 0.5. The energy eigenvalues were computed by the RAPW program adopted to the BESM-6 computer, using the crystal potentials constructed from Liberman's charge densities for the free-atom configuration $6d^2 7s^2$ and Kohn-Sham exchange. The γ_e's obtained from these are shown in Fig. 2.1. The variation is as expected from the T-F model. However, the electronic

Fig. 2.1 Variation of γ_e with T for Pb and Th for $V/V_\sigma = 0.55$

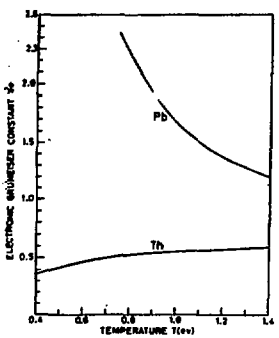

energy and pressure depart considerabily from the T^2 behaviour as used in shock wave calculations.

REFERENCES

[1] Godwal, B.K., Sikka, S.K. and Chidambaram, R., Phys. Rev. B (under publication).

[2] McMahan, A.K. and Ross, M. (1971) Phys. Rev. B15, 718-724.

4.1.3 Derivation of Crystal Potentials from Experimental Equation of State Data

(S.K. Sikka and B.K. Godwal)

There are now numerous data on equation of state of condensed matter both from static and shock wave high pressure experiments. These contain a wealth of information about the crystal potentials. We have systematically used the 0°K isotherms, derived from shock PV measurements to get the parameters for the Krasko and Gurskii [1] pesudopotential. It was found that upto pressures of 1 Mbar, a single set of pesudopotential parameters describe the PV data. This is in accordance with the fact that zero pressure values of bulk modulus, Grüneisen constant, etc. are often sufficient to calculate the high pressure PV data. Some of the fitted isotherms are shown in Fig. 3.1. For thorium, the computed

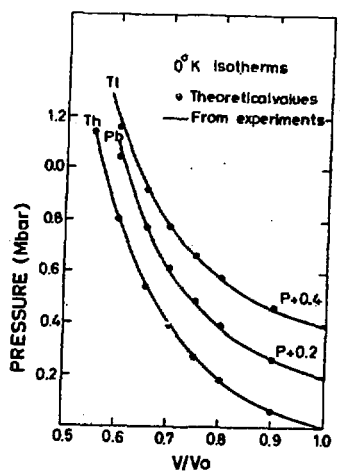

Fig. 3.1 Crystal potentials from 0°K isotherms

bulk modulus of 0.49 Mbar from the fitted pesudopotential, may be

compared with the experimental values ranging from 0.491 to 0.539 Mbar. The phonon frequencies at zero pressure, obtained from this pesudopotential for Th are within 20% of the experimental values [2].

REFERENCES

[1] Krasko, G.L. and Gurskii, Z.A. (1969) Zh. eksp. teor. Fiz. 9, 59.

[2] Reese, R.A., Sinha, S.K. and Peterson, P.T. (1973) Phys. Rev. 88, 1332.

4.1.4 X-Ray Transport in Ni Plasma

(B.K. Godwal)

Mizui et al [1] have observed enhanced transmittance of laser light through foils of high Z metals like Au, Ni and Al, compared to that through a low Z metal foil. These high Z plasmas were produced by them using high power Nd-glass lasers with a 1.06 μm, 200 psec pulse at intensities from 10^{14} to 7 x 10^{14} w/cm^2. In order to explain the experimental observations, substantial energy transport is attributed to x-rays, emitted from the critical density to the solid density region. In our view their results provide a link between experimentally observed transmittance and x-ray energy transport. To check this, the x-ray transport for Ni plasma was evaluated from the models of opacity calculations developed earlier by us [2, 3]. The results of our investigations showed that the x-ray source length satisfies black body condition i.e. $\ell_{PL} < X_L < \ell_{RO}$ (7.0 x 10^{-4}cm $<$ 67.1 x 10^{-4} cm $<$ 2.2 x 10^{-2} cm) where ℓ_{PL}, X_L and ℓ_{RO} are free-Planck mean free path, x-ray source length and free Rosseland mean free path. It was further noted that x-ray transport can be computed in the optically thick limit, and that the x-ray transport increases with foil thickness.

REFERENCES

[1] Mizui, J.N. et al (1977) PRL 39, 619.

[2] Godwal, B.K. and Sikka, S.K. (1977) Pramana 8, 217.

[3] Godwal, B.K. and Sikka, S.K. (1978) Pramana 11, 47.

4.2 High-Pressure Phase Transformations and Electronic States and Processes in Solids

4.2.1 Electronic Structure of Omega Phase of Titanium and Zirconium-Theoretical and Experimental Study

(Y.K. Vohra, S.K. Sikka and R. Chidambaram)

Under high pressures, hcp (α-phase) Ti and Zr transform to a

more open hexagonal structure (ω -phase, AlB_2 type). Also, in some alloys of Ti and Zr with d-rich transition metals, metastable ω -phase is formed during quenching and ageing. The ω -phase is a distorted bcc structure and contains two non-equivalent lattice sites A and B which differ in coordination number and the nearest neighbour distances. There have been various empirical suggestions regarding the electronic structure of the ω -phase i. e. localization of one d-electron and sd^2 hybridization at B-site. We have done band structure calculations for the ω -phase of Ti and Zr to check the empirical bonding suggestions and to explain its properties. The non-relativistic APW program [1] was used for electronic structure calculations. For comparison purposes we have also recalculated the band structure of the α -phase with the atomic charge densities which were used in case of the ω -phase.

The computed electronic density of states (DOS) curves for α -Zr and ω-Zr are shown in Fig. 1.1 and Fig. 1.2 respectively (the curves for Ti are similar). The discriminating features of the band structure of the ω -phase as compared to the α-phase are the reduced s-d spacing, a broad d-band without sharp resonances and the location of the Fermi level. In case of the α -phase, the Fermi level lies in a valley while in case of the ω -phase, it lies near the centre of a broad maximum. However, there is no evidence of a localized atomic d-state in the DOS curves of the ω -phase as empirically suggested in [2] . The low energy peak in the DOS of ω -phase in analogy with the low energy peak structure found

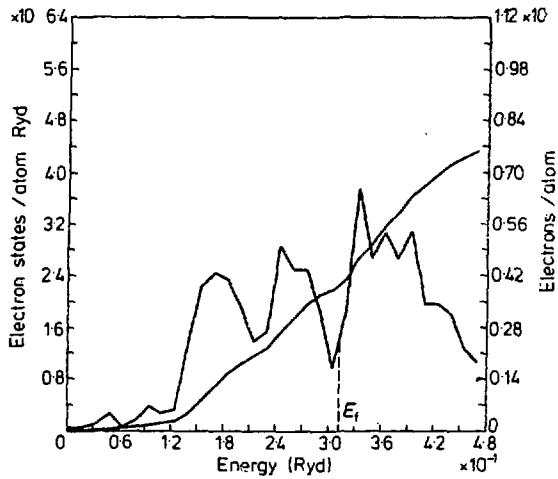

Fig. 1.1 Electronic density of states (DOS) and integrated electron/atom curves for α-Zr. The Fermi energy is indicated by broken line

in case of ZrB_2 (AlB_2-compound) and attributed to sp^2 bonding [3] may

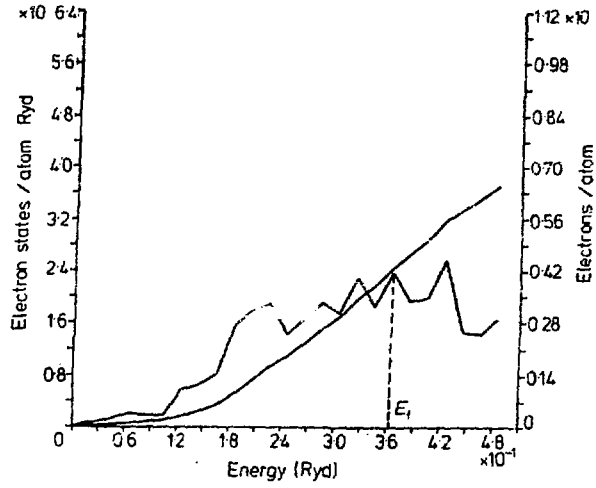

Fig. 1.2 Electronic density of states(DOS) and integrated electron/atom curves for ω-Zr. The Fermi energy is indicated by broken line

be in this case due to sd^2 bonding at B-site.

For XPS studies, ω-Ti and ω-Zr were synthesized under high pressures and high temperatures in the form of cylindrical specimens (0.6 cm dia and 0.8 cm height) using a cubic press at NPL, Delhi. The completeness of the bulk transformation was checked by neutron and x-ray diffraction methods. The XPS study on the α and ω-phases of Ti and Zr were carried out with an ESCA spectrometer at Institute of Science, Bangalore. Al K_α radiation (1486.6 ev) was employed for which the resolution of the instrument was between 1 to 1.5 ev. The samples were heavily etched by Ar^+ ion bombardment to remove surface oxygen. The spectra recorded for α-Zr and ω-Zr are shown in Fig. 1.3. The peak at 1 ev in the α-Zr pattern may be compared with the two peaks in the DOS curve which, due to resolution effects, will merge and manifest as a single peak in the experimental curve. In contrast, the spectrum for ω-Zr has a flat region with a dip at 4.6 ev. This is in agreement with our theoretical calculations for ω-Zr (Fig. 1.2) which predict a flat occupied *d*-band width of 3.5 ev or so.

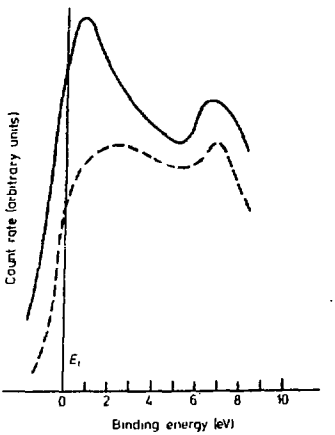

Fig. 1.3 XPS spectra of α-Zr (full curve) and ω-Zr (broken curve) recorded with Al K_α radiation after prolonged etching to remove surface oxygen. The two curves have been displaced with respect to each other along the y-axis for comparison. The zero on the energy scale refers to the Fermi energy. The peak at 6 to 7 ev from E_f is attributed to residual oxygen

REFERENCES

[1] Vohra, Y. K. in Annual Report 1975-1976.

[2] Jamieson, J. C. (1963) Science 140, 72.

[3] Ihara, H., Hirabayashi, M. and Nakagawa, H. (1977) Phys. Rev. B16, 726.

4.2.2 Electronic Basis for Omega Phase Stability in Group IV Transition Metals and Alloys

(Y. K. Vohra)

It is now well known [1] that relative stability of different crystal structures in transition metals is decided mainly by the bonding contribution of the d-band (U_d^{bond}) which is further related to the changing number of d-electrons across a transition metal series [1]. We have applied this d-band occupancy criterion to the problem of stability of omega structure in Group IV transition metals and alloys.

A free energy diagram (called unified phase diagram) has been drawn (Fig. 2.1) at room temperature and pressure as a function of change in the number of d-electrons based on the expected variation of U_d^{bond} with increase in d-electrons for the three competing crystal structures i.e. hcp(α), bcc (β) and simple hexagonal (ω). Here, ΔN_d^o is the change in d-band occupancy corresponding to the minimum in the free energy of the ω-phase. ΔN_d^1 and ΔN_d^2 correspond to the free energy curves cross-over for α-ω and β-ω respectively. It is shown [2] that such a representation gives a unified picture of omega phase formation during various pressure and thermal treatments in

different systems. The composition of ω-phase in aged alloys correspond

Fig. 2.1

The free energy curves for α, β and ω structure as a function of the change in d-band occupancy of typical omega forming AB alloy system. These curves are drawn at room temperature and pressure. Here A is a group IV transition metal element while B is any d-rich β-stabilizer

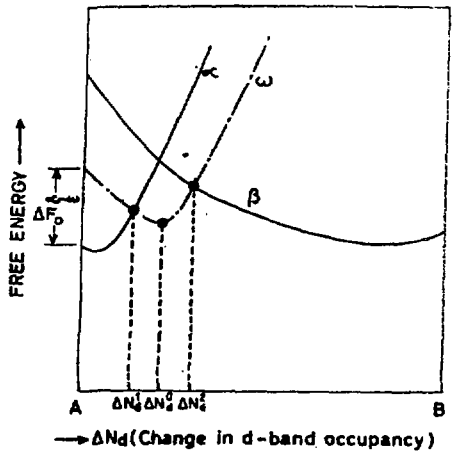

to the minimum in the ω-free energy curve and experimental values of ΔN_d^o for various alloy systems are shown in table 2.1. From the data it is clear

Table 2.1: The Composition of ω-Phase at Pseudoequilibrium state During Ageing and the Corresponding Change in d-band Occupancy for Various ω-forming Alloy Systems

Alloy	Alloying content in aged (at %)	N_d^o in aged (electron/atom)
Ti-V	13.8 ± 0.3	0.138 ± 0.003
Ti-Cr	6.5 ± 0.2	0.130 ± 0.004
Ti-Mn	5.1 ± 0.2	0.153 ± 0.006
Ti-Fe	4.3 ± 0.2	0.172 ± 0.008
Ti-Nb	9 ± 2	0.090 ± 0.020
Ti-Mo	4.3 ± 0.4	0.086 ± 0.008
Zr-Nb	10 - 11	0.100 to 0.110

that ΔN_d^o is characteristic of the alloy system and is dependent on the alloying element. This dependence on the alloying element is attributed to the breakdown of rigid band model as there are distortions produced in the d-band as a result of alloying. The occurence of ω-phase under pressure is explained by the fact that pressure gives rise to increase in d-band occupancy ($s \rightarrow d$ transfer [3] and the PV term in the free energy also tends to stabilize high

density ω-phase. Also, it can be seen from the unified phase diagram that ω-phase free energy increases rapidly in B-rich compositions. So it appears that application of pressure on omega forming alloy systems will cause $\alpha \rightarrow \omega$ - transformation only in solute lean phases. However systematic work is required to complete the phase diagram of the omega forming alloy systems with pressure.

REFERENCES

[1] Pettifor, D.G. (1977) J. Phys. F4, 613, Calphad 1, 305.

[2] Vohra, Y.K. (under publication in Acta Metallurgica).

[3] Svechkarev, I.V. and Paniflov, A.S. (1974) Phys. Stat. Sol. (b) 63, 11.

4.2.3 High Pressure Studies on Group IV Transition Metals

(Y.K. Vohra)

The phase diagram of Group IV transition metals is shown in Fig. 3.1. The high pressure ω-transformation shows extensive hysteresis in P-T plane.

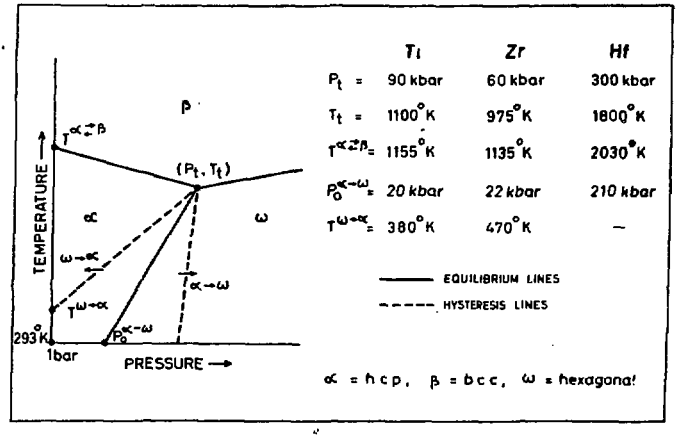

Fig. 3.1 Schematic phase diagram of titanium, zirconium and hafnium

An earlier high pressure study on Ti [1] established the isothermal martensitic nature of the $\alpha \rightarrow \omega$ transition. Also, measurements of the rate of transformation as a function of pressure show a C-curve behaviour [2]. It is noticed that ω-transformation occurs in Ti and Zr under shock wave compressions of microsecond durations. All these experimental features are related to the kinetics of ω-transformation under static and dynamic pressures.

Table 3.1 Theoretical Values of Energy of Critical State, Bulk Athermal Martensitic Start Pressure for $\alpha \rightarrow \omega$ and $\omega \rightarrow \alpha$ Transformation for Ti, Zr and Hf.

Element	α-phase cell constants in Å	ω-phase cell constants in Å	$\Delta V^{\alpha-\omega}$ cm^3/mole	Elastic++ constant (C_o) in dynes/cm^2 and strain parameter (γ_o)	ΔF^* cals/mole	$P_o^{\alpha-\omega}$ kbar	$P_{M_s}^{\alpha\rightarrow\omega}$ kbar	$P_{M_s}^{\omega\rightarrow\alpha}$ kbar
	a_o = 2.951	a_o = 4.625		C_{66} = 3.52x10^{11}				$P_{M_s}^{\omega\rightarrow\alpha} < 0 = -17$
Ti			0.165		146	20	57	ω-retained in a metastable state at room pressure
	c_o = 4.679	c_o = 2.813		γ_o = 0.18				
	a_o = 3.232	a_o = 5.039		C_{66} = 3.53x10^{11}				$P_{M_s}^{\omega\rightarrow\alpha} < 0 = -24$
Zr			0.177		194	22	68	ω-retained in a metastable state at room pressure
	c_o = 5.147	c_o = 3.136		γ_o = 0.18				
	a_o = 3.195			C_{66} = 5.20x10^{11}				+ 184
Hf+		-	0.45		274	210	236	ω-can not be retained in a metastable state at room pressure
	c_o = 5.051			γ_o = 0.18				

+ For Hf, $\Delta V^{\alpha-\omega}$ and $P_o^{\alpha-\omega}$ are tentative only and are yet to be confirmed by experiments.

++ Elastic constant values given are α-phase at room temperature and pressure. Consequently all the pressures listed here corresponds to room temperature.

To explain these observations, we have done theoretical calculations of the kinetics of $\alpha \rightleftharpoons \omega$ transformation in these metals. Estrin [3] showed that the energy of the intermediate state (ΔF^*) per unit volume during the course of transformation is

$$\Delta F^* = \frac{C_c \gamma_0^2}{2\pi^2}$$

where Co is the initial elastic modulus and γ_0 is the strain which transforms the lattice of the α -phase into that of the ω -phase. The intermediate state occurs at strain $\gamma^* = \gamma_0/2$. The following expressions for the martensitic start pressure for the forward ($P_{M_s}^{\alpha\to\omega}$) and backward ($P_{M_s}^{\omega\to\alpha}$) transformation can be derived [4] .

$$P_{M_s}^{\alpha\to\omega} = P_0^{\alpha-\omega} + \frac{C_0\gamma^2}{2\pi^2 \Delta V^{\alpha\to\omega}}$$

$$P_{M_s}^{\omega\to\alpha} = 2P_0^{\alpha-\omega} - P_{M_s}^{\alpha\to\omega}$$

where $P_0^{\alpha-\omega}$ is the equilibrium transformation pressure and $\Delta V^{\alpha-\omega}$ is the volume change at the transition. The theoretical results are summarized in table 3.1 and it can be seen that $P_{M_s}^{\omega\to\alpha} > 0$ for Hf so that, in contrast to Ti and Zr, the ω -phase of Hf cannot be retained in a metastable state.

The Hf phase diagram drawn to scale is shown in Fig. 3.2. To check the

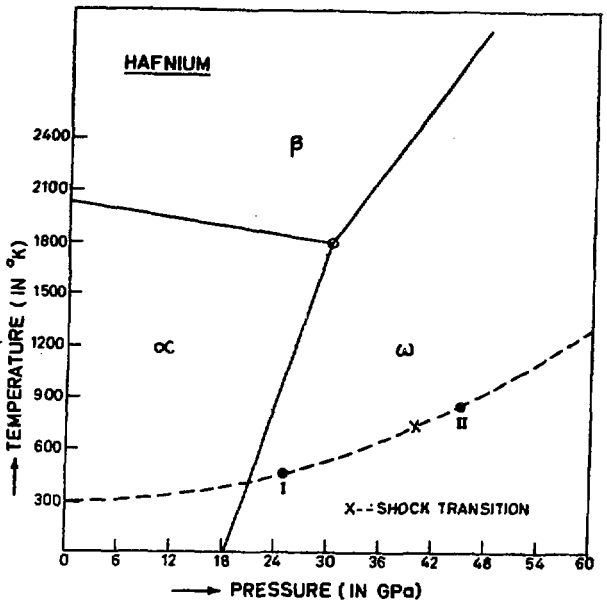

Fig. 3.2

Phase diagram of hafnium. Dashed curve represents the (T-P) state of shock compression. The shocked state achieved in two experiments (I and II) along with shock transition point are indicated on the dashed curve

non-retention of the ω -phase in Hf, two shock experiments (I and II in Fig. 3. 2) one below and another above the shock transition point were done. The shock recovered samples were phase analyzed using x-rays to see the possible retention of ω -phase. In both the experiments, no ω -phase was

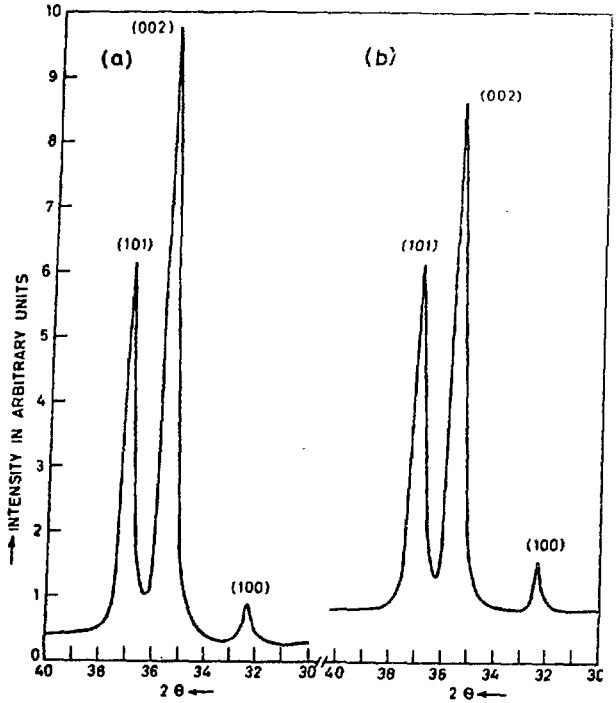

Fig. 3. 3 X-ray diffraction pattern of the plane face of hafnium cylindrical crystal bar sample (a) pre-shock sample showing prominent (002) texture (b) post-shock recovered sample showing texture retention

picked up in the bulk of the recovered samples, though a surface oxide layer was formed.

All the Hf-samples used in the study were having preferred orientations (texture). Metallographic and x-ray studies on shock recovered samples show that the texture of the grains is retained during shock compression (Fig. 3. 3).

This fact is in agreement with the results of Johnson et al[5] on other materials. More experiments have been planned on other hexagonal close packed metals.

REFERENCES

[1] Vohra, Y.K., Sikka, S.K., Vaidya, S.N. and Chidambaram, R. (1977) J. Phys. Chem. Solids 38, 1293.

[2] Zilbershtein V.A., Chistotina, N.P., Zharov, A.A., Grishina, N.S. and Estrin, E.I., (1975) Fiz. Met. Metal. 39, 445.

[3] Estrin, E.I., (1974) Fiz. Met. Metal. 37, 1249.

[4] Vohra, Y.K. (1978) J. Nuclear Materials 75, 288.

[5] Johnson, Q., Mitchell, A.C. (1972) Phys. Rev. Lett. 29, 1369.

4.2.4 Deviations from Matthiessen's Resistivity Rule for Metals

(Surinder M. Sharma)

It is known that for very small concentrations of impurities, the temperature dependent resistivity and residual resistivity interfere to give rise to a total resistivity which is usually higher than their sum [1]. This difference is called the deviation from Matthiessen's Rule (DMR). It has been observed [2] that DMR has some general features which are independent of type of impurity. For all polyvalent metals, critical residual resistivity marking the onset of DMR changes with temperature as T^2 and the amount of critical resistivity increases with complexity of Fermi surface. It had been suggested by Kagan and Zhernov [3] that such an interference between resistivity due to phonons and residual resistivity results from the change of character of the Boltzmann equation. It is because electron-phonon umklapp scattering is very anisotropic while impurity scattering is isotropic. To evaluate the relative effect of these two types of scattering, detailed calculation was done for Indium. The Boltzmann equation was solved by iteration. Computed results were in reasonable agreement with experimental data.

It was realised that competetion between impurity and umklapp scattering is of extreme importance in deciding about the conditions under which deviations from Matthiessen's rule will become observable. So we proposed that the crieterion for deriving the systematics of critical resistivity should be modified. It was suggested that it is the near equality of respective relaxation times rather than corresponding resistivities which should be the crieterion for the onset of deviations. Based on this crieterion the correct temperature dependence (T^2) of critical resistivity was deduced. A plausible explanation for the general dependence of critical resistivity on complexity of Fermi surface was also given.

REFERENCES

[1] Bass, J. (1972) Adv. Phys. 21, 431.

[2] Cimberle, M.R., Bobel, G., and Rizzuto, C. (1974) Adv. Phys. 23 639.

[3] Kagan, Yu. and Zhernov, A. P. (1971) Sov. Phys. JETP 33, 990.

4.2.5 Experimental Facilities for Studies of High Pressure Phase Transformations and Electron States in Solids

(S. K. Sikka, Y. K. Vohra, S. M. Sharma and R. Chidambaram)

(a) Apparatus for Electrical Resistance Measurements upto 100 kbar

For investigating the phase transitions in materials under high pressures, an apparatus for measuring electrical resistance at high pressure has been set up at the Purnima Laboratory. The pressure on the sample is generated by the standard Bridgman opposed WC anvils, pressed by a 100 ton hydraulic press. The press can be operated both manually and electrically with a preset loading rate. To obtain very good stability (i.e. no change of load at a particular value for long times) an isolation valve is used between the ram and the pump. The electronics employed for resistance measurements contains, a constant current generator, D. C. amplifier and a micro voltmeter. Using the two probe method, the anvils have been calibrated by observing Bi I-II, II-III and V-VI phase transitions.

(b) Positron-2γ Angular Correlation Apparatus

An apparatus to measure the momentum distribution of electrons in solids by observing the angular correlation of the 2γ photons resulting from the annihilation of positron-electron pairs has been set up. The annihilation photons are detected by standard coincidence technique by NaI scintillation counters, each of them 2 meters from the centre of the sample. The size of the NaI crystals employed is 76 mm in diameter and 51 mm thick. The two detectors and the source-sample assembly are mounted on three separate tables, which are not interconnected as in conventional set ups. The moving detector rotates around the vertical axis passing through the centre of the sample. Provision has also been made to rotate the sample about its axis in the positron beam. This feature will be useful in single crystal samples where the annihilation spectra have to be recorded in different directions. The counting of photons for preset times and the stepping of the moving detector from one position to next has been automated (for details see section C). Initial measurements were done by a 30 mCi Co^{58} source. Now the shielding has been improved for the use of more intense Cu^{64} sources. The annihilation spectrum from ω-Zr sample using a 120 mCi Cu^{64} source is shown in Fig. 5.1.

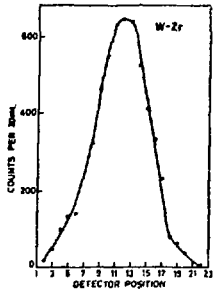

Fig. 5.1 Raw angular correlation data on ω-Zr using 120mCi Cu^{64} source

(c) Automation for Positron Angular Correlation Experiments

(S.N. Momin and R.N. Khunte)

A control unit for scanning coincident counting of γ-ray intensities as a function of the angle between the fixed and moving detectors has been designed and fabricated using digital ICs. The control unit drives the geared d.c. motor and sets the detector in motion which is sensed by the optical digitizer. The detector could be advanced in steps of 1 mm or 2 mm (2 mm corresponds to one milliradian) with positioning accuracy of 0.02 mm. The programmable counting timer can be preset from 1 to 9999 seconds and the final coincident intensity data counts are output on a serial printer. The control unit provides the preselectable scanning range (100 points maximum) and could perform scanning either in forward or backward direction with automatic reversal. The schematic functional block diagram is shown in Fig. 5.2.

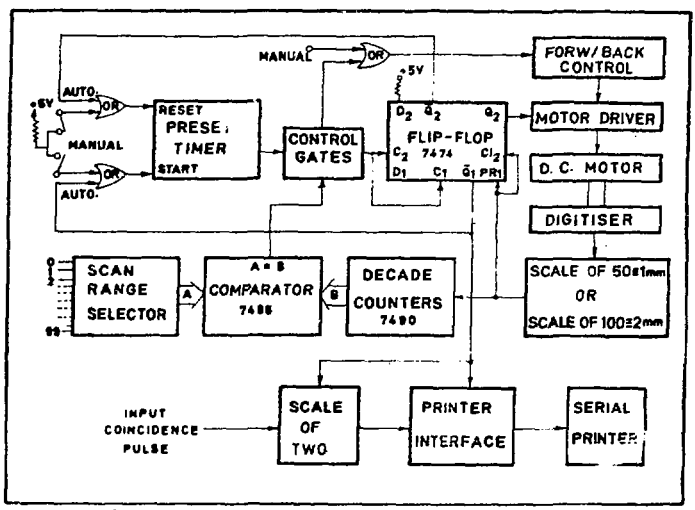

Fig. 5.2 Schematic diagram of the control unit for positron correlation experiment

4.2.6 Computer Programs Developed in the Section for BESM-6 Computer

(1) APW-augmented plane wave energy band program with facilities for plotting of energy bands and density of states. (Y. K. Vohra)

(2) RAPW-relativistic augmented plane wave energy band program. (B. K. Godwal)

(3) PEW-pesudopotential energy band program. (B. K. Godwal and S. K. Sikka)

(4) PCE-pesudopotential cohesive energy program. (S. K. Sikka)

(5) PLD-pesudopotential lattice dynamics program. (Surinder M. Sharma)

4.3 Search for New Ferroelastics and Ferrogyrotropics and the Study of Their Properties

4.3.1 Orthoboric Acid: an Unusual Ferroelastic

(V. K. Wadhawan)

The discovery of the ferroelastic effect in H_3BO_3 crystals was reported in the previous Annual Report. Further studies on domain-wall orientations, and a detailed analysis of the crystal structure, have led to the following main conclusions about this remarkable ferroelastic. For details regarding these results, the original papers may be consulted [1, 2, 3].

(a) H_3BO_3 belongs to the Aizu species $6/mmm\ F\bar{1}$. The space group of the prototype phase is postulated as $P6_3/mcm$.

(b) The spontaneous strain for this crystal at room temperature is about 0.2, and it has a vanishingly small coercive stress. This value of the spontaneous strain is one to two orders of magnitude larger than that for any of the other 100-odd known ferroelastics.

(c) This crystal is an order-disorder ferroelastic. In fact, it may well be the first member of an entirely new class of ferroelastics having giant spontaneous strains and low coercive stresses.

(d) Atomic mechanisms for the motion of the various types of domain walls under stress have been proposed [1, 2]. Some of these mechanisms involve proton transfers along the O-H...O bonds in small, six-sided loops. This type of stress-induced cooperative proton transfer should also occur in potassium dihydrogen phosphate, another order-disorder ferroelastic.

REFERENCES

[1] Wadhawan, V. K. (1978) Mat. Res. Bull. 13, 1-8.

[2] Wadhawan, V. K. (1977) Nucl. Phys. & Solid State Phys. (India), 20C, 404-407.

[3] Wadhawan, V. K. (1978) Abstract no. 16.1-28 in the Collected Abstracts of the Eleventh International Congress of Crystallography, Warszawa, Poland.

4.3.2 Potassium Chlorate, a New Ferroelastic with an Antiferroelastic Phase Above 250°C

(V. K. Wadhawan)

Observation of the ferroelastic effect in $KClO_3$ crystals has been reported recently from our laboratory [1]. The crystals are monoclinic-pseudoorthorhombic at room temperature and undergo a transition to an orthorhombic phase at 250°C [2]. They are well-known for their iridescence property, which disappears above the phase transition temperature. At the present stage of the work it appears that the ferroic species for $KClO_3$ at room temperature is 4/mmm F 2/m (s). This postulate has some peculiar consequences which are under investigation. However, the following conclusion can already be drawn with a reasonable amount of certainty. The orthorhombic phase above 250°C is an antiferroelastic phase. Antiferroelasticity as a possible phenomenon was postulated a decade ago by Aizu [3], but no actual examples of its occurence in non-antiferroelectric non-antiferromagnetic crystals had been reported so far. An antiferroelastic crystal has a crinkled lattice, which can be smoothed by applying a suitable uniaxial stress. The 'unit cells' in such a crystal are distorted in opposite senses alternately, so that the true unit cell actually comprises a pair of these oppositely distorted halves.

REFERENCES

[1] Wadhawan, V. K. (1979) Abstract no. 14.12, Tenth National Conference on Crystallography, B. H. U., Varanasi.

[2] Ramachandran, G. N. and Lonappan, M. A. (1957) Acta Cryst., 10, 281.

[3] Aizu, K. (1969). J. Phys. Soc. Japan, 27, 1171.

4.3.3 Switchable Gyrotropics

(V. K. Wadhawan)

Switchable gyrotropics, or ferrogyrotropics, are those optically active crystals, the optical rotation of which can be switched in sign (or magnitude), in at least one direction, by applying a suitable external field. This

phenomenon has been examined recently by the author [1, 2] in the framework of Aizu's concept of ferroicity. The case of dicalcium strontium propionate has been analysed in some detail as an illustration of the procedure for enumerating the ferrogyrotropic orientation states of any given crystal.

Ferrogyrotropy may or may not be accompanied by ferroelectricity, ferromagnetism and/or ferroelasticity. If it is not, the crystal is called a 'pure' ferrogyrotropic. Konak et al [3] have derived and tabulated 13 possible species of equitranslational, single-transition-parameter pure ferrogyrotropic. A scrutiny of the 773 ferroic species shows that four additional species of pure ferrogyrotropics are also possible [2]. These four species, namely 4/mmm F$\bar{4}$, 6mm F 3, 6/mmm F 32, and m3m F 23, represent partial ferrogyrotropics, and have four orientation states each, whereas the remaining 13 have only two orientation states each.

Ni-Cl boracite, $BaMnF_4$, $RbNO_3$, and some related crystals, are suggested as new potential ferrogyrotropics. The first two of these could be ferromagnetic ferrogyrotropics, of which no examples are known so far.

REFERENCES

[1] Wadhawan, V. K. (1978) Nucl. Physics & Solid State Phys. (India), Vol. 21C (In the press).

[2] Wadhawan, V. K. (1979) Acta Cryst. A35, (In the press).

[3] Konak, C., Kopsky, V. and Smutny, F. (1978) J. Phys. C: Solid State Phys., 11, 2493.

4.4 Rock Mechanics Phenomenology of Underground Peaceful Nuclear Explosions

4.4.1 Effect of Porosity on the Cratering Efficiency of Underground Peaceful Nuclear Explosions in a Shale Medium

(Satish C. Gupta, S. K. Sikka and R. Chidambaram)

The shale rock near the detonation point of the Pokaran peaceful nuclear explosion was relatively dry and of variable porosity. Using our one-dimensional spherical symmetric rock mechanics code [1] we have studied the effect of porosity on the cratering efficiency of this shale, as measured by the kinetic energy imparted to it by the explosive. Unlike the parametric studies by others in which the important rock parameters have been treated to vary independently we have taken into account in our study, the simultaneous variation of shear strength and compactibility which are affected by change in porosity. A realistic model coupled with experimental measurements was used to represent this variation of both the above rock parameters with porosity. The calculated spall velocities, peak pressures and kinetic energies show

that the cratering efficiency of this shale is first enhanced with increase in porosity and then degraded. This is due to the fact that, at low porosities, the strength effects are more significant and at high porosities, the effects due to compressibility are more dominant. Calculations also showed that the overall cratering efficiency of this shale is lower compared to, say, Bear Paw shale and basalt rocks, in which USA has carried out explosions.

REFERENCES

[1] Gupta, Satish C., Sikka, S.K. and Chidambaram, R. "OCENER - One dimensional computer code for nuclear explosion effects in rocks" BARC report- 1023 (1979).

4.4.2 A Non-Self Similar Blast Wave Method to Predict the Early Time Ground Motion Phenomena Due to Underground Peaceful Nuclear Explosion

(S.K. Sikka, Satish C. Gupta and M.P. Ranga Rao*)

In our program of developing analytical methods for studying the effects of underground nuclear explosions in rocks, we have modified and applied the Porțel-Zaker method, for shock propagation in solids, to evaluate the early-time profiles of pressure versus radius, shock position versus time, etc. Our modification consists of taking into account the departure of rocks from the 'linear shock velocity - particle velocity' equation of state and a model for the initial state of the explosion. Application of this non-self similar method for nuclear explosions in granite and alluvium media has been made. Fig. 2.1 shows the shock decay

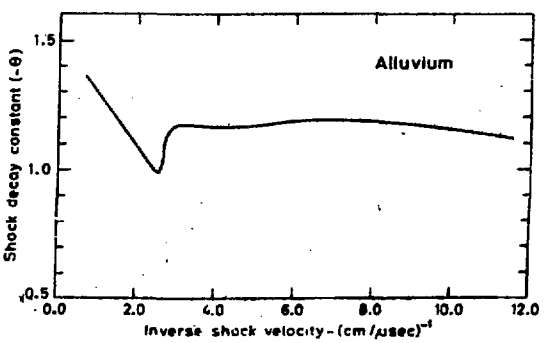

Fig. 2.1

Shock decay constant vs inverse shock velocity for alluvium

---

*. Indian Institute of Technology, Powai, Bombay.

constant (Θ) versus the inverse of shock velocity for alluvium. The increase in Θ for lower shock velocities in this curve was found to be essential for matching the observed shock position versus time profile (Fig. 2.2).

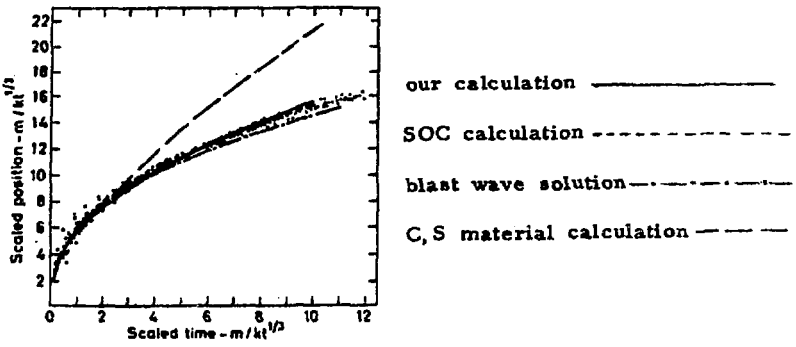

Fig. 2.2 Shock position vs time for alluvium

Further work, in which the strength of the rock is also included, is in progress.

5. SEISMOLOGY

5.1 Seismological and Microbarograph Services

(S.K. Arora, T.K. Basu, R.N. Bharthur, M.K. Bhat, C.A. Krishnan, P.C. Mitra, A.G.V. Prasad, K.K. Sankaran, H.S.S. Sharma, T.V. Sridharan, K.R. Subbaramu and T.G. Varghese)

The activity of the Section is centered around the problem of detecting and identifying underground and atmospheric nuclear explosions. The data necessary for this work is obtained from a continuously operated medium aperture L-shaped seismic array of twenty short period seismometers (1 sec. period) and a triangular array of three long period seismometers (20 sec. period) located at Gauribidanur, 80 km north of Bangalore.

Continuous measurement of atmospheric pressure variations was carried out in the period range 6-600 sec. Effort is being made to develop hard-ware for obtaining on-line phase-summed time series.

An ECIL made TDC-12 computer was installed at the array in 1972. It was utilised for some period for on-line detection and computation of some parameters useful for approximate location of tele-seismic sources; several computer programmes were also developed for off-line use of TDC-12 computer.

Since the work of this Section is largely a cooperative endeavour for seismic source discrimination studies, it is reported under a few major headings, together with concerned staff. This report is thus not an evaluation of work of individual members, but is a composite structure reflecting the different types of work being carried out.

5.1.1 Monitoring Statistics

On an average the seismic array at Gauribidanur detects about 10 seismic signals every day. The majority of these are due to tremors taking place on various places in the crust or upper mantle of the earth. A few of them are due to man made sources which include chemical shots for mining purposes or underground nuclear explosions for peaceful or military purposes.

The following table gives the summary of events whose sources are classified to be nuclear explosions as inferred from our data.

U.G. = Underground; Atm= Atmospheric

Year	Source located in Nevada USA	Sites in USSR	Lop Nor, China	Tahiti Isl. France
1977	5 U.G.	19 U.G.	1 Atm.	2 U.G.
1978	8 U.G.	24 U.G.	-	1 U.G.

All these events, except the atmospheric explosion by China detected by the microbarograph array, have an estimated yield in the range 20-150 kilotons of TNT. The yield of Chinese atmospheric nuclear explosion is estimated to be in the range 25-50 kilotons of TNT

5.1.2 Bulletin Services

The Section prepares a regular bulletin of events and exchanges them bilaterally with other national and international seismic centres.

5.1.3 Regional Seismicity

The short period medium aperture array has provided with reasonable accuracy the location of the source of the tremors. A systematic study of tremors originating in the southern part of India was carried out to find the epicenters and their relation with the tectonic and geological features. The Fig. 1.1 gives the distribution of epicenters as obtained

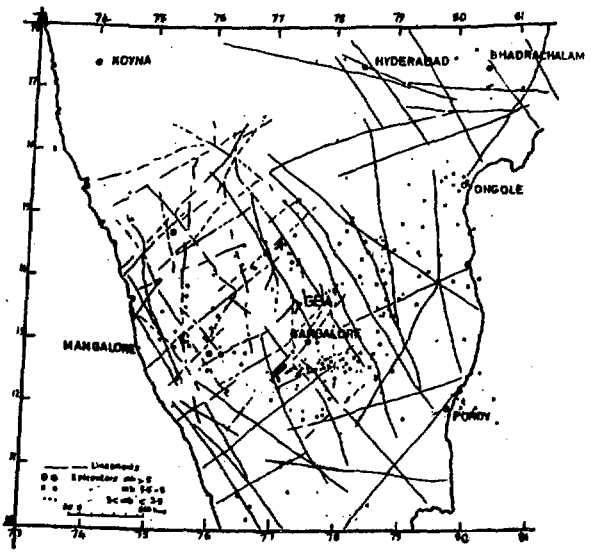

Fig. 1.1 Epicenters of earth tremors recorded at Gauribidanur (1968-1975) shown against the background of lineaments

from the Gauribidanur data for local tremors during the period 1968-75 together with the lineaments as observed in LANDSAT imagery. The

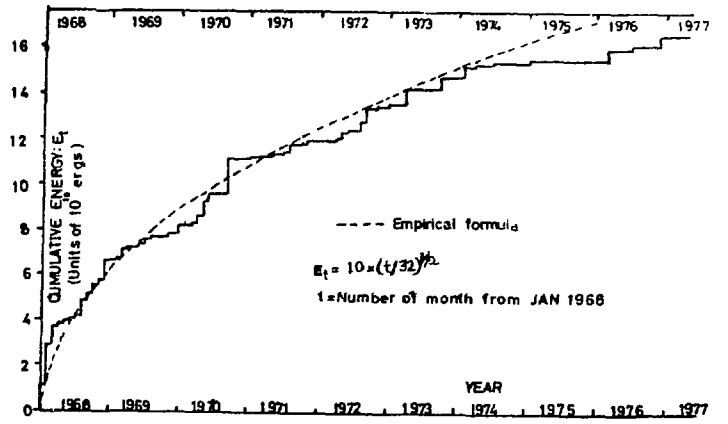

Fig. 1.2 Variation of cumulative energy release from Koyna as deduced from GBA data during 1968 to 1977

study is being continued with the special attention to tremors arising from Koyna. The Fig. 1.2 shows the cumulative energy release from Koyna as observed at Gauribidanur.

5.2 Development of Seismological Instrumentation

(M.K. Bhat, V.S. Kamath, V.G. Kolvankar, V.N. Nadre, G.J. Nair, B.S.S. Rao, F. Roy, N. Satyanarayana, B.M. Shah, S.V. Sharma, S. Srinivasa Murthy, M. Suryavanshi, T.G. Varghese and Vijai Kumar)

5.2.1 Seismometer

Special alloy, Ni-Span C leaf springs which are vital parts of the seismometer were successfully developed and fabricated with the help of Analytical Chemistry Division and Atomic Fuels Division of BARC. With this success a completely indigenous short period seismometer is now fabricated in our Section. One such unit together with associated electronics and recording system is being field-tested at Gulmarg and found to function satisfactorily at a magnification of 200,000 at 1 cps.

The seismic noise level at High Altitude Research Laboratory, Gulmarg, was measured recently (Sept. 1978) by our seismometer and was found to be about 5 milli microns during night time and increase to about 200 milli microns during day time. Some of the recent typical seismic signals recorded by this are shown in Fig. 2.1. The data obtained at HARL, Gulmarg is useful in conjunction with the Gauribidanur data for locating the source of teleseismic signals. Preliminary observations show that several tremors recorded at HARL by our unit are not

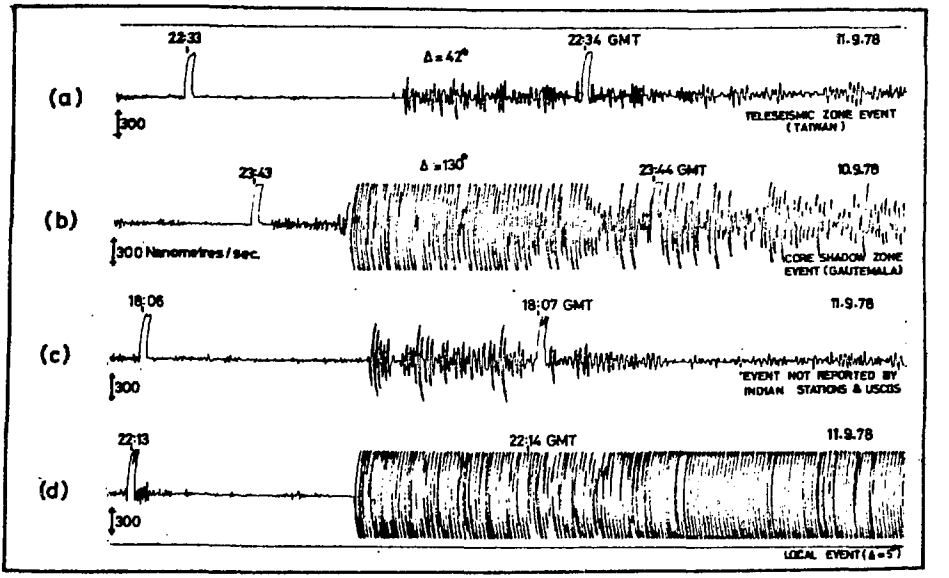

Fig. 2.1 Typical seismic recordings at Gulmarg

reported either by Indian or Foreign Observatories.

5.2.2 Microbarograph

The calibration system of the microbarograph was improved to obtain daily automatic calibration for input signals of different period in the range 5 sec-1000 sec by utilising integrated circuit technology. This unit controls the solenoid valve to isolate the microbarograph transducer from the atmosphere and starts the calibration motor to produce sinusoidal pressure changes of known amplitude and period (Fig. 2.2).

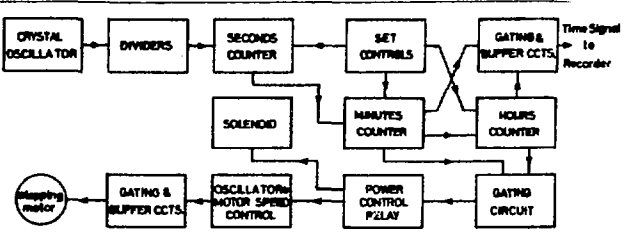

Fig. 2.2 Block diagram of the automatic calibration and timing system for microbarograph

A complete microbarograph system with automatic calibration fabricated in the Section is being field tested. Continuous record of pressure fluctuations is made and it is found that the amplitude of normal background varies from a few microbars to few hundred microbars.

5.2.3 Seismometer Calibration

Operator controlled procedures for obtaining response function of short period and long period seismic systems quickly and accurately have been developed and standardised using TDC-12 computer. This procedure takes only one minute for calibration of one instrument, which includes digitisation of data and computation of the response function. This facility has greatly enhanced the task of keeping all instrument responses within tolerable limits. Typical response curves of short period and long period instruments are given in Fig. 2.3.

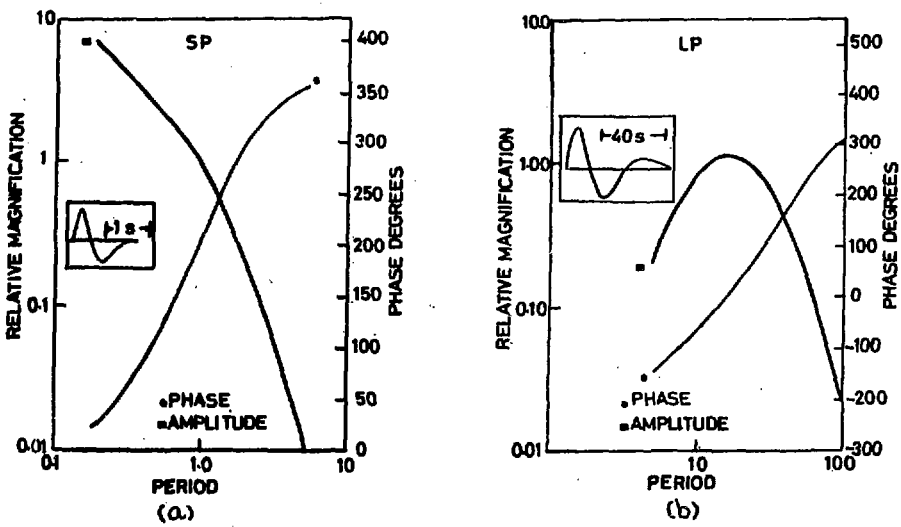

Fig. 2.3 (a) Short period and (b) long period seismometer system responses. Input signals are shown in the inset

5.2.4 FM to Digital Converter

Following the recent developments in multi-channel digital data acquisition for computer analysis, the frequency modulated seismic signals were directly digitised using frequency multiplying and counting. This ensures a larger dynamic range at low system noise. The system developed for the purpose can take three channels of data at variable sampling

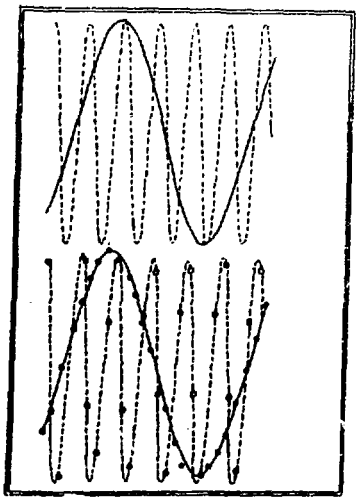

Fig. 2.4 Analog and digital representation of 2 volts zero to peak, 1 Hz and 5 Hz waveforms

rate upto 20 samples per second and provides 12 bit accuracy in digital representation. It also provides an interface to record this data alongwith accurate time information on a digital stepping recorder. Typical output from the unit is shown in Fig. 2.4. The top figure shows the input and the lower figure shows the digital output superposed on the input.

5.2.5 Tape Labelling Unit

When large number of analog seismograms are transcribed on to a library tape, it is necessary to label the tapes as well as the events serially to facilitate retrieval of seismic data at a future date. This unit (Fig. 2.5) provides serial code very much similar to vela time code and,

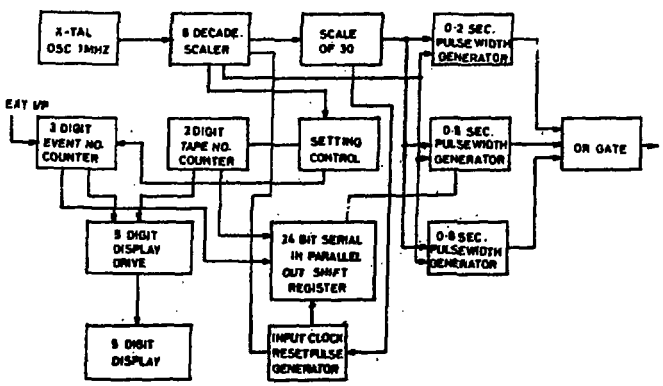

Fig. 2.5 Block diagram of the tape labelling unit

has a capacity to code events numbers from 0 to 999 and library tape number from 0 to 99, which can be chosen by the operator. Distinct pulses every second are marked on the tape along with th labelled information which is repeated every 30 seconds. ... format of the code is such that the tape search and control unit which reads vela time code can also read this code for retrieving the seismic data.

5.3 Seismological Research

(S.K. Arora, A.R. Banghar, T.K. Basu, R.N. Bharthur, Ram Datt, G.S. Murty, G.J. Nair, K.J. Rao, F.Roy, T.G. Varghese and Vijai Kumar)

5.3.1 Auto-Regression Method of Detection of Weak Signals in Noise

Akaike's method of determining optimum auto-regression model for stationary time-series is adopted to detect transient signals in noise background using the 'One-step-ahead-prediction' property of auto-regression model. Fig. 3.1 shows a few typical records of noise at different seismo-

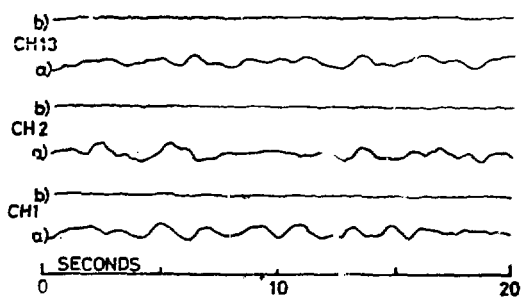

Fig. 3.1

Test of stationarity of time-series by auto-regression model of typical GBA seismic noise

meters of short period Gauribidanur array (traces each 1, 2 and 13) sampled at equal intervals of time (usually 1/26 second). An optimum auto-regression model is obtained for the first half of the traces 'a', using which an 'error' series is obtained by subtracting the actual values by the corresponding 'one-step-ahead'-predicted values for the whole time series and shown in the traces 'b' drawn on the same scale. It is seen here that the second half of 'error' series is not noticeably different from the first half. This enables one to introduce a prescription to detect a signal in the latter half of the time series as follows:

A new time series called the spike series is generated such that a spike of unit magnitude exists at all instants when the 'error' exceeds a threshold, otherwise the spike does not exist at that instant of time. The choice of 'genuine' spike is then made by time shifted 'AND' and 'ADD' operations carried on the spike series of all channels on which a teleseismic signal is expected. A typical case when a transient is superposed

with zero lag on four noise series is shown in Fig. 3.2. The lowest trace is the transient pulse and the traces 'a' are the perturbed time series with the transient added to noise. One can hardly notice any signal in traces 'a' in the channels 1 and 2. The top trace 'e' is the result of 'ADD' operation and trace 'd' is the result of 'AND' operation on the traces 'c' of all four channels. Thus the presence of a signal is indicated even though it is not visible on all the channels. This method has the advantage that coherency properties of the signal are not needed to detect it.

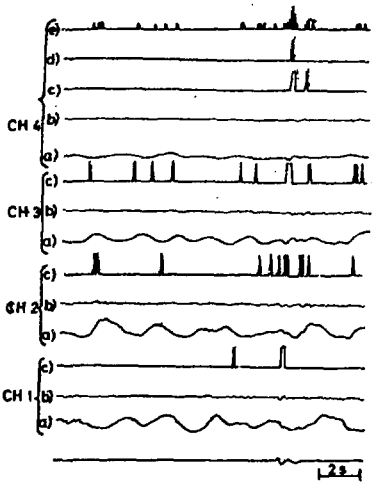

Fig. 3.2

Detection of weak signals by auto-regression model of time-series

5.3.2 Signal detection by Fisher's Randomness Test of Akaike's Final Prediction Error

One of the merits of auto-regression model of stationary time series is its ability to "predict" one step ahead of a given time window the value of discrete time series sampled at equal intervals. This enables one to generate an "error" series which can be tested for randomness and stationarity at a given level of confidence and answer the question whether a given succeeding window of time series contains a "signal" or not.

To illustrate this, an optimum auto-regression model for 10 second interval of Gauribidanur Seismic noise sampled at 26 samples/sec is first constructed using Akaike's Final Prediction Error method. One transient pulse (two cycles of one-second period sine wave) was added to the succeeding 10 seconds of noise series. Trace A in Fig. 3.3. is the segment of noise series containing the transient. Trace B is error series of trace A obtained by Akaike's Final Prediction Error method and trace C

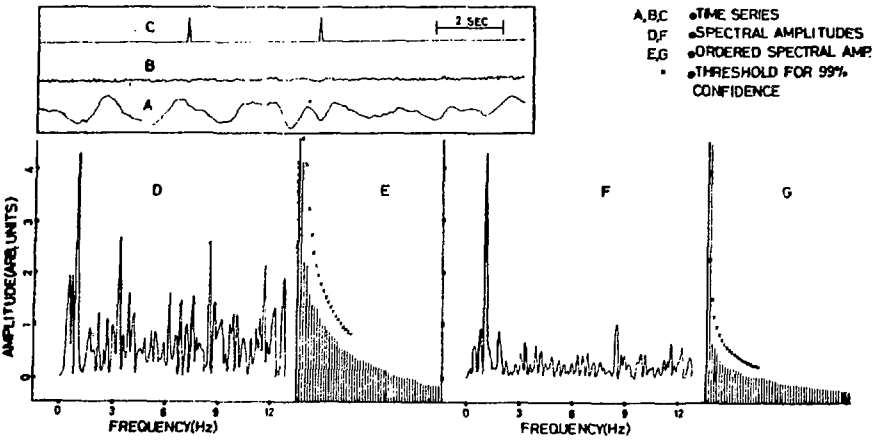

Fig. 3.3 Test of significance of spectral amplitudes by Fisher's method

is spike series obtained as described elsewhere (See 5.3.1).

Portions of error series are Fourier analysed by FFT in the two cases, one containing the transient and the other not containing it, and the corresponding spectral amplitudes are tested for randomness by Fisher's test at 99% confidence limit. Traces D & F are the spectral amplitudes of error series without and with a transient, while traces E and G show the corresponding Fisher's test. The crosses in E and G represent threshold values, above which the corresponding spectral amplitude is significant (not random!). Thus we see in G that the error series containing the transient has one significant peak at 99% confidence limit, while in the case of no transient none of the spectral amplitudes are significant. Adaptation of this method for multi-channel data is straight forward.

5.3.3 Nth Root Method of Signal Detection

Analysis of the coda of seismic events renders valuable information on the nature of the Seismic velocity gradients in the signal transmission path, provided the weak arrivals are detected and identified on the basis of their arrival times and apparent phase velocities. The technique, which has been found useful in achieving this objective is illustrated in Fig. 3.4. The left hand top trace in this figure is a signal to noise ratio enhanced seismogram of an earthquake signal. The centre top trace is the time averaged product obtained by adding the array outputs into two groups, multiplying the two partial sums and averaging the product over an interval of time. The right hand top trace is similar except that an N^{th} root(N=4) of the output from each seismometer has been taken before forming the partial sums and these partial sums have been raised to the

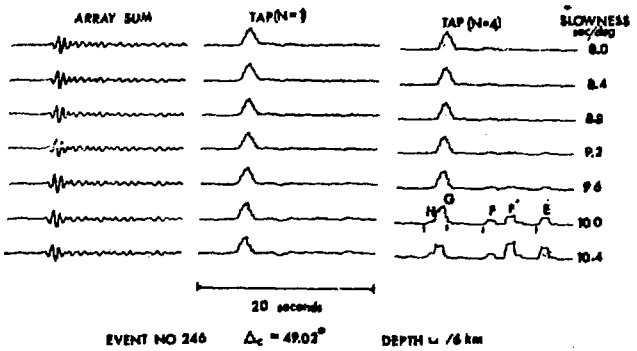

Fig. 3.4 Typical examples of Nth root method of detection of weak signals embedded in the seismic coda

N^{th} power. The traces in the remaining lines have been similarly obtained by varying the array steering slowness in steps of 0.4 second/degree. The N^{th} root process, as this figure illustrates, enhances weak arrivals, which are otherwise embeded in the coda of the wavetrain and enables them to be detected and identified.

5.3.4 STA/LTA Method of Signal Detection

Taking into account of the variation of noise amplitude with time is essential in any on-line detection system to keep the false alarm rate

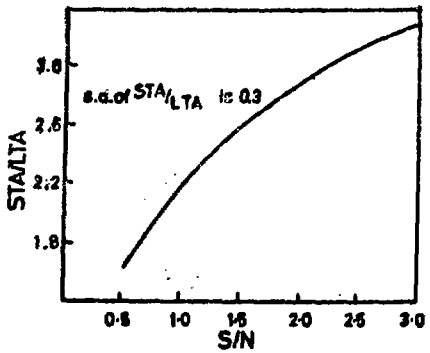

Fig. 3.5 Variation of the ratio of short term average (STA) to long term average (LTA) for different values of signal to noise ratio

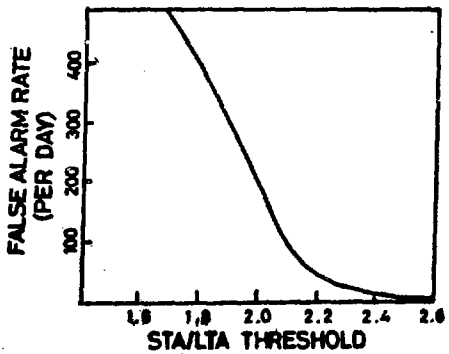

Fig. 3.6 Variation of false alarm rate with STA/LTA ratio

within tolerable limits. A method has been adopted in which the ratio of short-term average (STA) over 0.8 second interval to long term average (LTA) over 16 second interval is compared with a preset value for detecting seismic signals in the presence of variable noise back ground. Fig. 3.5 shows the dependence of STA/LTA on the "signal to noise" ratio obtained by super-posing on predominently 2 second period noise various scaled transient signals of 0.8 second period. The reduction of the false alarm rate with increase of STA/LTA threshold is also shown in Fig. 3.6. False alarm rate of 400 per day corresponds to 0.4% false decisions approximately.

5.3.5 Processing of Events on TDC-12

The data processing system (Fig. 3.7) which was built around the TDC-12 computer at Gauribidanur to detect events on-line, has been augmented to obtain quick information on signal parameters such as its apparent phase velocity, signal amplitude, period, P-wave spectral ratio, signal complexity, by playing back the analog data tapes directly into the computer. The system also provides digital seismic data on events, which are used on the BESM-6 computer to carry out further detailed analysis. The details of the processing of data using this system, the software used and the format of the available information are given separately in a BARC report.

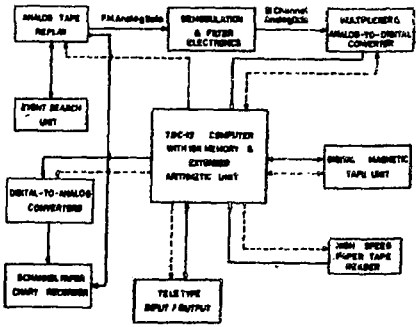

Fig. 3.7

Block diagram of the data processing system

5.3.6 Response of Regional Seismic Networks

In field deployment of regional seismic surveillance networks in regions of known crustal structure, economising on the number of stations to reduce both operational problems and cost is an important aspect. Keeping this in view the location capabilities of different triangular network constituted by a bare minimum of four seismic sensors were evaluated (Fig. 3.8). The network performances were determined on the basis of overall shifts in hypocenter, epicenter and origin time, these parameters being computed by reconstructing a profile of large number of assumed sources at two representative depths (0 and 5 km) using an iterative method.

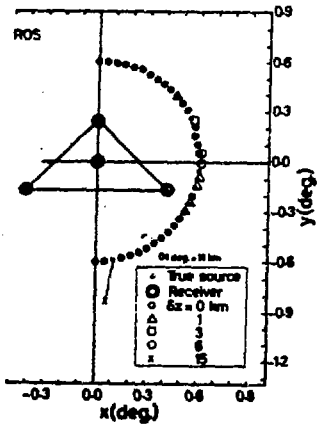

Fig. 3.8

Response of a typical quadripartite network in locating seismic sources outside the net

It is shown that a right angled triangle with its orthogonal arms comparable in length with the radial distance to epicenters is the best suited configuration (3 sensors at the vertices and 1 centrally placed) for locating sources surrounding the network. However, if the sources happen to be situated within the outer boundaries of a net, the response of one type of net is not appreciably different from that of another, but comparatively much better than that for any of the 4-element "source-outside" configurations. Reducing the network aperture is found to render its performance poor. On the other hand, notwithstanding the network geometry, an increase in the number of sensors produces a definite improvement in the estimates of source parameters. The performance of the optimum net is shown to remain practically invariant with focal depth upto few kilometers. The location errors in the constructed examples are attributed to be mainly due to the effect of layering.

The above study of the relative performance of quadripartite systems was repeated for a profile of relatively deep-seated sources at 10 Km depth. No significant change in the network response was noticed so long as the hypocentral distances were not larger than the network aperture. In support of this result, the response of sufficiently small aperture net was shown to deteriorate gradually with increasing source depth.

5.3.7 Crustal Structure Near Gauribidanur

Investigations of the structure of the earth's crust near Gauribidanur in Southern India were made. In this study high-quality seismograms of 215 events recorded at Gauribidanur array (GBA) provided the pertinent data. The events include (a) small chemical explosions conducted near the array site, (b) bulk Deep Seismic Sounding (DSS) charges fired 85-300 km away from GBA along a segmentally continuous profile from Kavali on the eastern margin to Udipi near the west coast, (c) rockburst in the Kolar

Gold Fields (KGF) about 120 km southeast of the array cross-over point, and (d) local tectonic earthquakes which occured at distances upto 350 km from GBA giving wide azimuthal coverage as well as good signal correlation along the array. To avoid any ambiguities regarding identification of phases in the background of high-frequency signals due to reverberation and scattering (P and S coda), uncontaminated first arrivals (direct and refracted) and clear reflected phases were mainly employed in the analysis.

The main findings of this work are as follows:

(i) Two distinct granitic layers, viz. Granite-1 having a thickness of 8.7 km overlying Granite-2 of thickness 10.5 km, are underlain by a 17.2 km thick basaltic layer which extended down to the Moho discontinuity at a depth of about 36 km.

(ii) The entire body-wave data used are consistent with a 3-layer crustal model.

(iii) Group-velocity dispersion data corresponding to short-period surface-waves (Rayleigh type) from explosions suggest a possible 200-250 metre thick outermost layer of weathered material (Fig. 3.9).

(iv) The Moho is found dipping (a localised feature) to the extent of about 4° in the northeast directions between 40° and 55° with respect to Gauribidanur.

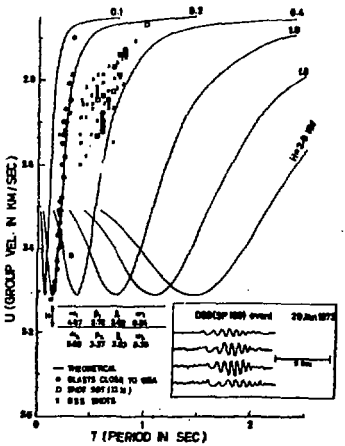

Fig. 3.9

Group velocity dispersion curves indicating possible existence of 200-250 meter thick outermost crustal layer of weathered material

(v) Direction dependent variations of P and S velocities and layer thicknesses being within a few per cent, the layered structure is inferred to be more or less uniform in Gauribidanur and adjacent regions.

(vi) Regional travel-times constructed for various crustal phases are expected to facilitate location of seismic sources in Southern India with an accuracy far better than what can be achieved using a global average model. Hence they would lead to a more reliable seismicity pattern for the peninsular shield.

5.3.8 Travel Time Curve From Warramunga Array Data

Over two hundred events in the Pacific ocean, which were analysed using data from the Warramunga Seismic array in Northern Australia, were utilized to derive an accurate regional P-wave travel time curve (Fig. 3.10) in the distance range $15^{\circ} - 45^{\circ}$. Apart from the well-known triplications near 20° and 24°, the data indicated triplications at epicentral distances near 12°, 26°, 29.5°, 39.5° and 42°. Later arrival branches corresponding to these triplications were identified using non-linear array processing techniques and it was demonstrated that, even in the teleseismic distance range, the later arrival branches of the triplications could be resolved on the basis of slowness and travel times of the arrivals on these branches. Another important feature of these data has been a shadow zone for the first arrival branch which began at about 16° epicentral distance and indicated the presence of a low-velocity zone in the uppermantle.

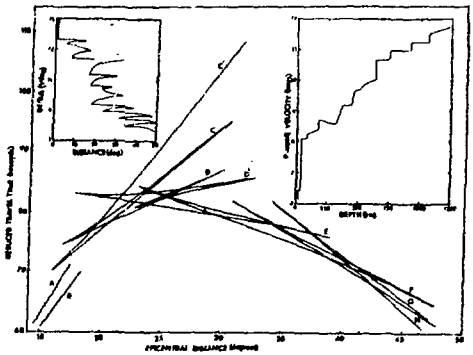

Fig. 3.10

P-wave travel time and velocity model inside earth deduced by array data analysis

5.3.9 Velocity-Depth Relationships

The slowness and travel time data from the Warramunga Array were inverted to obtain the P-wave velocity structure upto a depth of 1200 Kms. The velocity distribution which has been derived (Fig. 3.11) is characterized by a low-velocity zone between 210 and 330 km depths and high velocity gradients at depths near 330, 450, 640, 750, 920 and 1050 kms. A significant feature of this velocity model is the very small velocity gradients in the depth ranges 640-750 and 750-920 km, respectively, which produce low amplitude arrivals in the coda of the seismic events in the teleseismic distance range.

Fig. 3.11

P-Δ curve and the corresponding velocity model with most observational uncertainties beyond 14° included

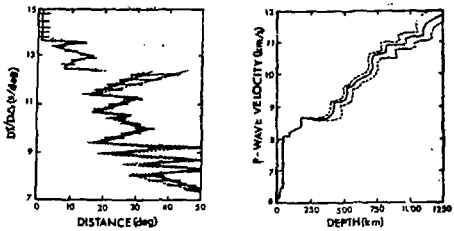

5.3.10 Depth Limits on the Seismic Velocity Structure

The process of inverting slowness epicentral distance (p-Δ) and travel time-epicentral distance (T-Δ) data is associated with a non-uniqueness of the solution, viz. for a given set of (p-Δ) and (T-Δ) data, there exists an infinite number of velocity-Depth (V-D) relationships which satisfy these data. An envelope of the T-Δ and p-Δ data was constructed by taking into account the observational uncertainties and measurement errors into the data and the corresponding V-D envelope was obtained through the method of extremal inversion (Fig. 3.11) in order to estimate the uncertainties in the array data. Computations showed that the velocity discontinuities in the interior of the earth could be scaled with accuracies ranging between 15 and 45 km in depth.

5.3.11 Seismic Ray Tracing

Computer software for obtaining travel times of first and later arrivals from earthquakes from different hypocentres, for known velocity structures, has been written on the BESM-6 computer. Tables were computed to provide corrections to travel times and epicentral distances for events which occured at finite depths from the earth, so that data on deep focus earthquakes could be utilized, along with that on shallow focus earthquakes, to construct a travel time curve.

5.3.12 Problems of Source Identification

Simplicity of signal waveform combined with compressional "first motion" is generally considered to be of diagnostic value in discriminating underground nuclear explosions against earthquakes. However, cases may occasionally arise when these discriminants are not adequate. For example in Fig. 3.12 the two signal traces (a) and (b) are simple transients though the trace (b) is relatively more complex than (a). It is known that seismograms of earthquakes are usually more complex and of longer duration than those of explosions of about the same strength in a given region. To ascertain the true nature of the sources of these two events, the teleseismic P-wave data of seven stations for event (a) and nine stations for event (b) were analysed to determine the source depth. It turned out that the event (a) had a source at depth 50 ± 10 km in Southern

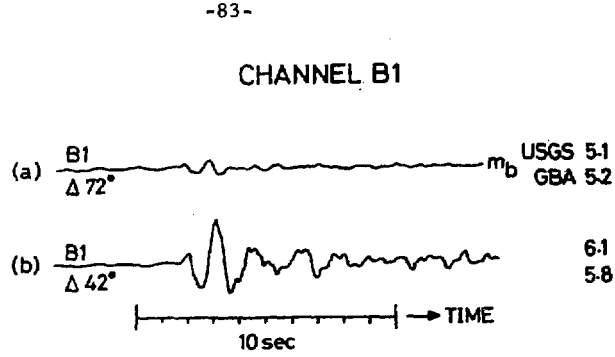

(a) Kamchatka earthq. : 7 Apr 1978

(b) Caspian Sea expl. : 18 Dec 1978

Fig. 3.12 Typical earthquake and explosion records obtained at Gauribidanur

Kamchatka region whereas the event (b) was characterised by a shallow-focus (of the order of 5 km depth) north of Caspian Sea in the Western Kazakh region of USSR. On this basis the preferred conclusions were that event (a) is an earthquake and the event (b) could be a shallow earthquake or an underground explosion. It was later on confirmed from the USGS reports that the event (b) is an underground nuclear explosion. Hence focal depth estimation can serve as a useful discriminant. Attempts are underway in this Section for alternative supporting evidence of shallow focal depth of event (b) apart from the teleseismic P-wave data.

5.3.13 Focal Mechanisms of Earthquakes

As a part of continued work on seismic source discrimination, fault plane studies were carried on for earthquakes in the Himalayan region. Six earthquakes that occurred along Burma-India Border, along the Himalayas and in the Hindukush were studied. The first motions of P and PKP and the polarisation (or first motions) of S waves were used for this investigation. Two of these earthquakes occurred along Burma-India border. One of these mechanisms indicates a predominant component of thrust faulting, whereas, other mechanism is characterized by a large component of normal faulting. Of the two earthquakes that occurred along the Himalayas, mechanism solution of one earthquake (Kinnaur earthquake of 19th January 1976) indicates a normal faulting, while the earthquake that occurred in northwestern Kashmir shows a large component of thrust faulting. Majority of earthquakes that occur along the Himalayas and Hindukush are characterized by a large component of thrust faulting, hence, normal faulting mechanism for Kinnaur earthquake is unusual for that region. Hence, it seems worthwhile to observe seismicity of Himalayan region more closely than is done so far.

5.3.14 Interfacial Waves

The theoretical model of a loosely bonded interface developed earl :r in the Section was generalised to the case when the bonding parameter could be related to an externally imposed pressure. For this, a non-linear model akin to the compression of metallic powders was invoked, thus introducing two empirical parameters in the model. The recent experimental data of Lee and Corbley on the speed of interfacial waves between elastic solids is examined by an optimum choice of the empirical constants by the least square error criterion. The comparison between theory and experiment is shown in Fig. 3.13. The physical meaning of the empirical constants is being studied.

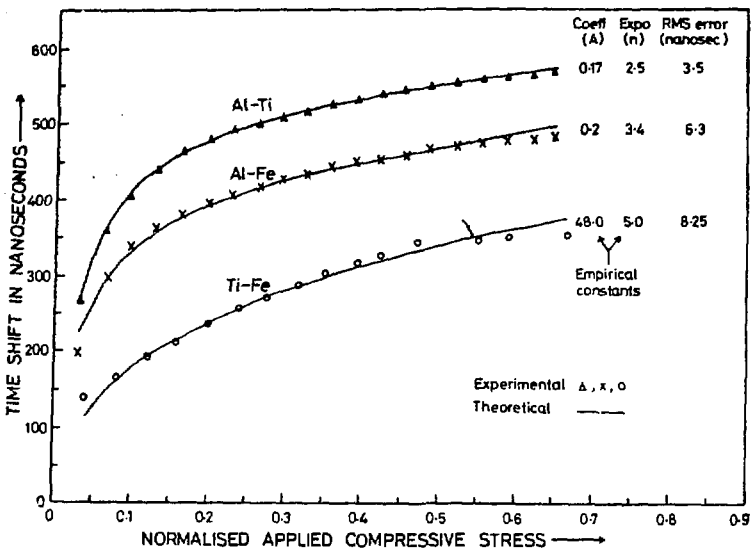

Fig. 3.13 Test of loose bonded model of solid-solid interface

5.3.15 On Propagation and Attenuation of Love Waves

The period equation for Love waves was derived for a layered medium, which is composed of a compressible, viscous liquid layer sandwiched between homogeneous, isotropic, elastic solid layer and homogeneous, isotropic half space. In general, the period equation will admit complex roots and hence love waves will be dispersive and attenuated for this type of model. The general disperson relation is mathematically complex, hence, numerical results were obtained for mathematically interesting case when thickness H and coefficient of viscosity η of a liquid layer tend to zero so as to maintain the ratio $P = H/\eta$ = a constant,

since this limit corresponds to imperfectly bonded interfaces. Numerical values for phase velocity, group velocity, quality factor (Q) and displacement in the elastic layer and half space have been computed as a function of the dimensionless frequency for first and second modes for various values of the parameter $\underline{P}$. It is shown that Love waves are not attenuated when P = 0 and ∞ . The computed values of Q for first and second modes indicate that when $\underline{P} \neq 0, \infty$, the value of Q attains minimum value as a function of dimensionless angular frequency. It was also shown that for P about 20, elastic solid layer effectively decouples from the rest of the half space.

5.4 Collaborative Projects in Seismology

(V.G. Kolvankar, A.G. Kulkarni, V.N. Nadre, B.S.S. Rao, N. Satyanarayana, K.R. Subbaramu, M. Suryavanshi and T.G. Varghese)

The expertise developed in the Section is finding its applications. A contract has been signed by BARC to supply 20 units of timing system (see 5.4.1) developed in the section to be installed in Seismology Project under UNDP to study the seismicity of South East Asia. Similarly, a rockburst research unit is established consisting of a network of surface array of 11 geophones to locate the rockbursts at Kolar Field. The design, development and installation of the array is done by the Section, while the funding and logistic support is given by Bharat Gold Mines. Fig. 4.1

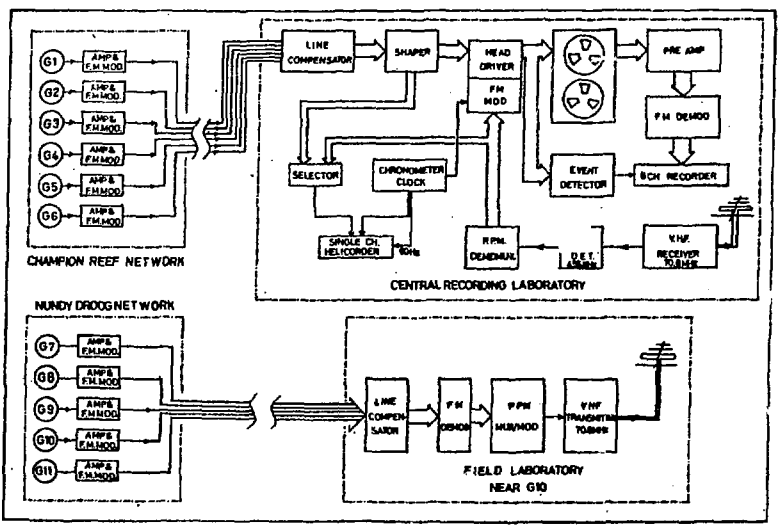

Fig. 4.1 Principal features of the Kolar Gold Field Rockburst Research setup

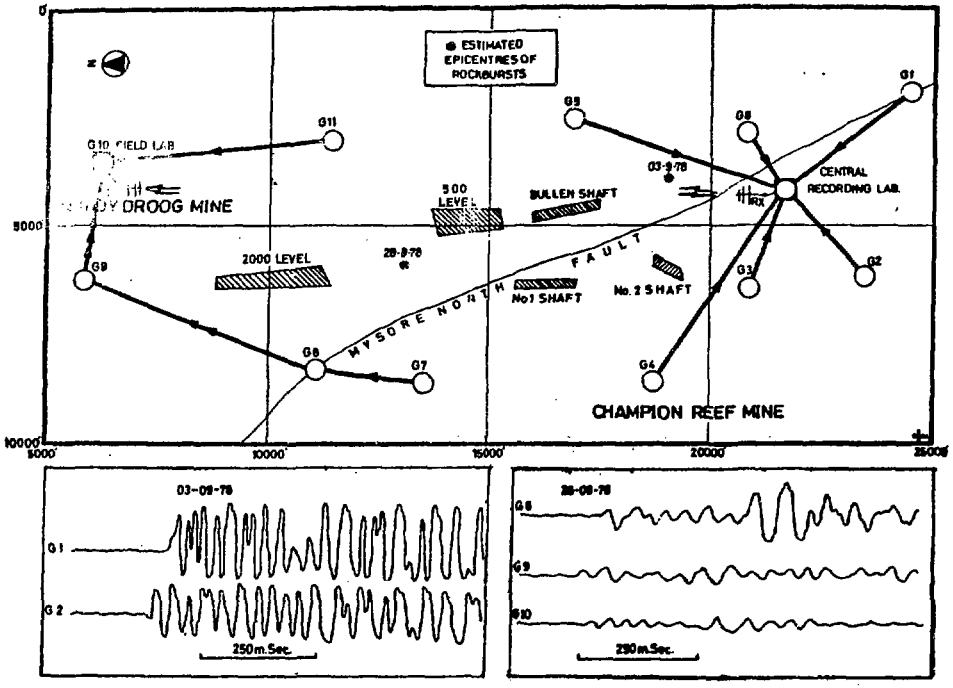

Fig. 4.2 Layout of geophones G1 to G11 and typical rockburst signals

shows the block diagram of field set-up which became operational in September 1978. Fig. 4.2 shows the layout of geophones and typical rockburst signals recorded by the network. (See 5.4.2 to 5.4.5).

5.4.1 Timing System

One of the essential parameters in the recording of seismic signals is the universal time measured to an accuracy of 0.05 second. A timing system (Fig. 4.3) is designed and fabricated which has a stability better than 1 PPM over a period of one year in a temperature range of 0 to 70°C. It can be synchronised with world time within an accuracy of 8 milliseconds. In addition to slow as well as fast coded timing signals it can provide accurate 60 Hz square pulses for driving helicorder at uniform speed.

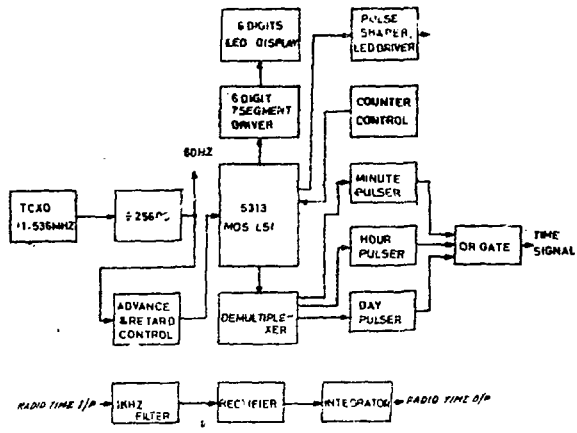

Fig. 4.3

Block diagram of the timing system

5.4.2 Field f.m. Telemetry Unit

A network of low noise geophones were installed at sites, shown in Fig. 4.2. The low level outputs of these sensors are amplified 10,000 times and frequency modulated on a 540 Hz centre frequency carrier with 33-33 % deviation. The amplifiers are a.c. coupled to eliminate noise in the frequency band below 1Hz as well as d.c. offsets in the amplifiers. The f.m. geophone signals are telemetered (Fig. 4.2) via the same d.c. line which feeds power to the system, to the field laboratory and the central recording laboratory. The system has a signal pass-band of 1Hz to 180 Hz with less than 3% f.m. distortion. The frequency passband of signals to be telemetered could easily be extended from d.c. to few KHz.

5.4.3 Multichannel Data Acquisition System

A multichannel data transmission system was developed to transmit high quality analog data from the remote sensors in Nundydurg mines to the Central recording laboratory. The system (Fig. 4.4) accepts 15 channels of analog data at a sampling rate of 80 samples per second with a band width of 0 to 30Hz. The geophone signals from locations 7 to 11 (See Figs. 4.1 and 4.2) are transmitted via cables to field laboratory where they are time division multiplexed, pulse position modulated and telemetered on a 70.8 MHz carrier by wireless transmitter to the recording laboratory. Here the V.H.F. signal is received, detected, pulse position demodulated and demultiplexed to recover the original multichannel data. The pulse position modulated signal has a deviation of ± 250 microseconds for the full dynamic range. In order to conserve R.F. power and to achieve continuous unattended transmission, a traffic ratio of 1:6 was found suitable. The system has an overall cross-talk better than 50 dB between the channels and linearity better than 1%.

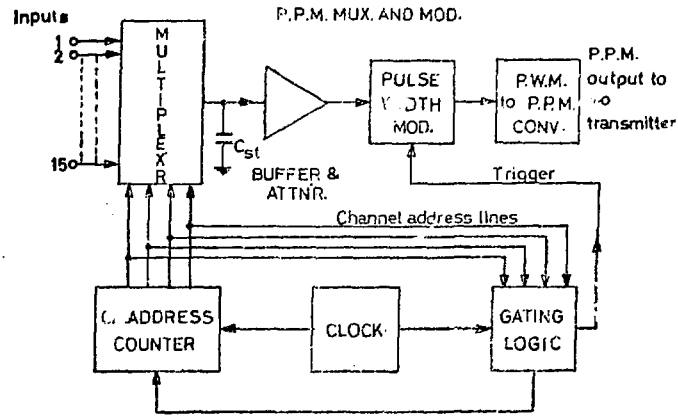

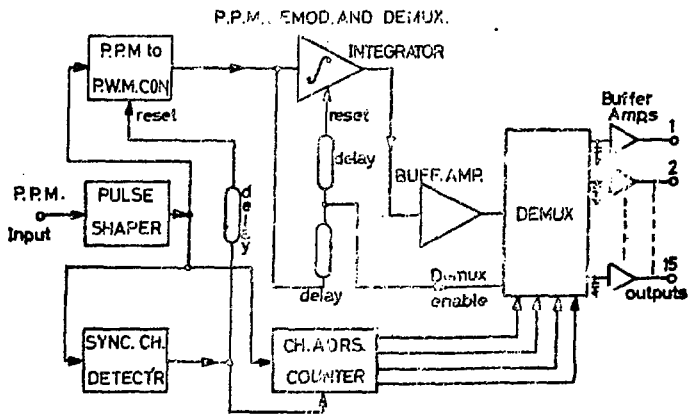

Fig. 4.4 Block diagram of multi-channel analog data acquisition system

5.4.4 F. M. Record and Replay Electronics

For keeping a permanent analogue record of events for analysis as well as to provide online hard copy of the tremors, the f. m. geophone signals are recorded on a 1" width, 24 track magnetic tape. The record electronics filters the f. m. signals which are received from field geophone nos. 1 to 6, in 300Hz-800 Hz pass band, shapes and records them on

magnetic tape. Direct geophone signals no. 7 to 11 received via wireless telemetery are frequency modulated and recorded. Replay electronics picks up the low level f.m. signals from tape, amplifies and demodulates them to retrieve their original analogue forms. The system has a dynamic range of 70 dB for signal in the frequency band 0-35 Hz with less than 3% total harmonic distortion. Signal frequency band width can easily be extended upto 20 KHs by choosing suitable centre frequency and tape speed. Some sample wave forms recorded by the array are shown in Fig. 4.2. Of these the traces on the left hand side are the signals (telemetered as in article 5.4.2) of an event on 3 September 1978, the very first event to be recorded after the array became fully operational. The lower two waveforms on the right hand side are rockburst signals of an event on 28 September 1978, which gave detectable energy at two of the geophone locations, 9 and 10 from where the signals are telemetered partly by cable and partly by V.H.F. (see article 5.4.3).

5.4.5 Event Trigger Unit

For analysis of seismic events, a hard copy of seismogram is needed. It is uneconomical to have a record of 24 hour daily data. To produce a seismic signal only when needed an on-line unit is developed and installed which produces a seismogram when simultaneous occurence of seismic signals having magnitude greater than a threshold in at least a chosen number of channels out of a total number of channels, is registered. A typical record of an event detected and recorded is shown in Fig. 4.5.

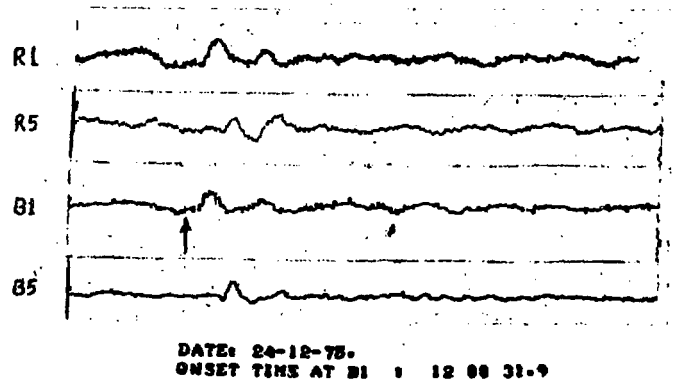

Fig. 4.5 Typical seismic records triggered by the event trigger unit

Papers Published/Accepted for Publication in Scientific Journals, etc.

1. A universal empirical relation for the variation of k_{eff} with core dimensions of bare and reflected small fast systems
Anil Kumar, M. Srinivasan, T.K. Basu and K. Subba Rao
Atomkernenergie, 30, 39 (1977).

2. On-line monitoring and data reduction of seismic events at Gauribidanur array
R.N. Bharthur, B.S.S. Rao and F. Roy
BARC Report 920 (1977).

3. Kinetics of zero energy fast reactor Purnima
S. Das and M. Srinivasan
BARC Report 957 (1977).

4. Saha's ionization equation for high Z elements
B.K. Godwal and S.K. Sikka
Pramana 8, 217 (1977).

5. Measurements of physics parameters of a subcritical system using correlation technique
B.K. Godwal, M.R. Phiske and M.P. Navalkar
Atomkernenergie 27, 227, (1977).

6. DL-leucyl-glycyl-glycine
K.N. Goswami, V.S. Yadava and V.M. Padmanabhan
Acta Cryst. (1977) B33, 1280.

7. Unfolding of fast neutron spectrum from foil activation data for Purnima
O.P. Joneja, D.V.S. Ramakrishna and M.P. Navalkar
Atomkernenergie 30, 45 (1977).

8. Some seismic results of the Rajasthan explosion of 18th May, 1974
G.J. Nair
AWRE report AG 224, June 1977.

9. Measurement of the effect of the reactivity of materials in a fast reactor (in Russian)
V.R. Nargundkar, T.K. Basu, K. Chandramoleshwar, P.K. Job and K. Subba Rao
Atomnaya Energiya, 42(5), 383 (1977).

10. Evidence of multiplicity in the travel time curve beyond 30 degree
Ram Datt and K.J. Muirhead
Phys. Earth Planet Inter. 15, 28-38 (1977).

11. Role of BARC in the design of earthquake resistant structures
T.G. Varghese and S.K. Arora
Proc. 6th Conference on Earthquake Engg. (1977).

12. An instrument for measuring large ground motion transients
Vijai Kumar
BARC Report I-460 (1977).

13. Impurity effects and reaction kinetics of the pressure-induced $\alpha \rightarrow \omega$ transformation in Ti
Y.K. Vohra, S.K. Sikka, S.N. Vaidya and R. Chidambaram
J. Phys. Chem. Solids 38, 1293 (1977)

14. The crystal structure of onitin, a phenolic illudoid sesquiterpene from the fern onychium auratum
V.K. Wadhawan, S.K. Sikka and R. Chidambaram
Acta Cryst. (1977), B33 428

15. Comments on technical note 'A simple relationship of maximum Δk due to compaction of unmoderated fissile materials and use of Trombay Criticality Formula for same
Anil Kumar and M. Srinivasan
Accepted for publication in "Nuclear Technology".

16. Shape factors of non-critical small fast assemblies and their use in k_{eff} calculations
Anil Kumar, K. Subba Rao and M. Srinivasan
Accepted for publication in "Atomkernenergie".

17. An integral version of the Los Alamos density exponent formula for critical mass variation
Anil Kumar and M. Srinivasan
Atomkernenergie 31, 249 (1978).

18. Neutron emission from a 100 joule plasma focus
Anurag Shyam and M. Srinivasan
Appl. Phys., 17, 425 (1978).

19. Relative performance of different triangular networks in locating regional seismic sources
S.K. Arora, T.G. Varghese and T.K. Basu
Proc. Ind. Acad. Sci (E and P Sciences-4), 87A, 1978.

20. On propagation and attenuation of love waves
A.R. Banghar
Accepted for publication in Proc. Ind. Acad. Sci. A

21. Neutron multiplication studies in beryllium for fusion reactor blankets
T.K. Basu, V.R. Nargundkar, P. Cloth, D. Filges and S. Taczanowski
Accepted for publication in Nucl. Sci. Eng.

22. Exploitation of Gauribidanur array for seismic monitoring
T.G. Varghese, F. Roy, B.S.S. Rao, M.P. Suryavanshi and R.N. Bharthur
Phys. Earth and Planet. Interiors (1978).

23. Extinction corrections in structure refinement
R. Chidambaram and A. Sequeira
Advances in Crystallography, Ed. R. Srinivasan, Oxford and IBH (1978), pp 47-62.

24. भूकंपों की भविष्यवाणी: कुछ तकनीकी पक्ष
कालूलाल रॉय
वैज्ञानिक, 10(4), अक्टूबर - दिसंबर, 1978

25. Opacities of high temperature high Z plasmas
B.K. Godwal and S.K. Sikka
Pramana (1978), 11, 47.

26. X-ray transport in Ni plasma
B.K. Godwal
Accepted for publication in Phys. Lett.

27. Electronic Grüneisen parameter in shock Hugoniot equation of state of aluminium
B.K. Godwal, S.K. Sikka and R. Chidambaram
Accepted for publication in Phys. Rev. B.

28. Effect of porosity on the cratering efficiency of underground peaceful explosions in a shale medium
Satish C. Gupta, S.K. Sikka and R. Chidambaram
Accepted for publication in Proc. Indian Acad. Sci. A.

29. Strength curves for shales and sandstones under hydrostatic confining pressures
Satish C. Gupta and S.K. Sikka
BARC Report 968 (1978).

30. Use of non-fission neutron sources for the breeding of U^{233} from thorium
P.K. Iyengar and M. Srinivasan
Physics News, 9(3), 1(1978). Also in the "Report on the Seminar on Thorium", Edited and Compiled by M.R. Balakrishnan, BARC (1977).

31. Purnima - A PuO_2 fuelled zero energy fast reactor at Trombay
P.K. Iyengar, T.K. Basu; K. Chandramoleshwar, S. Das, P.K. Job, S.K. Kapil, V.R. Nargundkar, C.S. Pasupathy, M. Srinivasan and K. Subba Rao
Accepted for publication in Nuc. Sci. and Engg.

32. Experimental determination of the k_{eff} variation of Purnima-I fast reactor during insertion of core into reflector
P.K. Job and M. Srinivasan
Atomkernenergie, 34, 58 (1978).

33. Calculations for tritium breeding per source neutron for fusion blanket models
O.P. Joneja, K. Subbukutty and M.P. Navalkar
Atomkernenergie 33, 11 (1978)

34. A precision neutron diffraction study of tetragonal RbH_2PO_4
A.R. Khargouli, B.A. Wahab, E. Ajaj and A. Sequeira
Acta Cryst. B34, 1040(1978).

35. Auto-regressive method of detection of weak signals in noise for monitoring precursors
G.S. Murty, G.J. Nair and P. Roy
Accepted for publication in Ind. Journ. of Meteorology and Geophysics.

36. F.M. to digital conversion of seismic array data
G.J. Nair
BARC Report, I.467, 1978.

37. Pulse neutron logging, a modern approach to petroleum exploration
M.P. Navalkar
Training School Journal, 1978.

38. Amino acids: systematics of molecular structure conformation and hydrogen bonding
M. Ramanadham and R. Chidambaram
Advances in Crystallography, Ed. R. Srinivasan, Oxford and IBH (1978), pp. 81-103.

39. Cavity radius estimation for contained peaceful nuclear explosions- an analytic approach
M. P. Ranga Rao, and S.K. Sikka
Proc. Indian Acad. Sci. 87A, 13 (1978)

40. भूकंपों की पूर्व घोषणा: विज्ञान, प्रशासन व समाज
रामदत्त
वैज्ञानिक, 10(4), अक्टूबर - दिसंबर, 1978

41. आपके इलाके में भूकंप आ जाए तो.....
सलत कुमार अरोड़ा
वैज्ञानिक, 10(4), अक्टूबर - दिसंबर, 1978

42. An on-line TDC-312 computer controlled neutron diffractometer
A. Sequeira, S.N. Momin, H. Rajagopal, J.N. Soni, R. Chidambaram, Dilip Kumar, R. Rao and V.M. Gopu
Pramana 10, 289 (1978)

43. Recording techniques in neutron diffractometry
A. Sequeira
Advances in Crystallography, Ed. R. Srinivasan, Oxford and IBH (1978), pp 159-182.

44. Critical resistivity of deviations from Matthiessen's rule for polyvalent metals
S.M. Sharma
Accepted for publication in Phys. Rev. B

45. Surface barrier detector fabrication and fast neutron spectrometry
R.V. Srikantiah, O.P. Joneja, J.S. Coachman, H.J. Shetty and M.P. Navalkar
Atomkernenergie 32, 198 (1978)

46. Preliminary safety analysis report for Purnima II: BeO reflected U-233 uranyl nitrate solution reactor experiment
M. Srinivasan, A.K. Ray, K. Chandramoleshwar, S. Das, P.K. Job, P.C. Mayankutty, B.K. Patil, C.S. Pasupathy and K. Subba Rao
BARC/I-488 (1978).

47. A simple technique of fabrication of paraboloidal concentrators
M. Srinivasan, L.V. Kulkarni and C.S. Pasupathy
Accepted for publication in "Solar Energy".

48. Analysis of small cylindrical fast system by monte carlo method
K. Subbukutty and M.P. Navalkar
Atomkernenergie 31, 21 (1978).

49. Time dependent calculations by neutralised collision method
K. Subbukutty, S.B.D. Iyengar and M.P. Navalkar
Atomkernenergie (1978), 32, 203 (1978)

50. पिछले दस वर्षों के विनाशकारी भूकंप
तापस कुमार बासु और सलत कुमार अरोड़ा
वैज्ञानिक, 10(4), अक्टूबर - दिसंबर, 1978

51. भूकंपों का वैज्ञानिक पहलू
विजय कुमार
वैज्ञानिक, 10(4), अक्टूबर - दिसंबर, 1978

52. Kinetics of phase transformations in Ti, Zr and Hf under static and dynamic pressures
Y. K. Vohra
Jour. Nuclear Materials 75, 288 (1978)

53. Electronic Structure of omega phase of titanium and zirconium
Y. K. Vohra, S. K. Sikka and R. Chidambaram
Accepted for publication in J. Phys. Metal Phys. F.

54. Electronic basis for omega phase stability in group IV transition metals and alloys
Y. K. Vohra
Accepted for publication in Acta Metallurgica.

55. Ferroelastic effect in orthoboric acid
V. K. Wadhawan
Mat. Res. Bull. 13, 1 (1978)

56. Ferroelastic effect in barium chloride dihydrate
V. K. Wadhawan
Curr. Sci. (1978), 47, 534 (1978)

57. Gyrotropy, an implicit form of ferroicity
V. K. Wadhawan
Accpeted for publication in Acta Cryst. A.

Papers Presented/Accepted for Presentation at Symposia, Seminars, Conferences, etc.

1. Temperature-dependent electronic contribution to shock Hugoniot equation of state of aluminium
B. K. Godwal, S. K. Sikka and R. Chidambaram
Nuclear Physics and Solid State Physics Symposium, Univ. of Poona, Pune (1977).

2. The crystal structure of DL-leucyl-glycyl-glycin
K. N. Goswami, V. S. Yadava and V. M. Padmanabhan
National Conference on Crystallography, University of Madras, Madras (Jan. 1977).

3. Surface barrier spectrometers for calibration of fast neutron in Mev range
O. P. Joneja, R. V. Srikantiah, M. R. Phiske, J. S. Coachman and M. P. Navalkar
International Specialists Symposium on Neutron Standards & Application, 1977, N. B. S. Washington

4. Feasibility studies of carbon-oxygen method for oil well logging
D. V. S. Ramakrishna, S. K. Sadavarte and M. P. Navalkar
DAE Symposium on Isotopes in Industries, 1977.

5. Impurity dependent changes in the intrinsic resistivity of Indium
S. M. Sharma
Nuclear Physics and Solid State Physics Symposium, Univ. of Poona, Pune (1977).

6. A neutron diffraction study of the structure and conformation of glycyl-L-threonine. $2H_2O$
A. Sequeira, H. Rajagopal and V. M. Padmanabhan
National Conference on Crystallography, Madras (1977).

7. Critical Experiments with ^{233}U
M. Srinivasan
Report on the Seminar on Thorium, Edited and Compiled by M. R. Balakrishnan, BARC (1977).

8. High pressure electronic structure of Titanium in relation to its alloying behaviour with transition metals
Y. K. Vohra and S. K. Sikka
Nuclear Physics and Solid State Physics Symposium, Univ. of Poona, Pune (1977).

9. 'Orthoboric Acid' an unusual Ferroelastic
V, K. Wadhawan
Nuclear Physics and Solid State Physics Symposium, Univ. of Poona, Pune (1977).

10. Ferroelastic effect in Orthoboric acid
V. K. Wadhawan
Seventh National Conference on Crystallography, Univ. of Madras, Madras, Jan. 1977.

11. Experimental studies of neutron multiplication from beryllium (n, 2n) reaction in CTR blankets
T. K. Basu, P. Cloth and V. R. Nargundkar
10th Symposium on Fusion Technology, Padua, Italy (Sept. 1978).

12. Equation of state of thorium
B. K. Godwal, S. K. Sikka and R. Chidambaram
Nuclear Physics and Solid State Physics Symposium, IIT, Bombay (1978).

13. Monte carlo calculations for intermediate energy standard neutron field
O. P. Joneja, K. Subbukutty, S. B. D. Iyengar and M. P. Navalkar
International Conference on Neutron Physics and Nuclear Data for Reactor and other Applied purposes, held at Harwell, Sept. 1978.

14. Status report on reactor dosimetry
M. P. Navalkar
Presented at IAEA meeting of WGRRM, 1978.

15. A neutron diffraction study of DL-aspartic acid
H. Rajagopal, S. N. Momin, M. Ramanadham and A. Sequeira
National Conference on Crystallography, Vallabh Vidyanagar (1978).

16. P-wave low velocity zone in the upper mantle
Ram Datt and K. J. Muirhead
III Symp. on Earthquake Engg., University of Roorkee, Oct. 1978.

17. P-wave low velocity zone in the upper mantle
Ram Datt
6th Symp. on Earthquake Engg., Roorkee University, 1978.

18. An objective approach in the determination of the travel time curve,
Ram Datt
Symp. on Seismology, Kurukshetra University, 1978.

19. On inversion of slowness and travel time data from arrays
Ram Datt
Symp. on Seismology, Kurukshetra University, 1978.

20. Neutron diffraction study of biological molecules using medium flux reactors
A. Sequeira
Proc. Int. Symp. 'Biomolecular Structure Conformation Function and Evalution' Madras (1978).

21. A comparative study of some methods of extinction correction in neutron diffraction
A. Sequeira, H. Rajagopal and R. Chidambaram
Absts. XIth Int. Cong. Crystallography, Warsaw (1978).

22. Corrections for severe secondary extinction in neutron diffraction
A. Sequeira, H. Rajagopal and R. Chidambaram
National Conference on Crystallography, Vallabh Vidyanagar (1978).

23. The phase problem in Neutron Crystallography
S. K. Sikka
Invited talk at Eighth National Conference on Crystallography, Sardar Patel University, Vallabh Vidyanagar (1978).

24. High pressure-some theoretical aspects
S. K. Sikka
Nuclear Physics and Solid State Physics Symposium, IIT, Bombay (1978).

25. A macrobarographic system for the measurement of infrasound
Vijai Kumar
Twenty-second Technical Convention of Inst. Electronics Engineers, New Delhi, 1978.

26. Theoretical and experimental study of electronic structure of ω-Zr
Y. K. Vohra, S. K. Sikka and R. Chidambaram
Nuclear Physics and Solid State Physics Symposium, IIT, Bombay (1978).

27. 'Orthoboric Acid', a Novel Ferroelastic
V. K. Wadhawan
Eleventh International Congress on Crystallography, Warsaw, Poland (1978).

28. 'Gyrotropy'
V. K. Wadhawan
Nuclear Physics and Solid State Physics Symposium, IIT, Bombay (1978).

29. The crystal and molecular structure of L-prolyl-L-alanine monohydrate
V. S. Yadava and V. M. Padmanabhan
National Conference on Crystallography, Sardar Patel University, Anand (Feb. 1978).

30. The structure of L-prolyl-L-alanine monohydrate
V.S. Yadava and V.M. Padmanabhan
Eleventh International Congress of Crystallography, Warsaw (Aug. 1978).

AWARDS AND DEGREES (M.Sc./Ph.D.)

Name	Guide	Title	Award and Year
S. Das	Dr. R. Chidambaram	Dynamic measurement of reactivity in Purnima zero energy fast reactor	M.Sc., Bombay (1977)
Ram Datt	Dr. K.J. Muirhead	A "P" wave velocity structure for the upper mantle and transition zone, using the Warramunga seismic array	Ph.D., Australian National University(1978)
S.K. Arora	Dr. P.K. Iyengar	Crustal structure near Gauribidanur in Southern India from the Gauribidanur data of local earthquakes, rock-bursts and chemical explosions	Ph.D., Bombay (1978)
Vijai Kumar		Microbarographic detection and location of atmospheric nuclear explosions and evaluation of underground nuclear explosion parameters based on close-in measurements	Indian National Science Academy Young Scientist Award (1977)

Talks Organised/Delivered by Nt. P. D. Staff (1977-78)

S. No.	Speaker	Topic	Date	Auspices
1.	K.R. Subbaramu	Earthquakes (Kannada)	12-6-77	All India Radio, Bangalore
2.	O. P. Joneja	Tritium breeding measurements in Lithium Blankets	19-7-77	Reactor Physics Seminar
3.	K. Subba Rao	Monte Carlo methods in neutronic calculations	29-10-77	Reactor Physics Seminar
4.	R. Chidambaram	Atomic Energy	Oct. 77	Border Security Force Officers, New Delhi
5.	K.R. Subbaramu	Seismic Array Station	Nov. 77	Rotary Club, Madhugiri
6.	A. Sequeira	Neutron scattering from biomolecules	Dec. 77	IPA Seminar on Neutron scattering
7.	Dr. R. Diamond MRC Laboratory of Molecular Biology, Cambridge, U.K.	Application of computer graphics to the interpretation of the structure of tobaco mosaic virus at 2.8A resolution	2-1-78	Physics Colloquium
8.	Prof. T. L. Blundell Laboratory of Molecular Biology, Birkbeck College University of London U.K.	Structural evidence for gene duplication and fusion in the evolution of proteins	13-1-78	Physics Colloquium
9.	S. Das	Coupled Core Kinetics Theory and experiment	21-1-78	Reactor Physics Seminar

S. No.	Speaker	Topic	Date	Auspices
10.	K. Chandramoleshwar	Brief Description of Purnima II Reactor	21-2-78	Purnima II Safety Seminar
11.	P.K. Job	Physics Calculations	21-2-78	Purnima II Safety Seminar
12.	S. Das	Dynamics of Power Excursions in Purnima II	21-2-78	Purnima II Safety Seminar
13.	C.S. Pasupathy	Safety Consideration in the Design of Purnima II	21-2-78	Purnima II Safety Seminar
14.	Dr. Krishan Lal National Physical Lab. New Delhi	Defects in nearly perfect crystals	22-2-78	Physics Colloquium
15.	V.K. Wadhawan	Ferroelastic Effect in Orthoboric Acid	2-3-78	Physics Colloquium
16.	Vijai Kumar	Science ki Duniya (Hindi)	8-6-78	All India Radio, Bombay
17.	Vijai Kumar	Bharat Mein Bhookamp Vigyan (Hindi)	5-7-78	All India Radio, Bombay
18.	S.K. Arora	Pahad (Hindi)	6-8-78	All India Radio, Bombay
19.	A. Sequeira	Digital control by computers for scientific experiments	7-10-78	IPA seminar on computers and Physics
20.	S.K. Arora	Bhookampaki Bhavishyavani (Hindi)	14-10-78	All India Radio, Bombay

S. No.	Speaker	Topic	Date	Auspices
21.	K. K. Kannan	Structure and function of proteins by x-ray diffraction analysis	Oct. 78	Symposium held at Mahabaleshwar on the Role of Chemistry in Biological processes
22.	R. Chidambaram	Neutron scattering and its application to biological systems	Oct. 78	Symposium held at Mahabaleshwar on the Role of Chemistry in Biological processes
23.	G.S. Murty	Seismological data acquisition and interpretation	Nov. 78	BARC Workshop on Experimental Data
24.	K. K. Kannan	Structure and function of proteins	Nov. 7, 78	Physics Colloquium
25.	Dr. Alexandre Novak Infrared and Raman Spectroscopy Laboratory, CNRS, France	Applications of infrared and Raman spectroscopy to the problems of hydrogen bonding	23-11-78	Physics Colloquium
26.	M. Ramanadham	Triclinic lysozyme: a case study of the refinement of protein structures	28-11-78	Physics Colloquium
27.	Dr. J.H. Hodgson Project Manager UNDP Project in South East Asia, Manila	Seismology in South-East Asia	5-12-78	

S. No.	Speaker	Topic	Date	Auspices
28.	Prof. Francois Fillaux, Infrared and Raman Spectroscopy Laboratory, CNRS, France	Low-frequency vibrational spectra of N-methylacetamide-comparison of infrared, Raman and Neutron inelastic scattering	14-12-78	Physics Colloquium
29.	K.R. Subbaramu	Seismic Array Station	Dec. 78	Science Association National College, Gauribidanur

Lectures Organised/Delivered by Nt. P. D. Staff (1977-78)

S. No.	Speaker	Topic	Date	Auspices
1.	S.K. Sikka	Materials Science	Jan-April 77	25 lectures delivered to 20th batch trainees
2.	CUS*	Isotope Separation	3-2-77	Group Discussion
3.	S.M. Sharma	Band Theory	April-May 77	4 lectures delivered to 20th batch trainees
4.	Y.K. Vohra	Advanced Solid State Physics	April-June 77	15 lectures delivered to 20th batch trainees
5.	S.C. Gupta	Defect Solid State	May-June 77	6 lectures delivered to 20th batch trainees
6.	S.K. Sikka	Architecture of Crystals	May 77	3 lectures given to 16th batch of post graduate teachers
7.	CUS*	Fusion Power	28-6-77	Group Discussion
8.	CUS*	Techniques in Material Science	22-9-77	Group Discussion
9.	S.K. Sikka	Solid State Science	Sept-Dec 77	8 lectures and quiz delivered to 21st batch trainees
10.	T.G. Varghese	Seismic Instrumentation	Oct-Nov 77	A course of lectures delivered to trainees and operators, UNDP Project, Manila

S. No.	Speaker	Topic	Date	Auspices
11.	P.K. Job	Reactor Statics and Kinetics	Oct-Dec 77	A course of 30 lectures delivered to the Chemical and Metallurgy Trainees of 21st batch
12.	Y.K. Vohra	Solid State Science	Dec 77-April 78	20 lectures delivered to 21st batch trainees
13.	CUS*	Accelerators	6-3-78	Group Discussion
14.	S.M. Sharma	Boltzman Equation	March 78	4 lectures delivered to 21st batch trainees
15.	P.K. Job	Elementary Reactor Physics	April 78	A course of 10 lectures delivered to the Chemistry Trainees of 21st batch
16.	B.K. Godwal	Statistical Physics	April-June 78	3 lectures delivered to 21st batch trainees
17.	S.K. Sikka	Quantum Fluids	May 78	4 lectures delivered to 21st batch trainees
18.	S.K. Sikka	High Pressure Physics	May 78	Lecture delivered to 17th batch of post graduate teachers
19.	V.K. Wadhawan	Structural Phase Transitions	May 78	Lecture delivered to 17th batch of post graduate teachers

S. No.	Speaker	Topic	Date	Auspices
20.	Y.K. Vohra	Band Structure Studies	May 78	Lecture delivered to 17th batch of post graduate teachers
21.	B.K. Godwal	Statistical Physics	July-Dec 78	25 lectures delivered to 22nd batch trainees
22.	H. Rajagopal	Computer programming	Sept-Dec 78	A course of 20 lectures delivered to [illegible] trainees of 2[illegible] batch
23.	CUS*	Waste Disposal	24-10-78	Group Discussion
24.	Anil Kumar	Computer Programming (Numerical Methods)	Oct-Dec 78	A course of 10 lectures delivered to the Physics trainees of 22nd batch
25	P.K. Job	Reactor Statics and Kinetics	Oct-Dec 78	A course of 30 lectures delivered to the Chemical and Metallurgy trainees of 22nd batch
26	A. Sequeira	Neutron diffraction studies of biomolecules	Dec. 78	A course of 3 lectures at Madurai Kamaraj University

---

* Club Under Six: A group constituted of Nt. P. D. staff members from the training school with less than six years research experience.

NEUTRON PHYSICS DIVISION STAFF

Dr. P.K. Iyengar	Director, Physics Group
Dr. R. Chidambaram	Head, Neutron Physics Division

Purnima Laboratories

1. Dr. P.K. Iyengar
2. Shri M. Srinivasan

3. Dr. V.R. Nargundkar*
4. Shri K. Subba Rao
5. Shri K. Chandramoleshwar
6. Shri C.S. Pasupathy
7. Shri S. Das
8. Shri T.K. Basu+
9. Shri P.K. Job
10. Shri Anil Kumar
11. Shri L.V. Kulkarni

12. Shri Anurag Shyam
13. Shri S.K.H. Auluck

Reactor & Applied Neutron Physics

1. Dr. M.P. Navalkar

2. Dr. O.P. Joneja
3. Shri J.S. Coachman
4. Shri M.R. Phiske

5. Shri S.B.D. Iyengar
6. Shri G.V. Acharya $
7. Shri K. Subbukutty

8. Shri D.V.S. Ramakrishna
9. Shri S.K. Sadavarte
10. Shri Jagir Singh

11. Shri B.B. Gaikwad

Biological Crystallography & Automation

X-Ray Diffraction

1. Dr. V. M. Padmanabhan
2. Dr. V.S. Yadava
3. Shri Surendra Sinh
4. Dr. K.N. Goswami[++]

Neutron Diffraction

1. Dr. R. Chidambaram
2. Dr. A.S. Sequeira
3. Shri S.N. Momin
4. Shri H. Rajagopal
5. Smt. S.N. Bhakay-Tamhane
6. Shri R.N. Khunte
7. Dr. A.R. Kharagouli[**]

Protein Crystallography

1. Dr. K.K. Kannan
2. Dr. M. Ramanadham[@]

Solid State Phenomena

1. Dr. R. Chidambaram
2. Dr. S.K. Sikka
3. Dr. V.K. Wadhawan
4. Shri B.K. Godwal
5. Shri S.C. Gupta
6. Shri Y.K. Vohra
7. Shri S.M. Sharma

Seismology Section

Head: Shri T.G. Varghese[£]
Dr. G.S. Murty

Staff based at Bombay

1. Dr. G.S. Murty
2. Shri H.S.S. Sharma
3. Dr. S.K. Arora
4. Dr. Ram Datt

5. Shri A.R. Banghar
6. Shri Vijai Kumar Jain
7. Shri G. Jayachandran Nair
8. Shri V.G. Kolvankar
9. Shri Falguni Roy
10. Shri C.A. Krishnan
11. Shri K. Jayachandra Rao
12. Shri B.M. Shah
13. Shri V.N. Nadre
14. Shri T.K. Basu
15. Shri S.V. Sharma

Staff based outside Bombay

Delhi

1. Shri T.V. Sridharan
2. Shri P.C. Mitra

Gauribidanur

1. Shri K.R. Subbaramu
2. Shri R.N. Bharthur
3. Shri B.S.S. Rao
4. Shri M.K. Bhat
5. Shri M.P. Suryavanshi
6. Shri K.K. Sankaran
7. Shri N. Satyanarayana
8. Shri V.S. Kamath
9. Shri A.G. Kulkarni
10. Shri A.G.V. Prasad
11. Shri Muddurama
12. Shri T.J. Thomas
13. Shri S.S. Murthy

Administrative Staff

1. Smt. Usha Narayan
2. Shri K.N.N. Pillai
3. Shri K.P. Rajasekharan
4. Shri D. Diwakaran

* On deputation to KFA, Jülich, West Germany from July 1, 1977 to September 30, 1978.

\+ On deputation to KFA, Jülich, West Germany from April 1, 1977 to September 30, 1978.

@ On leave for post-doctoral research work at University of Washington, Seattle, USA from June 1, 1977 to August 31, 1978.

++ Visiting Scientist from Jammu University during May/June, 1977.

** Visiting Scientist from the Nuclear Research Institute, Baghdad during April 1977.

$ At present working independently on specially assigned problems.

£ Deceased